DEVELOPMENT OF CHEMIRESISTOR BASED NANOSENSORS TO DETECT VOLATILE CANCER BIOMARKERS

A Thesis

Submitted to the Faculty

of

Purdue University

by

Shitiz Vij

In Partial Fulfillment of the

Requirements for the Degree

of

Master of Science in Mechanical Engineering

May 2019

Purdue University

Indianapolis, Indiana

THE PURDUE UNIVERSITY GRADUATE SCHOOL
STATEMENT OF COMMITTEE APPROVAL

Dr. Mangilal Agarwal, Chair

Department of Mechanical and Energy Engineering

Dr. Andres Towar

Department of Mechanical and Energy Engineering

Dr. Sohel Anwar

Department of Mechanical and Energy Engineering

Approved by:

Dr. Jie Chen

Head of the Graduate Program

This thesis is dedicated to my parents.

ACKNOWLEDGMENTS

I would like to thank my father Kapil Kumar Vij and my mother Dikshha Vij for their love, support, affection and their motivation to pursue my dreams to study in the United States. I would like to extend my hearty thanks to my advisor Dr. Mangilal Agarwal who provided me an opportunity to work on this project. I would also like to thank him for his constant supervision, guidance and support during the work on this project. This project might not be possible without his encourangement and support throughout my masters at IUPUI. I would like to thank my thesis committee members Dr.Sohel Anwar and Dr.Andres Tovar for being highly understanding during submission deadlines and for their valuable comments and support. I am thankful to Jerry Money for his timely reminders for submission and any academic help needed during the time of my project. I would also like to thank Dr.Ali Daneshkhah for his support and assistance in the design and development of experiments and his assistance conducting experiments and Nojan Aliahmad for his assistance with the FESEM instrument.

I would also like to acknowledge the National Science Foundation (NSF) to support this project under grant no. 1502310. Integrated Nanosystems Development Institute (INDI) is also acknowledged to provide instrument and facilities used for successful completion of this project including the JEOL7800F Field Emission Scanning Electron Microscope awarded through NSF grant MRI-1229514 and Bruker X-Ray Diffraction System awarded through NSF Grant MRI-1429241.

TABLE OF CONTENTS

Page

LIST OF TABLES

LIST OF FIGURES

Figure Page

SYMBOLS

μ	micro
Δ	change
%	percent
Ω	ohm

ABBREVIATIONS

GCMS	Gas Chromatography Mass Spectroscopy
SPM-GCMS	Solid Phase Microextraction Gas Chromatography Mass Spectroscopy
PTRMS	Proton Transfer Reaction Mass Spectroscopy
FTIR	Fourier Transform Infrared
XRD	X-Ray Diffraction
FESEM	Field Emission Scanning Electron Microscope
VOC	Volatile Organic Compounds
CPC	Conductive Polymer Composite
GNP	Gold Nanoparticle
CB	Carbon Black
CNT	Carbon Nanotube
IR	Infrared
SWCNT	Single Walled Carbon Nanotube
MWCNT	Multi Walled Carbon Nanotube
ANN	Artificial Neural Network
SAM	Self Assembled Monolayer
SAW	Surface Acoustic Wave
QCM	Quartz Crystal Microbalance
ppm	parts per million
ppb	parts per billion
IDE	Interdigitated Electrode
MOS	Metal Oxide Semiconductor
PEI	Polyetherimide

ABSTRACT

Vij, Shitiz. M.S.M.E, Purdue University, May 2019. Development of Chemiresistor Based Nanosensors to Detect Volatile Cancer Biomarkers. Major Professor: Mangilal Agarwal.

Researchers have shown links between various hydrocarbons and carbonyl compounds and diseases, such as cancer using exhaled breath analysis through gas chromatography/mass spectroscopy (GC/MS) analysis of volatile organic compounds (VOCs). Trained canines can detect these VOCs and can differentiate a patient suffering from cancer from a healthy control patient. In this project, an attempt has been made to develop highly sensitive sensors for the detection of low concentrations of aldehyde VOCs, such as nonanal, using conductive polymer composites (CPCs) and functionalized gold nanoparticles (f-GNPs). Facile methods have been used to enhance the sensitivity and cross-selectivity of the fabricated sensors towards nonanal. Interdigitated electrodes (IDEs) are fabricated through a photolithography process. Sensors of PEI/carbon black (CB) composite were developed via spin-coating of the material followed by the heat treatment process. Sensors of 1-Mercapto-(triethylene glycol) methyl ether functionalized GNPs are developed via drop-casting of nanomaterial and f-GNP/PEI sensors are fabricated by spin casting PEI film on top of f-GNPs. Fourier Transform Infrared (FTIR) analysis, X-Ray Diffraction (XRD) analysis, contact angle measurement, and Field Emission Scanning Electron Microscopy (FESEM) analysis was conducted to characterize the fabricated devices. The fabricated sensors have been tested with a low concentration of nonanal, nonanone, dodecane, and 1-octanol in dry air. Multiple sensors are fabricated to ensure sensors reproducibility. The sensors have been exposed repeatedly to the targeting VOC to

assess the repeatability of the sensors. PEI/CB sensor degradation was studied over a period of 36 days.

The fabricated PEI/CB film could detect (1-80 ppm) of nonanal with higher selectivity, than the f-GNPs. The sensor$'s$ sensitivity to nonanal was over fourteen times higher than 2-nonanone, 1-octanol, and dodecane. This shows the high selectivity of the fabricated sensor toward nonanal. In addition, the proposed sensor maintained its sensitivity to nonanal over time showing minimal degradation. The sensor response to nonanal at a relative humidity (RH) of 50% and 85% dropped less than 13% and 32% respectively. The Response of f-GNP sensors to nonanal (400 ppb - 15 ppm), dodecane (5 - 15 ppm), 1-octanol (5 - 15 ppm), and 2-nonanone (5 - 15 ppm) presented a sensitivity ($\Delta R/R_0$) of 0.217%, 0.08%, 0.192% and 0.182% per ppm of the VOCs respectively. Despite the high sensitivity to the targeting VOCs, the fabricated sensors were damaged in an environment with relative humidity (RH) at 45%. A thin layer of PEI over the film was developed to ensure the sensor could tolerate long-time exposure to water vapor in an environment with RH up to 85% and enhance the sensor selectivity towards nonanal. The f-GNP/PEI sensors with nonanal (400 ppb- 15 ppm), dodecane (100 -200 ppm), 1-octanol (5 - 15 ppm) and 2-nonanone (5 - 15 ppm) presented sensitivity ($\Delta R/R_0$) of 0.21%, 0.017%, 0.0438% and 0.0035% per ppm of the VOCs respectively. The sensor fabrication, characterization, testing methods, and results are presented and discussed.

1. INTRODUCTION

1.1 Objective

Early detection of tumor cells can help increase the survival rate of the cancer patients [1] and rapid and reliable detection of cancer cells in an early stage is a challenge for the researchers [2]. Various researchers have reported a non-invasive analysis of VOCs as a technique for anticipated diagnosis for cancer as the breath extracts of cancer patients show higher levels of several VOCs because of the exchange of gases between the alveolar air and the blood [3,4]. When a person is suffering from a disease, the metabolism of the body changes which alters the VOC concentration in blood. This blood interacts with alveolar air in the lungs resulting in an exhalation of VOCs slightly different than VOCs under normal conditions. These VOCs termed as biomarkers can be used to predict the disease from exhaled breath monitoring. Hence a fast, reliable, economic and portable technique is required for breath testing [5]. There are various methods used for detection of VOC fingerprints in breath such as magnetic resonance spectroscopy (MRS), nuclear magnetic resonance (NMR) and Mass Spectroscopy (MS) methods [6]. Among currently available methods GCMS is most preferred because of its sensitivity for specific molecules, high selectivity, and automation, with lower costs for detection [6]. Trained canines also present the possibility to detect these biomarkers and differentiate between a healthy person and a patient [7]. The major problem with using canines for breath sampling is time and money consumed to train the dogs, methodological weaknesses and different screening result in clinical studies [7, 8]. On the other hand, nanomaterial based sensor arrays have shown a fast, cheap and portable method presenting a solid foundation for breath sampling for the identification of VOC fingerprint in exhaled breath that can be linked to cancer [9–11]. It has already been shown by the literature review that f-

GNPs and CPCs possess better sensing properties such as controllable selectivity and sensitivity, low power consumption, lower response time than other nanomaterials like CNTs and graphene [12–14]. In this project, the goal is to detect a low concentration of aldehyde VOCs linked to different types of cancer by using CPCs and f-GNPs and propose the method to fabricate the respective sensors. Another aim is to reduce the sensitivity of f-GNP sensors to environmental variations such as humidity and enhance the selectivity towards nonanal by incorporating PEI film on top of drop-casted f-GNPs. The fabricated sensors should have the following properties: fast response time, high sensitivity to targeting VOCs with high selectivity, low sensitivity to environment changes like humidity, low degradation over time and the sensors should have a reproducible and repeatable response.

1.2 Outline of the Manuscript

The contents of the thesis are summarized in this section. After giving the objective in Chapter 1, Chapter 2 is focused on the literature review to show the importance of the development of chemiresistive sensors for the early detection of cancers by showing the cancer death toll. A list of biomarker VOCs is presented to determine potential targeting VOCs for the development of sensors. Existing gas sensing technologies are discussed and elaborated to show the importance of f-GNP and CPC nanomaterial-based chemiresistive sensors. Film fabrication techniques are also discussed with the goal to determine which fabrication methods would be suitable for the proposed application. In the last section, a brief overview of the conventional photolithography process is given.

Material and methods that were used to develop the sensors are presented in Chapter 3. This chapter describes methods used for the fabrication of IDEs, synthesis of the sensing material and development of the proposed sensors. The experiment test setup used for testing the fabricated sensors with different VOCs and water vapor

is presented in this chapter. The Sensing mechanism for PEI/CB and GNP is also presented in this chapter.

Chapter 4 present the results for material characterization of PEI/CB and PEI. This includes FTIR analysis, XRD Analysis, FESEM analysis, Contact Angle Measurement and Profilometer measurement of the fabricated films. The sensor results for PEI/CB and 1-Mercapto-(triethylene glycol) methyl ether functionalized GNPs with and without a PEI layer are presented in this chapter. In the end, a comparison has been presented in our work and other work in a related field.

Chapter 5 presents the conclusion made regarding the response of fabricated sensors towards various VOCs. This chapter also provides a brief overview of future work that can be done based on the present work.

2. LITERATURE REVIEW

2.1 Cancer Background and Biomarker Volatile Organic Compounds (VOCs)

Background

The Human body has trillions of cells which have a natural tendency to grow and divide to form new cells according to bodily needs. Cell division or replacement occurs when these cells become old or get damaged. Sometimes this natural order of cell replacement is disturbed in which the cells with damaged deoxyribonucleic acid (DNA) are neither replaced nor die but instead start replicating. These cells with damaged DNA result in uncontrolled and abnormal growth of damaged cells to form extra mass tissue called tumors. Cancer can be benign or malignant depending on the movement of the cancer cells to other body parts. This process of spreading and growing tumors is known as metastasis. There are external factors such as intake of tobacco, alcohol, poor diet, obesity, exposure of UV radiation, lack of physical activity and internal factors such as inherited genetics, a mutation from metabolism, change in hormonal conditions which can be a cause for cancer.

According to the World Health Organization (WHO) statistics, 8.8 million people died from cancer in 2015 and there is an exponential increase in the number of cases each year throughout the world. The number of new cancer cases and death estimation is done each year by the National Cancer Society and according to the most recent data, 1,735,350 new cancer cases and 609,640 cancer deaths are projected to occur in the United States in 2018 [15]. Accounting for half of the cancer deaths are prostate, lung and colorectal cancer for men and breast, colorectal and lung cancer for women [15], [16]. The number of cancer cases is different for each state in the

United States and according to a survey, 85% of the people with cancer are above 50 years of age [17]. The survival rate to major types of cancer is low. For lung cancer approximately, 85,000 out of 116,990 men and 71,200 out of 105,510 women dies which result in more deaths than any other type of cancer considering 26,000 men out 161,000 dies from prostate cancer and 41,000 women out of 252,000 die of breast cancer. Even though the survival rate for prostate cancer in men and breast cancer in women is much higher when compared to lung cancer but still the overall survival rate is low [17]. Deaths caused by cancer can be lowered by early diagnosis of cancer by focusing on detecting patients at as early a stage as possible. Delayed or late-stage diagnosis will consequently result in lower survival rate, higher cost of care, etc.

Biomarker VOCs

A broad definition is given by WHO describes a biomarker as "A substance, structure or process that can be measured in the body or its products and influence or predict the incidence of outcome or disease" [18] [19]. In a more precise manner, a biomarker can be described as an objectively measured characteristic that describes a normal or abnormal biological state in an organism by analyzing biomolecules such as DNA, ribonucleic acid (RNA), protein, peptide, and biomolecule chemical modifications [20]. More specifically for cancer, cancer biomarkers can provide a measure of cancer development, progression or response in a patient suffering from cancer. Biomarkers can be divided into three types:1) Diagnostic Biomarkers which are those that help to detect and identify a given type of cancer with specificity and sensitivity.2) Prognostic biomarkers which are used once diagnostic biomarkers are identified and the status of the cancer is established. These biomarkers help to predict the probable course of the disease and thus help to decide the dosage of the treatment.3) Predictive biomarkers help to classify individuals whether they are responding to medication or not by observing the biomarkers before and after treatment.

Table 2.1. List of VOCs associated with Lung and Breast Cancer Based on Chemical Nature.

Cancer Type	**Chemical nature of VOC**	**VOC biomarkers**
Lung Cancer [21–26]	Alcohols	methanol, isopropanol, ethanol, 1-octanol, 1-propanol
	Aromatic Hydrocarbons	isoprene, benzene, toluene, styrene, naphthalene, propyl benzene, 1,2,4 trimethyl benzene, trichlorofluoro benzene, xylene,
	Aliphatic Hydrocarbons	heptane, decane, undecane, cyclopentane, 1-hexene, nonane, cyclohexane, methyl heptene, octane, pentane
	Carbonyl Compounds	**formaldehyde, propanal,, butanal, pentanal, hexanal,, heptanal, octanal, nonanal, decanal, acetone, butanone**
Breast Cancer [27–29]	Alcohols	heptane, decane, undecane, cyclopentane,1 hexene, nonane, cyclohexane, methyl heptene
	Aromatic Hydrocarbons	benzene, 1,2,4,5 trimethyl benzene
	Aliphatic Hydrocarbons	nonane, dodecane, undecane, tetradecane, 2,7,10 trimethyl dodecane,2-methyl propane
	Carbonyl compounds	**hexanal, heptanal, octanal, nonanal**

Table 2.2. List of VOCs associated with Ovarian and Prostate Cancer Based on Chemical Nature.

Cancer Type	**Chemical nature of VOC**	**VOC biomarkers**
Ovarian Cancer [10, 30]	Alcohols	ethanol
	Aromatic Hydrocarbons	styrene
	Aliphatic Hydrocarbon	hexadecane, propionitrile
	Carbonyl compounds	**nonanal**, decanal, 2-butanone
Prostate Cancer [31]	Alcohol	2,6-dimethyl-7-octen-2-ol
	Carbonyl Compounds	**pentanal, 3-octanone, 2-octanone,nonanal**

There is a large variety of VOCs that can be associated with different cancer types and predicting these biomarkers can help in the early identification of cancer. ONeill et al. used computerized classification to determine VOCs from breath samples of lung cancer patients using GCMS technique and reported 28 VOCs mentioned in the list with occurrence more than 90% [21]. Philips et al. reported a list of 22 VOCs discriminated between test group of patients with and without lung cancer with p values less than 0.0003 [22]. Phillips et al. reported five compounds to predict the presence or absence of breast cancer in women [27]. Another study shows a list of 11 VOCs from lung cancer patients that help to differentiate exhaled breath from a healthy person using solid phase microextraction with gas chromatography [23]. In 2012, another article reported 15 VOCs out of 58 with high discriminant power from exhaled breath of colorectal cancer patients and a healthy person [32]. Besides lung and breast cancer, another study shows the development of a sensor array with five different sensing materials to detect different VOCs from exhaled breath of ovarian

cancer patients [10] and nonanal has also been reported as the main biomarker (with the smallest p-value) for detecting ovarian cancer from tumor-free subjects [30].

Assessment of VOCs investigated with patients suffering from cancer indicates that a majority of these VOCs could be categorized as carbonyl compounds, alcohols, aliphatic hydrocarbons, and aromatic hydrocarbons.

Alcohols - Nutrition, husbandry, and environmental factors influence VOC composition due to growth and metabolism effects in our body that result in the accumulation of metabolites that are exhaled in the breath [33]. Alcohols are easily dissolved in water, therefore it is found in body tissues and fluids and is rapidly absorbed in the blood [5]. A significant decrement in the concentration of 1-octanol was noticed between colorectal cancer patients and the healthy person [34]. Elevated levels of 1-octanol were reported in women suffering from breast cancer [29]. Proton transfer reaction mass spectroscopy (PTRMS) and solid phase microextraction with gas chromatography and mass spectroscopy (SPM-GCMS) were used to analyze the breath samples from lung cancer patients and methanol was reported as one of the targeting biomarker having p=0.01 [24]. A GNP based flexible sensor was fabricated to detect ethanol as one of the target biomarkers from women suffering from ovarian cancer [10]. A significant decrement in the concentration of 1-octanol was noticed between colorectal cancer patients and the healthy person [34]. Elevated levels of 1-octanol were reported in women suffering from breast cancer [29].

Carbonyl Compounds - Formaldehyde was also reported as one of the target VOCs from breath in lung cancer patients [35] and from urine headspace in prostate cancer patients [36]. Smith et al. reported higher levels of acetaldehyde in the range of 100 ppb if moderately size lung cancer tumors are present [37]. Poli et al. worked specifically on aldehydes and mentioned propanal, butanal, pentanal, hexanal, heptanal, octanal, and nonanal and made the comparison between the exhaled level of VOCs between NSCLC and the control group [38]. Formaldehyde and pentanal were

reported as one of the potential biomarkers among 21 VOCs for lung cancer patients [24]. Higher incidence of acetaldehyde and pentanal were reported for patients suffering from prostate cancer [31] [39]. Heptanal, hexanal, octanal, and nonanal have been reported with significant concentration difference between breast cancer patients and healthy people [28]. When compared with healthy patients nonanal and decanal levels in urinary VOCs are elevated in renal cell carcinoma patients [40].

Aromatic Hydrocarbons - In 1988, five different chemical classes alkenes, cycloalkanes, polynemes, cyclopolyemes, and naphthalene were reported as biomarkers for lung cancer using computer classification screening technique giving isoprene, benzene, toluene, ethylbenzene, naphthalene and dichlorobenzene as biomarker VOCs [21]. Discrimination between the breath from lung cancer patients and healthy people were completed and several aromatic hydrocarbons such as styrene, propyl benzene, benzene, 1,2,4 trimethyl benzene, 1-methylethenyl benzene were reported as target biomarkers for lung cancer.[8] Amal et al. and Kahn et al. both have reported styrene as one of the main biomarkers for ovarian cancer patients [10, 30]. A combination of VOCs like ethylbenzene, benzene and styrene were reported as biomarkers from exhaled breath in non-small cells lung cancer patients [41].

Aliphatic Hydrocarbons - In 1985, several alkanes and monomethylated alkanes such as dichloromethane and octane were reported to successfully differentiate between two groups of limited patient populations [42]. A combination of various VOCs like heptane, decane, undecane, cyclopentane, cyclopropane was mentioned as biomarkers in a study using breath samples from people suffering from lung cancer [22]. Bouza et al. reported dodecane as one of the potential VOC biomarkers in oral cancer patients [43] and a significantly higher concentration of n-dodecane was seen using ion mass spectroscopy in lung cancer patients [25]. Another study gives dodecane, undecane, pentadecane as important biomarkers for breast cancer

patients [29] and mentioning hexadecane as one of the five biomarkers from exhaled breath in ovarian cancer patients [30].

2.2 Gas Sensing Technologies

Normally the sensing technologies for detection of gases can be based on the operating principle of the sensor and can be divided into five major types:
1) Acoustic Sensors 2) Optical Sensor 3) Mass Sensitive Sensors 4) Electrochemical Sensors and 5) Chemiresistive Sensors.

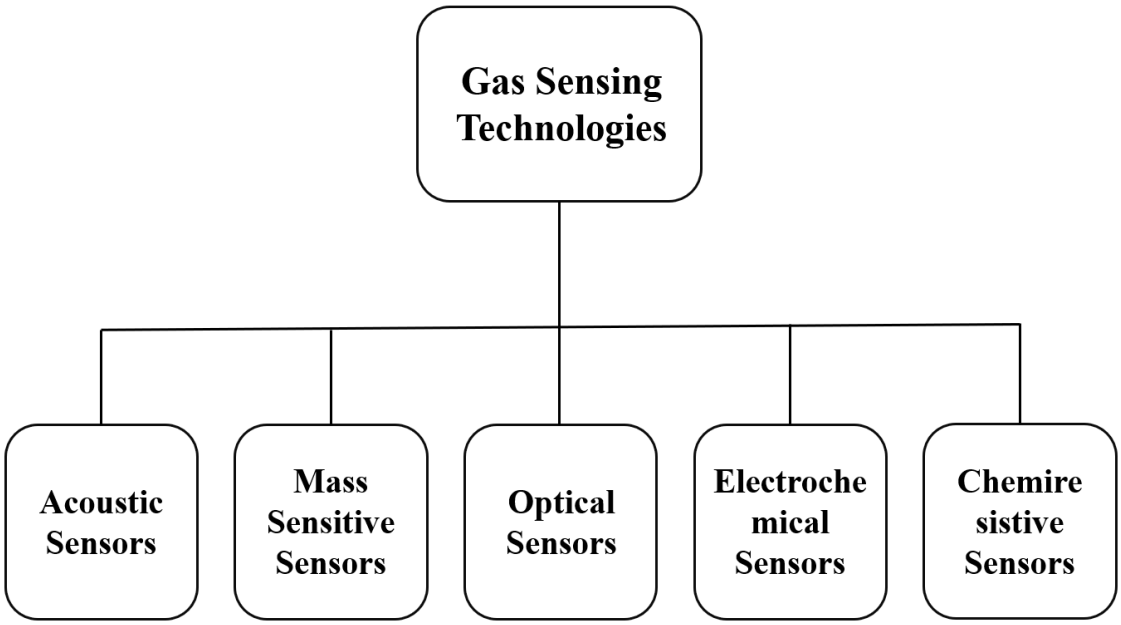

Fig. 2.1. Sensors based on different Sensing Technologies

2.2.1 Acoustic Sensors

Many different types of gas sensors are currently in use, but acoustic sensors are favored because of several advantages such as low detection limit, fast response time, ease of fabrication and low cost. Acoustic Sensors' working principle for detection

is based on the change in wave amplitude and velocity when interrupted by gaseous molecules as shown in Figure 2.2 [44].

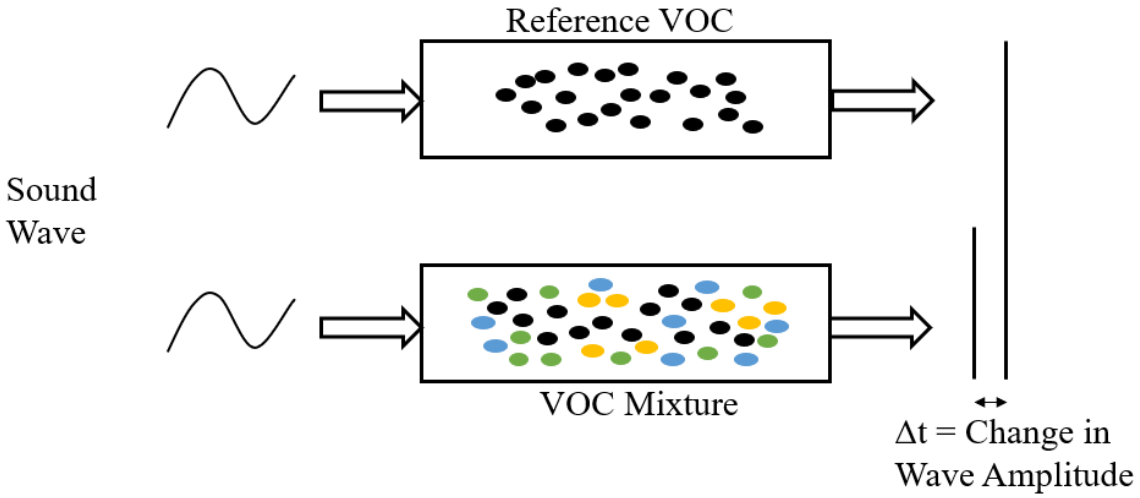

Fig. 2.2. Principle of Ultrasonic Detection

Viespe et al. in 2010 and 2018, presented a surface acoustic wave(SAW) sensor based on nanoparticles and CNT embedded in PEI polymer to increase the sensitivity of the sensors achieving faster response time and lower detection limit for VOCs such as methanol, ethanol and toluene [45,46]. Another article shows a SAW sensor coated with polyisobutylene thin film in combination with an artificial neural network (ANN) algorithm for detection of eleven biomarkers associated with lung cancer [47]. Penza et al. show a SAW sensor spray painted with CNT and further coated with SiO_2 to detect ethanol, toluene and ethyl acetate [48].

Although SAW sensors have various advantages, it has a few drawbacks such as sensitive to humidity, large measurement noise and a complicated signal processing system.

2.2.2 Mass Sensitive Sensors

Mass-sensitive sensors work on the principle of change in mass when a targeting molecule attaches to the sensor surface due to interaction. This mass change of the sensor can be noticed by a shift in resonance frequency either by a Quartz Crystal Microbalance (QCM) device, SAW device or by determining the bend of microcantilever beam.

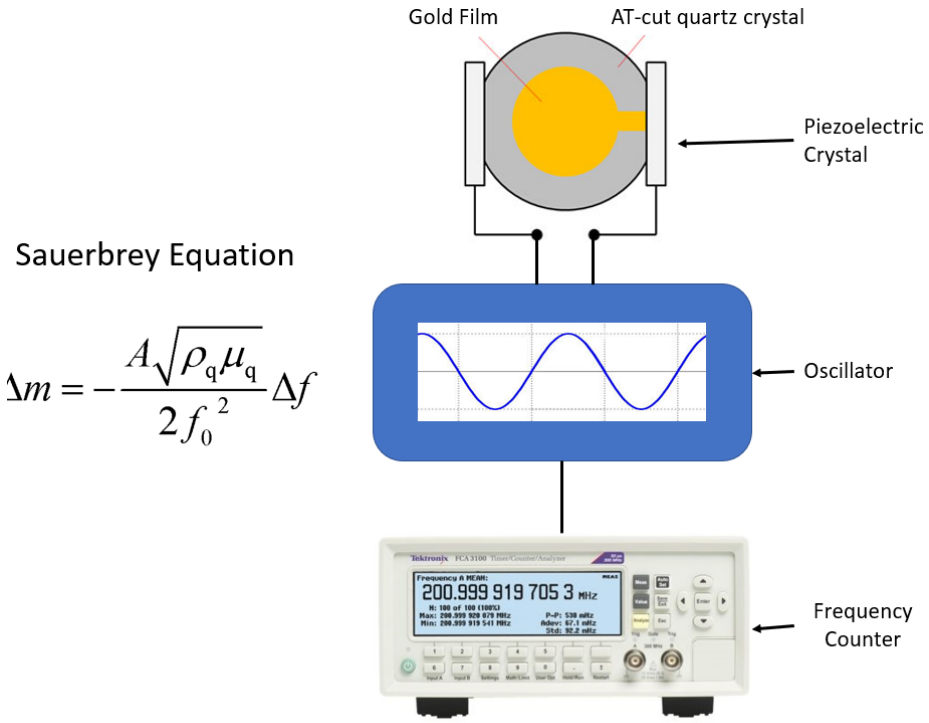

Fig. 2.3. Quartz Crystal Microbalance (QCM) Experimental Setup

A SAW sensor modified with sensitive polymer has detected VOCs like methanol, acetone, cyclohexane, benzene [49] and other articles have shown the use of a polymer coated micro cantilever to determine a mass change for n-octane, toluene, ethyl acetate and ethanol [50]. For a mass sensitive sensor, there are some major drawbacks such as high signal to noise ratio and requiring complex signal processing systems which prevents the wide usage of these sensors.

2.2.3 Optical Sensors

VOC detection using optical sensors can give real-time results due to relatively faster response time, high selectivity and sensitivity. Colorimetric and infrared sensors (IR) are also a type of optical sensor. They work on the principles of absorption spectra i.e. that every gas or vapor analyte can absorb light at a specific wavelength which can be determined using an optical detector as depicted in Figure 2.4.

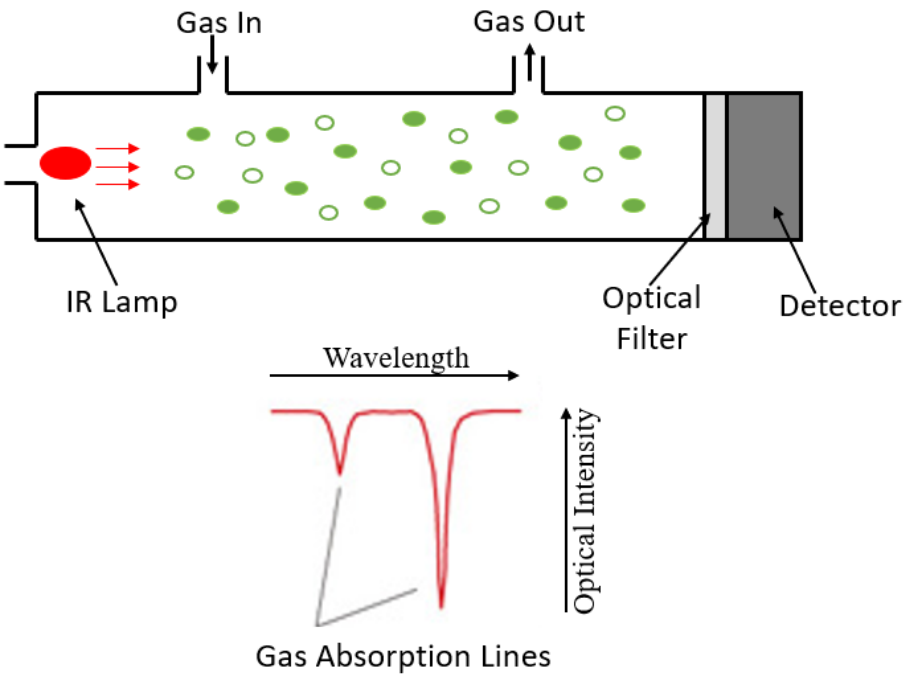

Fig. 2.4. Working Principle of Optical Gas Sensor

Lee et al. present an optical fiber sensor coupled with sensing layer of polyvinyl pyrrolidone (PVP) to detect acetic acid, benzene, dimethylamine, ethanol, and toluene by noticing the change in refractive index and reported the detection limit of 1 ppb to 10 ppb [51]. In 2006, a study by Janzen et al. reported a colorimetric sensor array using chemically responsive dyes to discriminate between various VOC groups such as alcohols, aldehydes, ketones, thiols, etc [52]. An optical sensor presents major advantages over other types of sensors, but they are very costly to fabricate due to

their miniaturization. Also, they have very complex electronics, low power output and short life time.

2.2.4 Electrochemical Sensors

Electrochemical sensors work on the principle of change in current due to oxidation/reduction reaction that happens at the electrode on the interaction of an analyte gas with the electrolyte. These sensors are divided into 3 groups by Janata et al. and Wilson et al. based on the type of change: 1) Change in voltage (potentiometer) 2) Change in current (amperometric) and 3) Change in conductivity (conductimetric) and polyurethane based implantable sensor was presented for the detection of glucose [53, 54]. Another article in 2010, reported an electrochemical sensor based on a polydimethylsiloxane (PDMS) membrane to detect benzaldehyde in the air [55]. Electrochemical sensors can give high sensitivity in real time and faster response, but their selectivity is low and unable to distinguish the presence of an unknown gas.

2.2.5 Chemiresistive Sensors

Chemiresistive Sensors work on the direct surface interaction between the sensing material and the gas molecules by a change in molecular structure due to different bonding methods. This change in molecular structure is measured in the change of resistance between the electrodes.

Researchers have reported different materials such as f-GNPs, conducting polymer, CPCs, CNTs, graphene and graphene oxide used as sensing materials to determine which of these can be used for the sensing vapors of different biomarkers [54–58].

Metal Oxide Semiconductor (MOS) Sensors

MOS sensors are one of the most common sensors with low cost and high sensitivity, making them useful for various applications such as indoor air monitoring,

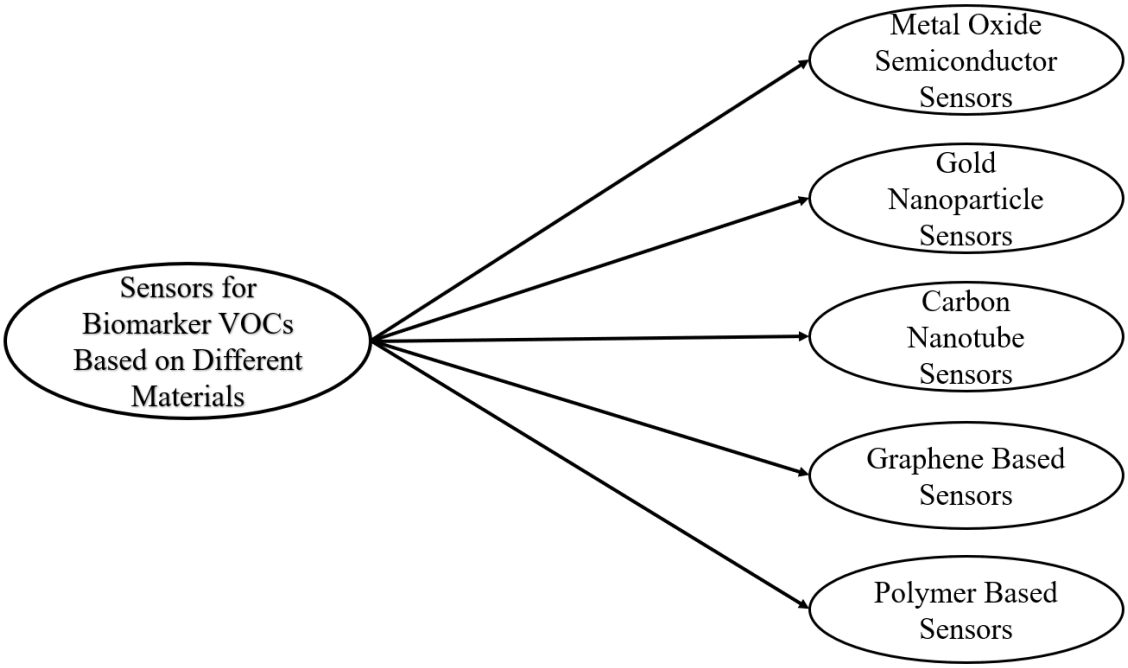

Fig. 2.5. Classification of Gas Sensors Based on Different Materials

fire detection, ventilation controls, etc. MOS sensors can be divided into two groups based on the oxidation states achieved: 1) Non-transition. 2) Transition.

The sensing material which is either a type-n or type-p undergoes reduction or oxidation when the gas particles diffuse into the sensing material surface. The sensing mechanism is explained through chemical absorption of oxygen into the metal oxide layer, creating an energy barrier preventing electron flow in the material resulting in an increase in resistance of the sensor [59].

Leidinger et al. and Schuler et al. both have reported a MOS sensor for detecting naphthalene, benzene, ethanol and benzaldehyde in the parts per billion (ppb) range even with or without the background environment [60,61]. A MOS sensor array with different metal oxides able to differentiate between different VOCs in a homogeneous mixture at different temperatures has been presented [62]. Some et al. presented a MOS sensor to increase the sensitivity of the sensor by temperature cycling and discuss various approaches to increase the selectivity of the sensor for gas discrimination

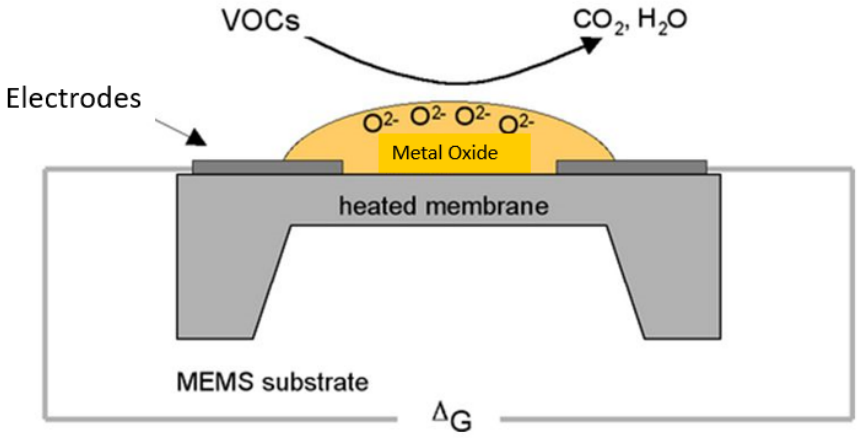

Fig. 2.6. Metal Oxide Semiconductor Sensor

in a mixture [63]. Another article presented an approach to increase the sensitivity of a MOS sensor by growing an ultra-thin grain with different material with high surface area and reported a change in resistance of 30% at 1 ppm hexane [64]. A long time has been spent by researchers to overcome the drawbacks such as slow response, high-temperature environment and long response time that prevents MOS sensors from being used for VOC detection related to different diseases.

Gold Nanoparticle Sensors

Since 1998, when Wohltjen and Snow first presented a GNP based chemiresistive sensor, nanoparticles and nanoparticles based material have attracted great interest due to their unique characteristics such as high sensitivity, fast and reversible response, low detection limit and low power consumption [65, 66]. Various researchers have reported that the properties of nanoparticles can be controlled by shape [67], size of the particle core [68], [69], length of the hydrocarbon chain connected to core [70]. Due to these controllable variations in the nanoparticles, it could be used for various applications such as biomedical diagnostics, optical sensing, and environmental monitoring.

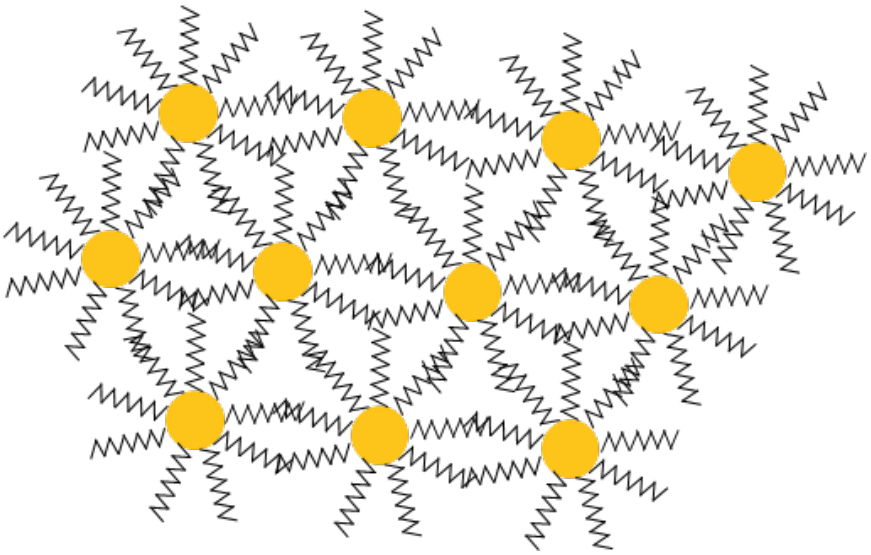

Fig. 2.7. Monolayer Protected GNP Schematic

For applications in chemical and vapor sensing of VOCs, the most commonly used nanoparticles are gold nanoparticles (Au_{NP}). The sensing mechanism that allows NP to sense vapor analyte is the change in electron tunneling. When a gaseous analyte comes in contact with the nanoparticles (NP) film, the average separation gap between the NP increases due to swelling caused by adsorption of molecules into NP matrix [71]. Joseph et al. studied the effects of alkylene chain length of alkanedithiol GNPs to study the response of toluene, 1-propanol, tetrachloroethylene and water and reported an exponential increase in the response to vapors with an increase in the length of alkanedithiol molecules [70]. An insight of absorption and swelling is given for GNP films using grazing-incidence small-angle X-ray scattering (GISAXS) were given for toluene, 1-propanol, 4-methyl 2-pentanone for dodecanethiol GNP [72]. Grate et al. reported the use of 7 different f-GNPs to determine the partition coefficient to estimate the mass absorbed per volume [66]. A novel urea thiol coated f-GNPs were proposed to increase the selectivity and sensitivity of a gas sensor for the detection of toxic VOCs in the air [73]. A sensor array was developed using 9 different functionalized GNPs to determine the 4 of the lung cancer biomarkers and train and optimize the sensor array for VOCs [74]. A study was done to investigate the mechanism of

charge transportation due to absorption of vapors to n-octanethiol protected GNPs and sensor performance for 25 vapors were presented and discussed [75]. Another study shows the response of the sensor array of 14 cross selective nanomaterials with biomarkers for different types of cancer and a comparison is made with GCMS breath analysis [16].

Table 2.3. List of Gold Nanoparticles previously used for Sensing Application Based on Different Functional Group.

Functional group	**f-GNPs**	**VOCs**
Hydrocarbon	Dodecanethiol GNPs Octanethiol GNPs Hexanethiol GNPs Decanethiol GNPs	Methanol, ethanol, butanol, propanol, tetrachloroethylene, hexane, toluene, 2-butanone, trimethylbenzene, octane, ethyl acetate, acetone, cyclohexane, acetonitrile
Alcohols	3-mercapto benzyl alcohol GNPs 4-mercapto phenol GNPs 11-mercapto-1-undecanol GNPs	Acetone, dichloromethane, methanol, ethanol, acetaldehyde, formaldehyde
Alkyl Group	4-methyl benzenethiol GNPs Butyl benzenethiol GNPs 2-ethyl hexanethiol GNPs 3-methyl-1-butanethiol GNPs 2-phenyl ethanethiol GNPs	Trimethyl benzene, dichloromethane, methanol, ethanol, toluene, acetone, ethyl acetate, styrene, nonanal, decanal, hexanol
Carboxylic Group	11-mercaptoundecanoic GNPs 3-mercapto propanoic GNPs	acetone, ethanol, benzene, ethylbenzene, toluene hexane, cyclohexane, acetonitrile

Carbon Nanotube Sensors

CNTs over the years have attracted many researchers to study its properties and characteristics due to its unique electronic properties for application in various fields. CNTs can be divided into two types: Single-Walled Carbon Nanotubes (SWCNTs) and Multi-Walled Carbon Nanotubes (MWCNTs). The response for CNTs is different for different vapor analytes based on the physisorption and chemisorption between the CNTs matrix and the analyte molecules [76]. Peng et al. reported an array of 10 different non-polymeric materials and CNTs to detect breath samples from lung cancer patients for styrene, hexane, decane, octane, and dimethyl benzene. This study also differentiated breath samples from healthy patients and comparing the results of breath samples of lung cancer patients by GC-MS [77]. A quantum resistive sensor was presented based on CNTs dispersed in a solution of different polymers to alter the selectivity of the sensor for the set of polar and non-polar VOCs related to lung cancer [78]. Another study shows the fabrication of non-functionalized and functionalized CNTs at different concentrations to study the response of non-polar alkane, polar analytes confirming lung cancer and water [79]. Although there are many advantages of using CNTs as a gas sensor, synthesis of defect-free CNTs is very difficult and costly, making it a challenging process to control the growth or dispersion of CNTs. Variation in the fabrication process will vary the surface and electronic properties of CNTs which will ultimately alter the interaction of CNTs and gaseous analytes [80]. The sensors have a slow response and a very slow desorption rate.

Graphene and Graphene Oxide (GO) Based Sensors

Graphene is one of the nanomaterials with mechanical robustness, excellent optical properties and high stability in harsh environments. Singh et al. presented a flexible wearable sensor based on reduced GO for detection of hazardous gases in the air such as NO_2, NH_3, hydrogen (H_2), hydrogen sulfide (H_2S), carbon dioxide (CO_2),

sulfur dioxide (SO_2), and humidity. Selective sensing of ethanol, methanol, acetone, hydrazine, THF, dimethylamine, nitromethane, and dichloromethane at the 500 ppb concentration level was reported hydrophilic GO and hydrophobic reduced GO [63]. A GO-based gas sensor was also reported for detection of low concentrations of nitrogen dioxide (NO_2) and ammonia (NH_3) in the air [81]. The major drawback with most of the graphene-based sensors is slow response and lower selectivity at lower concentration levels.

Polymer-Based Sensors

Polymer-based sensors are used because there are various VOCs which cannot be detected by MOS sensors below a certain threshold concentration and because polymer sensors can be made selective using different chemical composition polymers. The sensing mechanism for these sensors is based on the physisorption by hydrogen bonds, dipole/dipole interaction and dipole/induced dipole interactions when molecules of the vapor analyte interact with the sensing polymer [76, 82]. There are various advantages for using polymer-based sensors such as low cost of fabrication, simple and portable structure, low power consumption and varying sensitivity and selectivity on the polymer layer. Polymer-based sensors can be divided into two groups:
1) Intrinsically Conducting Polymers (ICPs)
2) Conducting Polymer Composites (CPCs)

ICPs - Conducting polymer has been readily investigated as a gas sensing layer because exposure of inorganic or organic gas molecules changes the electrical conductivity of the polymer layer. Jiang et al. proposed different materials of self-assembled monolayers (SAM) functionalized with Poly(3,4-ethylene-dioxythiophene)-poly(styrene sulfonate) (PEDOT:PSS) nanowires to detect low concentrations of VOC groups such as ketones, alcohols, alkanes, aromatics and amines [83]. An amine and nitro functionalized nano porous polymer was presented to detect ketone and alco-

hols between the range of 10 ppm to 3000 ppm using a difference in pore size of the fabricated polymer [84]. Lakard et al. reviewed doped polypyrrole (PPY) And polyaniline (PANI) polymers for sensing of VOCs like ethanol and acetone and explained the sensing mechanism of the sensors [85]. There is a limited number of conducting polymers such as PPY, PANI, Polythiophene (Pty) and their derivatives and their conductivity is not high enough to make a highly sensitive sensor which is one of the drawbacks for using conducting polymers. Other drawbacks include a shorter lifetime and temperature instability.

CPCs - Other ways to use polymers that are non-conducting are by using conducting material and synthesizing a composite through a solvent. This can give higher conductivity based on a conducting material and selectivity of a polymer to fabricate highly selective and sensitive sensors. In a recent study, Li et al. has presented a CPC using poly(lactic acid) (PLA) embedded with ramie fiber and CB and CNTs as conducting material and reported lower percolation threshold and stability [86]. Another article in 2018 by Li et al. reported a polycarbonate (PC) polymer dispersed in CB and CNTs for the detection of toluene, cyclohexane, and acetone [87]. MWCNT and poly(vinylidene fluoride) (PVDF) CPCs was 3D printed onto a platform for chemical sensing [88].

Further CPCs were investigated for the specific intention of detecting aldehydes. Mallya et al. presented an O-phenyl diamine (OPD) polymer to form a composite using CB in dimethyl propylene urea (DMPU) solvent for the detection of formaldehyde, acetaldehyde, benzaldehyde, acetone, ethanol, and methanol [89]. Mallya et al. presented another article reporting primary amine functionalized polyaniline for detection of aldehydes [90]. Various articles over the years have presented various polymer composites such as allyl amine/CB composite, PANI/poly(ethyleneimine), primary functionalized PANI and PPY coated fibers for the detection various aldehydes such as formaldehyde, acetaldehyde, and benzaldehyde [91–93].

After a literature review using research articles and online sources, polyetherimide (PEI) came to be one of the polymers that have not been researched extensively and shows properties of a good polymer that can be used for detection of aldehydes according to the polymer solvent chart. Alberici et al. studied the sensitivity of a PEI/sulfone polymer layer with different thicknesses for detection of 9 different VOCs and reported to have decreased the response time for five of the VOCs [94]. A Zeolite modified PEI sensor was fabricated for gas separation and an increase in selectivity for the mixture of gases was reported from 10% to 25% [95]. Asymmetric hollow PEI membrane for the removal of hydrogen sulfide from CO_2 was reported with near 100% efficiency with only 5% permeation of CO_2 [96]. A hollow fiber membrane of PEI was also discussed to remove impurities such as peptone, urea, sodium chloride, calcium chloride and magnesium sulfate in water [97]. Another article presents a carbon molecular sieve-based PEI shows an increase in selectivity for gas separation. PEI dense films have extensively been used for studies on gas permeation with high selectivity for all important gas pairs [98–100] and hollow fiber membranes of PEI have been used for removal of VOCs from the air [101]. Deng et. al have reported the fabrication of hollow fibers of PEI for VOC detection such as pentane, benzene, acetone, ethanol, methanol, etc. in the air [102].

2.3 Film Fabrication Technologies

In this section, an overview of different film fabrication techniques is given to explore a way to synthesize a PEI polymer as a sensing layer. A material deposition is mostly done by chemical deposition which can be defined as a method in which the liquid material is turned to a solid layer undergoing a chemical change at a solid surface. There are various methods of chemical deposition:

Dip Coating

Dip coating is one of the oldest methods to fabricate a film on to a substrate using the simple process of immersion of the substrate into the chemical solution. The variation of structures of the fabricated film differs because the condensed phase is different for every material [103]. Dip coating is divided into three technical steps which are as follows:

1) Immersion and dwell time - The substrate is dipped into the solution of the chemical precursor at a slow and jerk-free speed followed with a minimum threshold time to allow the substrate for complete wetting.
2) Deposition and drainage - Film deposition is entertained when the substrate is pulled up at a constant speed depositing a precursor thin layer and draining the excess liquid off from the substrate surface.
3) Evaporation: The solvent will evaporate from the deposited film after it is taken out of the solution. Heat treatment can be given for further drying the film and altering the chemical structure. This method normally gives a film thickness in the range of a few hundred nanometers depending on various factors such as speed for immersion and deposition, dwell time, evaporation environment, solution concentration and viscosity.

Blade Coating

Blade coating is a simple wet coating process where a film is fabricated by the action of moving a blade over the substrate. A single drop of the chemical precursor is dropped on the substrate and a clean and thin edge knife is rolled over the solution drop giving a film all over the substrate. The coating thickness is affected based on various factors: knife-substrate distance, rolling speed, viscosity, density and surface tension of the solution.

Langmuir-Blodgett (LB)

In this method, the surface of the substrate is dipped into the clean liquid (water) having an insoluble monolayer on the surface of the liquid. Molecules of insoluble material coating on the surface of the liquid have a hydrophobic tail and hydrophilic head. A monolayer is adsorbed on to the substrate because the hydrophobic tail of the molecules is attracted more to the solid substrate than the attraction of hydrophilic head to a high surface tension liquid. This method gives a film thickness in the range of a few nanometers. One major drawback of this method is that the polymer must be insoluble in the liquid.

Chemical Vapor Deposition

In a typical Chemical Vapor Deposition (CVD) process, the substrate is heated in a vacuum environment and the wafer is exposed to the precursor gas, with any catalyst if required, resulting in the deposition of the film on the surface. A conventional setup for a CVD system heats the substrate to be coated in an oven at 720^0C with gas flowing in the chamber. The by-products generated are removed with the gas flow in the chamber providing the thin film in the range of few nanometers. The major drawback with this method is properties of the precursors which needs to be volatile at room temperatures [104].

Spin Coating

A thin uniform film can be fabricated using one of the simplest methods, the spin coating technique. In this method, an excess of coating material is deposited all over the substrate through a controlled flow of a syringe or a dispensing nozzle. The substrate is then rotated at a slower speed (e.g. 500 rpm), called the spread speed, for a specific time to allow the material to spread uniformly over the substrate surface.

The speed is then ramped up to a high speed (e.g. 5000 rpm) to help achieve the thinning of the polymer and evaporation of the solvent using air flow.

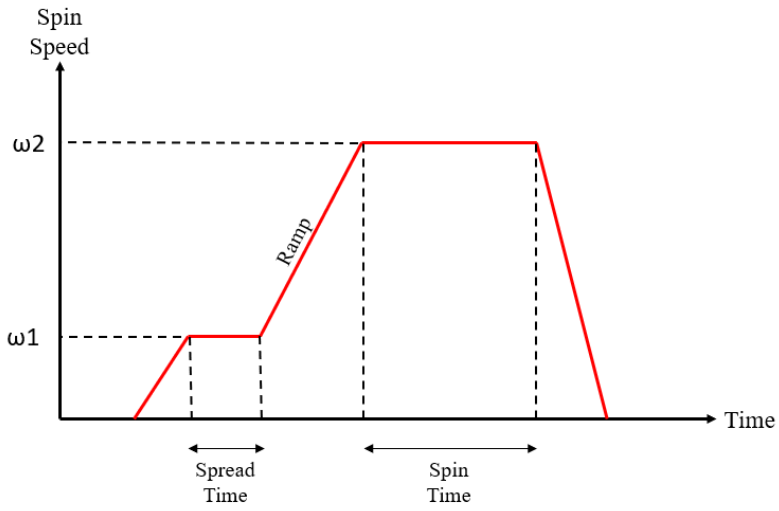

Fig. 2.8. The Spin Coating Theory

The thickness of the film fabricated from the spin coating technique varies due to various factors such as spin speed, spin time and viscosity and density of the chemical solution.

2.4 Photolithography

Photo or Optical lithography is a means to imprint a micro pattern on a substrate using light to pass through a mask pattern to a light-sensitive material called a photoresist. A sequence of procedural steps is followed for achieving the final pattern on the substrate and are as follows: substrate preparation, photoresist spin coat, prebake, alignment and exposure, post-exposure bake, development, inspection, etching, photoresist strip, and final inspection. A brief description and the importance of each step is described below.

1. Substrate Preparation: Surface preparation is done to achieve a higher adhesion of the photoresist material with the substrate. It is important because impurities

or contamination on the surface could lead to poor adhesion and defects in the final geometric pattern.

2. Photoresist Coating: A photoresist is a light-sensitive material which helps to get the pattern either by dissolving the covered dark portion (Negative photoresist) or by dissolving the portion exposed to light (Positive photoresist).A positive photoresist was used for spin coating.

3. Pre-Exposure bake or Soft bake: Some percentage of weight solvents are present in the spin-coated photoresist film. This pre-exposure bake is done to dry the photoresist film to remove any excess amount of solvent present and gives a stable film.

4. Alignment and Exposure: Light exposure through the mask will only expose the desired part of the positive photoresist and the exposed area will be soluble in the developer. There are three types of exposure techniques: i) Contact ii) Proximity and iii) Projection. The major factor that affects the IDE pattern is exposure time.

5. Development: This step is done to remove the area of the photoresist which is undesired. The developer is an aqueous base which will dissolve the photoresist which is exposed to a light source by breaking the bonds.

6. Hard Bake: Hard Bake is done to improve adhesion of the developed resist and stabilize it for the subsequent process by hardening the resist image to withstand etching process.

7. Inspection: Inspection is important to perform to check for defects due to impurities or particles and check the critical dimension of the pattern that will confirm the accuracy of the lithography process.

8. Etching: Etching is normally done using wet chemical acids or sometimes by dry plasma etching. The photoresist protects the layer below it from getting etched away giving the required pattern.

9. Photoresist Strip: Post etching for gold and chromium, the photoresist layer on top of the pattern must be removed.

10. Final Inspection: Final Inspection is done to ensure the pattern inspection, defects and impurity particles on the substrate and to optimize the various steps of the lithography process.

3. FABRICATION OF SENSORS

Material synthesis, fabrication, and experimental testing methods are described herein. Section 3.1 describes the material and fabrication methods used for the development of IDEs. Section 3.2 describes the materials and methods used for the development of PEI thin film, PEI/CB sensors, f-GNPs sensors and f-GNP/PEI sensors. Experimental testing set up for testing the sensors are described in section 3.3. The sensing mechanism of developed sensors are presented in Section 3.4

3.1 Fabrication of Interdigitated Electrodes (IDEs)

Fabrication of the IDEs was successfully accomplished by following conventional photolithography process using OAI HyberAlign Series 200 Mask Aligner and Exposure system. The system used for the fabrication of electrodes is presented in Figure 3.1. Mask Design was done using Coventor Ware 2012 and was printed on a soft transparent substrate by CAD/Art Service Inc. Figure 3.2 shows the design of the actual mask used and zoomed image of the electrode is also presented with it showing a gap of 10μm between the electrodes.

3.1.1 Materials

Silicon (Si) substrate with Silicon Dioxide (SiO2) and Gold (Au) coating (90 nm) was purchased from Hionix Inc. A positive photoresist S1813 was procured from MicroChem. An adhesion promoter MCC Primer 80/20 was obtained from MicroChem. The Microposit MF-321 developer was used for the developing step and was obtained from Rohm and Haas Electronic Materials LLC. Gold and Chromium etchant used for etching was purchased from Sigma Aldrich.

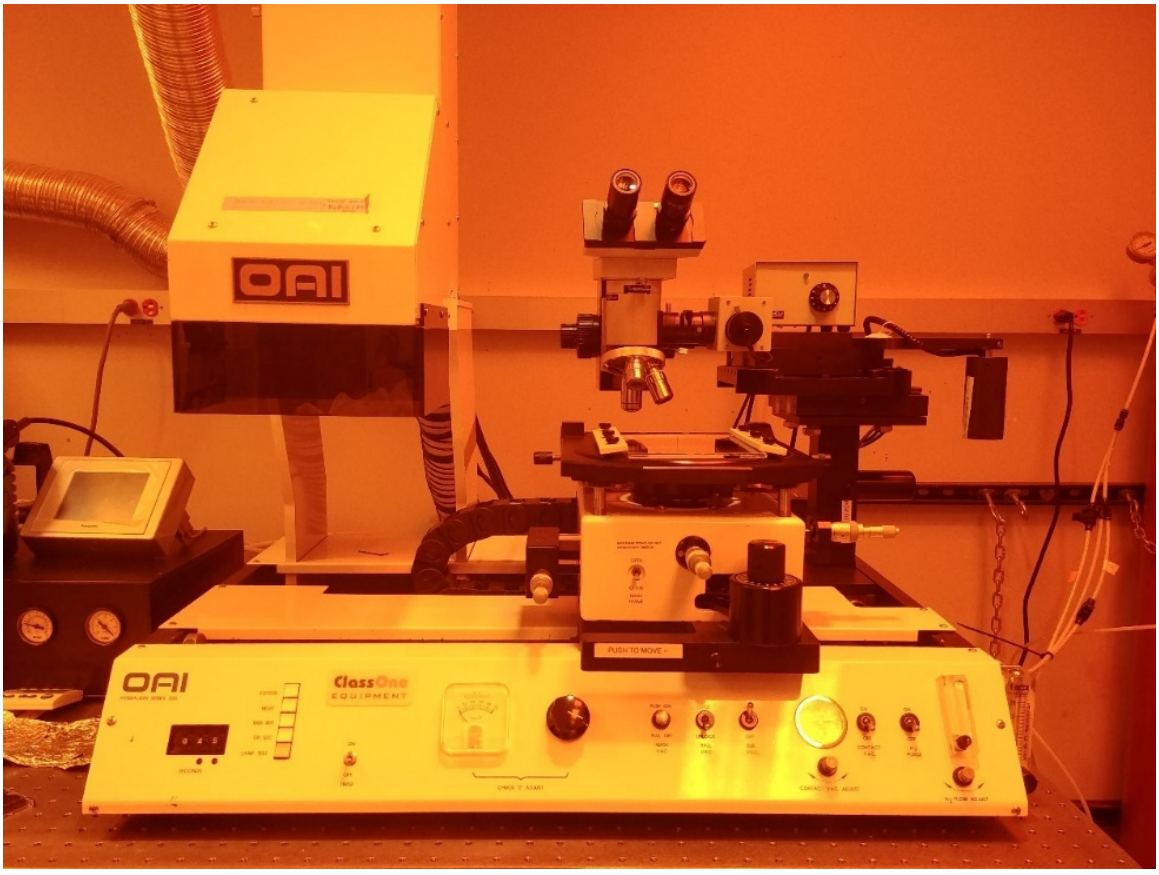

Fig. 3.1. OAI HyberAlign Series 200 Mask Aligner and Exposure System

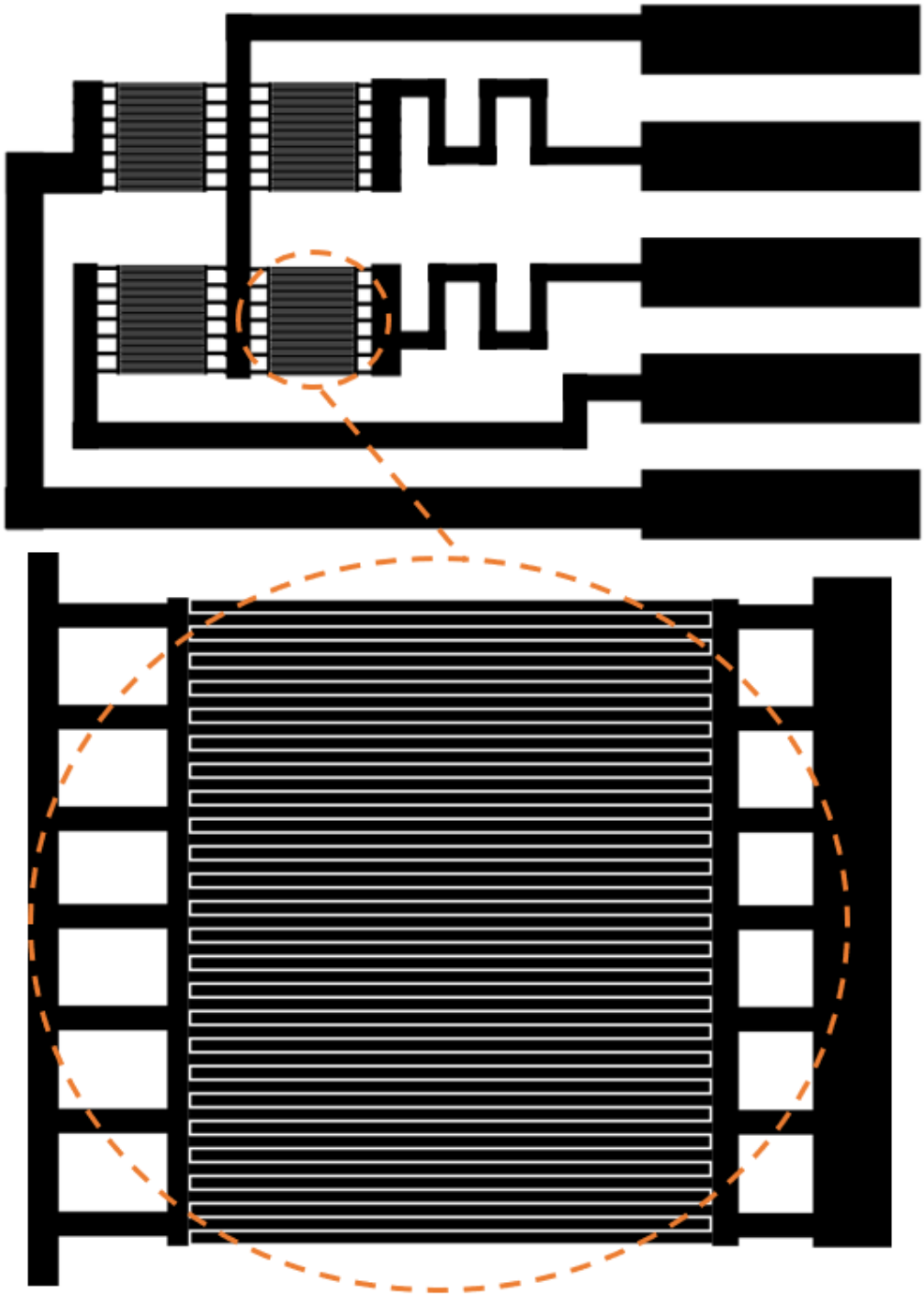

Fig. 3.2. Mask Image of Interdigitated Electrode

3.1.2 Photolithography Process

In surface preparation, the surface of the substrate is thoroughly cleaned by acetone, ethanol, and isopropanol (IPA) and washed with water for 1min to remove any oils and impurities on the surface. After cleaning, the surface is heated at 90^0C for 5 min to evaporate any chemical solvent left behind after cleaning. The cleaned surface is then spin-coated with an adhesion promoter- MCC Primer 80/20 at 400 rpm for 6 sec as spread time and at 3000 rpm for 40 sec as spin time which makes the surface hydrophobic and excellent for adhesion.

Photoresist S1813 was poured on to the substrate and was spin coated at 400 rpm for 6 sec and at 3000 rpm for 40 sec. There are various factors that affect the thickness of the photoresist film such as viscosity of photoresist, spin speed and spin time for the spin. The spin speed and time used for the photoresist, give a uniform thickness of 1.5 μm.

The soft bake is done at 90^0C on a hot plate for 15 sec. Higher temperatures could damage the photoresist film by decomposition of the resist mixture or cross-link at higher temperatures.

The printed soft mask is placed over the substrate with printed side touching the surface to avoid any light diffraction from the soft transparent sheet. For 20μm gap electrodes, exposure time of 3.9 sec was used and for 10μm gap electrodes, an exposure time of 4.1 sec was used. These times have been optimized after various experiments and careful pattern inspection.

In the developing stage, the exposed wafer is put in Microposit MF -321 developer in a beaker and shaken thoroughly using agitation technique for 1 minute. After developing, the wafer is washed with water for 30 sec.

Hard Bake is done on a hot plate at 90^0C for 15 min.

An optical microscope is used for the inspection to check for all the dimensions of the pattern and to look for any defects.

For the etching procedure, the substrate is first etched with gold etchant by putting the substrate into the etchant in a beaker and constantly shaking it using agitation technique for 20 - 25 sec. The substrate was washed for 30 sec with water to remove any residue of gold etchant. This will give a pattern with a photoresist layer, gold layer on top of the chromium layer through the surface. Then the substrate was etched with chromium etchant using the same protocol but for 20 sec for both electrodes of 20μm gap and 10μm gap. After etching, the substrate is washed with water for 1 min to remove any residue from the etching process.

The substrate surface was cleaned with acetone to remove the photoresist layer and then washed with water for 30 sec to remove acetone residue.

The final inspection was done to ensure the pattern inspection, defects and impurity particles on the substrate and to optimize the various steps of the lithography process.

Figure 3.3 shows an actual substrate after completing all the photolithography steps and a microscopic image of the fabricated electrode is also presented showing a gap of 10μm between the electrodes.

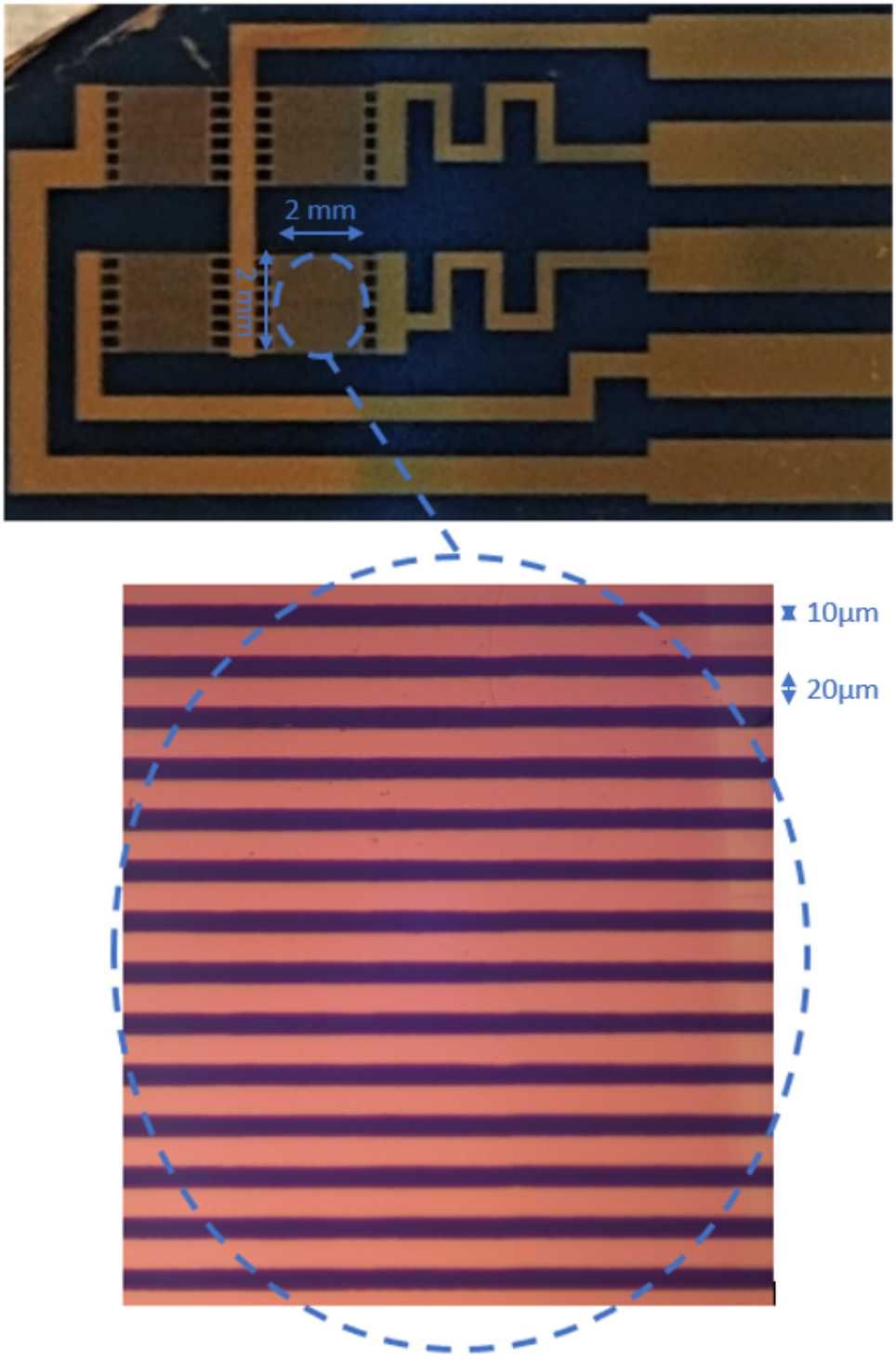

Fig. 3.3. Fabricated Interdigitated Electrode after Photolithography Process

3.2 Fabrication of Sensing Material

3.2.1 Materials

PEI and 1-Methyl-2-pyrrolidinone (NMP) were obtained from Sigma Aldrich. 1-Mercapto-(triethylene glycol) methyl ether functionalized GNPs was also purchased from Sigma Aldrich. Carbon Black (CB) was procured from Cabot Corporation.

3.2.2 Fabrication of PEI Film

PEI comes in pellet form and is heated in a vacuum oven at 200^0C for 4 hours to remove any moisture content. Vacuum dried PEI is dissolved in NMP to form a yellowish slurry composite of PEI/NMP by constantly heating the solution at 80^0C and constant rotation of 100 rpm using magnetic stirrers for 48 hours.

PEI/NMP composite was spin-coated at different speed of 3000 rpm, 5000 rpm and 7000 rpm and was quickly heated on a hot plate at 80^0C for the time of 0 sec, 30 sec, 120 sec, 300 sec, and 600 sec respectively at each spin-coating speed. This process is done to determine the effect of heat treatment on the polymer thickness film and to determine the optimized steps to follow for the fabrication of PEI as a sensing layer. The varying thickness of PEI based on different spin coating speeds and different heat treatment times are presented below in Table 3.1 and Figure 3.4. The values presented show that after 10 minutes, the reduction in thickness of PEI film is negligible and also from contact angle measurement of PEI film from Section 4.1.4 shows that heat treatment duration of 10 min or more gives the same contact angle values between the PEI film and a water droplet. Also, the thickness can be approximated for other speeds that are not included in the study.

Table 3.1. Thickness of PEI film at Different Spin Coating Speed at 80^0C with varying Heat Treatment Time.

Heat Treatment Time	**3000 rpm**	**5000 rpm**	**7000 rpm**
0 sec	30μm	19μm	5μm
30 sec	24μm	13μm	0.7μm
120 sec	14μm	6μm	0.67μm
300 sec	11μm	1μm	0.46μm
600 sec	9μm	0.9μm	0.45μm

3.2.3 Fabrication of PEI/CB Film

For PEI/CB film fabrication, the composite of PEI/CB with 100:5 w/w ratio was dissolved in NMP giving a slurry black paste. The solution was constantly rotated with the help of magnetic stirrers at 80^0C for 48 hours.

The spin coating method was used to develop a film of PEI/CB slurry over the fabricated IDEs. Speeds of 3000 rpm, 5000 rpm and 7000 rpm were used to synthesize a film over the electrodes. Quickly after that, the films were dried at 200^0C for 2 hours. This gave a series of the thickness of the PEI/CB film to determine the optimal thickness for the fabrication of PEI/CB sensor. The film was then allowed to be dried in a vacuum environment at 70^0C for another 48 hours. The profilometer measurements of PEI/CB film based on different spin coating speeds are presented in Section 4.1.5. This study was done to determine the most suitable film thickness for sensing nonanal.

Table 3.2. Thickness of PEI/CB film at Different Spin Coating Speed.

Speed	**Thickness**
1000 rpm	39μm
2000 rpm	21μm
3000 rpm	16μm
4000 rpm	13μm
5000 rpm	11μm
6000 rpm	8μm
7000 rpm	5μm

Fabrication of PEI/CB sensors

For synthesizing a PEI/CB sensor, PEI/CB composite was spin coated on the gold electrodes with a gap of 25μm, at a spread speed of 600 rpm for 6 sec and then the speed was ramped up to 3500 rpm and then rapidly heated on a hot plate at 200^0C for 2 hours and dried in vacuum at 70^0C for next 48 hours. The thickness of the film fabricated was 15μm. Spin coating speed of 3500 rpm was chosen because at lower speeds such as 1000 rpm and 2000 rpm the film becomes too thick (39μm and 30μm respectively), not giving the porous PEI/CB structure as presented in Section 4.1.3 due to excess material on the electrode thus reducing the surface area for interaction between the sensing film and the VOC analytes. At higher speeds such as 5000 rpm and 6000 rpm, the film gives a thickness of 11μm and 8μm respectively making the sensing layer thinner and also reducing the surface area for interaction. At 3500 rpm, the most porous structure of PEI/CB film giving the highest surface area among other film thickness to interact with VOCs was obtained.

3.2.4 Fabrication of f-GNP Sensor

1-Mercapto-(triethylene glycol) methyl ether functionalized GNP sensor was fabricated by the process of drop-casting on IDEs. The fabricated sensor was then dried in a vacuum environment for 24 hours. Drop casting methods give a non-uniformly distributed network of GNPs which shows much better sensitivity than layer-by-layer methods according to the literature review. The similarity of fabricated sensors depends on the accuracy of drop-casting equal amounts of GNP material over the electrodes. The depiction of the method is shown in Figure 3.4.

Fig. 3.4. Drop-Casting Method

3.2.5 Fabrication of f-GNP/PEI Sensor

For developing an f-GNP/PEI sensor, the speed of 600 rpm was used for a spread time of 6 sec and then ramped up to 6000 rpm for the next 1 min to spin coat PEI/NMP solution on top of f-GNPs over the IDEs. The substrate was then heated on a hot plate at 80^0C for 10 min to evaporate the excess solvent present in the spin-coated film. This gives a clear and transparent PEI film over the GNP. The fabricated sensor was then put in a vacuum without any application of heat for 48

hours. Spin coating speed of 6000 rpm was chosen to get the thinnest uniform film possible.

3.3 Experimental Setup

Air (78% nitrogen, 21% oxygen, 0.93% argon, 0.04% carbon dioxide and other gases, 0% relative humidity) was used as a carrier gas in the experimental setup because of the application to detect aldehydes in air. Figure 3.5 shows the experimental setup used for testing the sensors. Dry purified air purchased from Praxair flowed in a controlled flow by controlling the mass using mass flow controllers (MFCs) connected to the air tank. The controlled flow of air was bubbled through a liquid VOC flask to get the vapors of the targeting VOC. This VOC is then mixed in the mixing chamber with purified air coming from the air flask. A testing chamber with a volume of 250 cubic centimeters is used to put the fabricated sensor in a sealed tight environment where the sensor response is recorded. 450 standard cubic centimeters per minute (SCCM) was used as the air flow rate to avoid any variation that could arise from changes in air pressure. Different flow rates were used for VOCs to record the response of the sensor at different concentrations of targeting VOCs for multiple cycles. The standard deviation error bars are shown to present any deviation from the results. In order to show the selectivity of the proposed sensors, they have been also tested with dodecane (hydrocarbon), 1-octanol (alcohol), acetone (ketone), and ethanol (alcohol). Sensor$'s$ sensitivity to humidity was investigated by exposing them to water vapor at R.H of 50%, 70%, and 85%.

The experiments were conducted at 21^0C. A commercial humidity sensor (CO_2Meter Inc, Ormond Beach, FL, USA) was used to measure and validate the RH. VOCs concentrations are calculated and presented in parts per million (ppm) as follows:

$$Concentraion(ppm) = 10^6 X \frac{VaporPressure_{VOC}(mmHg)}{760} X \frac{MFCFlow_{VOC}}{TotalMFCFlow} \tag{3.1}$$

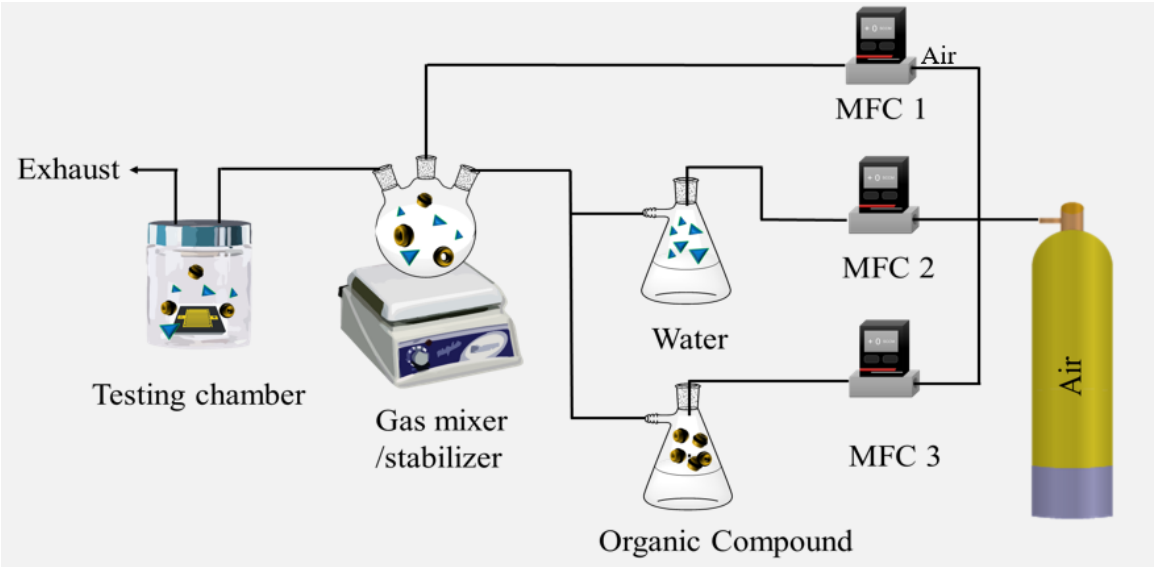

Fig. 3.5. Experimental Setup for Testing the Fabricated Sensors

A Keithley 2701 digital multimeter/data acquisition/data logging system (Beaverton, OR, USA) has been used to measure the actual resistance of the sensors. The data was transferred and collected in a personal computer using an RS232 interface. The presenting results are the average response of multiple sensors from the same batch which ensures the reliability of these findings. Figure 3.6 shows the actual setup that is used for testing the sensors including the digital multimeter used for recording the data.

3.4 Sensing Mechanism

3.4.1 PEI/CB Sensing Mechanism

Change in electrical conductivity of a PEI/CB composite during a sensing phenomenon is defined using the percolation theory[105] which gives statistical geometric description of the conductivity in a disordered system[106]. Wang et. al and Rahman et. al both presented that orientation and alignment of CB as well as their aspect ratio and weight percentage in the polymer matrix influence the electron tunneling

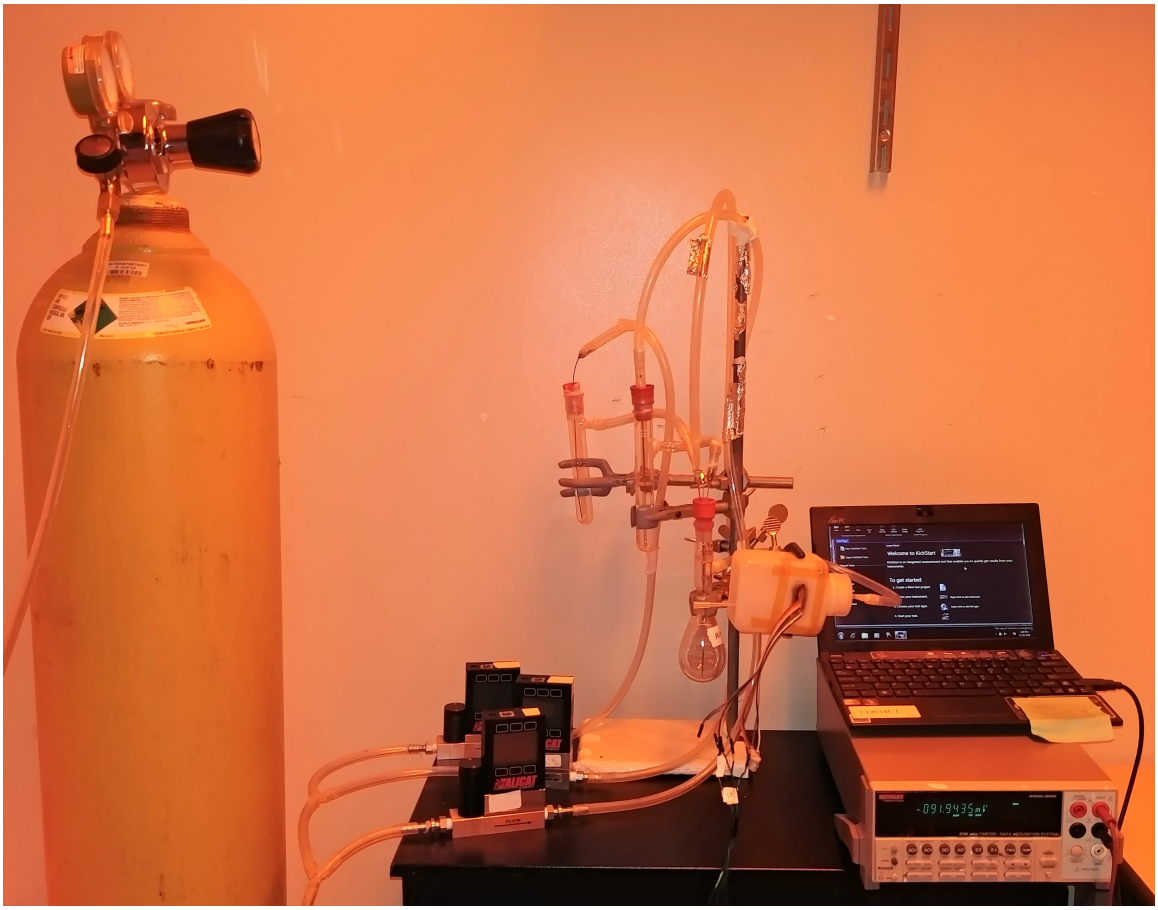

Fig. 3.6. Actual Experimental Setup for Testing the Fabricated Sensors

resistance[107], [108]. An infinite number of conducting paths are formed in the PEI matrix at percolation threshold volume concentration. When this conductive CB network embedded in PEI matrix, comes in interaction with any VOCs, swelling of the molecules occur due to physisorption of the gas into the polymer network which result in the change in electrical resistance of the CB network. This change in electrical conductivity above the percolation threshold volume is given by:

$$\sigma = \sigma_0(V - V_c)^t \tag{3.2}$$

[105]

where σ = conductivity in S/m

σ_0= constant

V = Filler volume fraction

V_c= percolation threshold

t = exponent based on material coating

It has been shown and reported that swelling of the polymer plays a major role [56, 106].

The structure of PEI is shown in Figure 3.7. Polyetherimide contains different chemical functions such as benzene rings, ether linkages (C-O-C), carbonyl groups (C=O) and C-N functions. When the PEI is molded, the long hydrocarbon chains align themselves so these reactive components interact to cause cross-linking between the chains giving PEI high chemical stability which results in high selectivity towards nonanal.

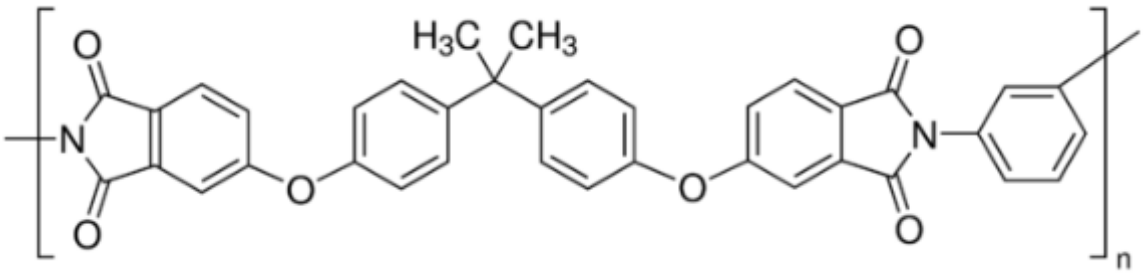

Fig. 3.7. Structure of Polyetherimide

3.4.2 Sensing Mechanism of f-GNPs

Various GNPs films have been used as a sensing element in chemiresistor sensor for vapor sensing of VOCs [107, 108]. The electrical resistance of Au_{NPF} changes when it detects an analyte, in either vapor or aqueous phase. This is explained by the fact that VOC analytes interact with f-GNP altering the films' principle method of electron transport, electron tunneling [109]. Under equilibrium conditions, the electron tunneling resistance RT of the Au_{NPF} is given by:

$$\frac{\Delta R}{R_0} = e^{\beta \Delta \delta}.e^{\Delta E_a/kT} - 1 \tag{3.3}$$

[71]

Where $\Delta\delta$ = change in edge to edge separation between gold cores

β= electron tunneling decay constant

E_A = activation barrier energy

k = Boltzmann Constant

T = temperature

The activation energy is given by,

$$E_A = e^2/(4\pi\epsilon_r\epsilon_0 r) \tag{3.4}$$

[110]

Where e = fundamental charge

ϵ_r = dielectric constant of the film

ϵ_0= vacuum permittivity

r = radius of gold nanoparticles

From the relation above, it is evident that NP size and surface functionalization plays an important part in sensing. Whenever a thin film of f-GNPs is exposed to organic gaseous analytes, there is adsorption of vapor molecules into a thin film which causes it to swell, resulting in an increase in the distance between the NPs [110]. This permeation causes changes in films; electrical impedance by the mechanism of electron tunneling. In other instances, it can be explained as charge transfer when surrounding the NP experience change in dielectric constant due to exposure of VOCs with a high dielectric constant.

In this project, 1-Mercapto-(triethylene glycol) methyl ether functionalized GNPs were used for their high sensitivity to different hydrocarbons because the f-GNPs present high sensitivity towards hydrocarbon VOCs. The structure of 1-Mercapto-(triethylene glycol) methyl ether functionalized GNPs is shown in Figure 3.8.

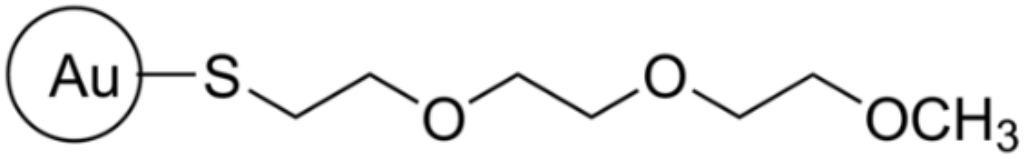

Fig. 3.8. Structure of 1-Mercapto-(triethylene glycol) methyl ether functionalized GNPs

Their high sensitivity towards different hydrocarbons is explained by the presence of double bonded oxygen atoms connected to alkyl groups adjacent to it making the oxygen highly unstable and quickly forming hydrogen bonds with hydrogen donor molecules such as alcohols, aldehydes, alkanes, etc. Double-bonded oxygen has two lone pairs of electrons which contribute to hydrogen bonding with different VOC molecules.

4. RESULTS

In this chapter, the results for material characterization using various techniques and fabricated sensor$'s$ results are presented. In Section 4.1 results for PEI with and without heat treatment and PEI/CB material characterization techniques are presented. These characterization techniques include FTIR analysis, XRD analysis, FESEM analysis, Contact Angle measurement and Profilometer measurement. Section 4.2 discusses the results for fabricated PEI/CB sensors with nonanal and other VOCs, sensor$'s$ response in high humidity (50% and 85%) and sensor$'s$ degradation as well. Section 4.3 and 4.4 present the results for f-GNP and f-GNP/PEI fabricated sensors with nonanal and other VOCs. Also, the response to water at different humidity concentrations is presented.

4.1 Material Characterization

Material Characterization is the process to determine the variation of material under various circumstances and changes in physical, chemical and structural properties leading to a higher understanding of the material.

4.1.1 Fourier Transform Infrared (FTIR) Analysis

A Nicolet iS10 FTIR Spectrometer from Thermo Scientific shown in Figure 4.1 was used to perform the FTIR analysis. The spectrometer was first run just in the air environment so that these reading can be removed giving light absorption peaks with the polymer layer only. FTIR peaks are located using Omnic software.

Fig. 4.1. Thermo Scientific Nicolet iS10 FTIR Spectrometer

FTIR Analysis of PEI and PEI/CB

Spin casting method was used to fabricate PEI and PEI/CB material on a special 25mm*4mm potassium bromide (KBr) disk shown in Figure 4.2. For each material speed of 3000 rpm was used for fabricating a film and then put in the vacuum environment to evaporate excess solvent present in the film.

Fig. 4.2. 25 x 4 mm KBr Disc used for FTIR Analysis

FTIR analysis of PEI and PEI/CB films were conducted and the results are presented in Figure 4.3. Suggested features are within 1 or 2 cm^{-1} of peaks reported in similar literature. This difference could be due to analysis variables such as environmental temperature and software or instrument calibration.

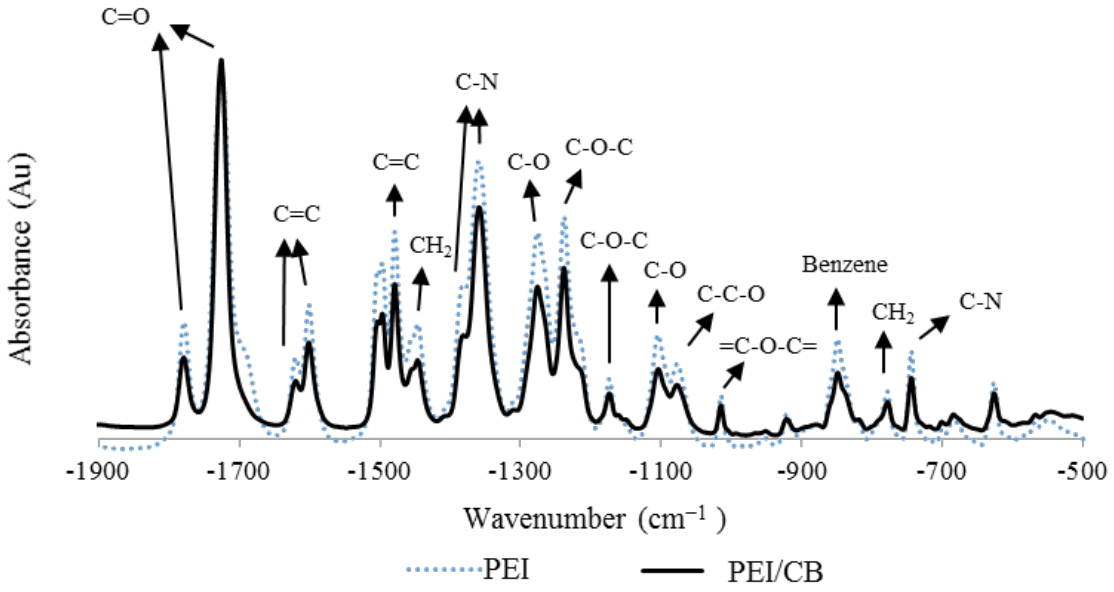

Fig. 4.3. FTIR Result for PEI and PEI/CB

PEI presents peaks at 626 cm^{-1}, 638 $^{-1}$ (rocking vibrations of methyl groups [111]) 684 cm^{-1}, 718 cm^{-1} (deformation of imide ring [112]), 744 cm^{-1}(C-N bending [113]

[114]), 778 cm^{-1}(CH2 rocking [115]), 819 cm^{-1} (C-H bending [116]), 849 cm^{-1} (out of plane benzene bending [117]), 850 cm^{-1} (Out-of-plane NH deformation [118]), 879 cm^{-1} (C-C-O symmetric stretch [118]), 921 cm^{-1} (coupling of C-C backbone stretching and the CH3 rocking mode [119]), 1014 cm^{-1} (=C-O-C= [120]), 1076 cm^{-1} (C-C-O asymmetric stretch [118]), 1105 cm^{-1}(C-O stretch [118]), 1173 cm^{-1} (C-O-C stretching [112]), 1237 cm^{-1} (aromatic ether C-O-C [113]), 1276 cm^{-1} (C-O stretching, ether groups) [121] [122], 1358 cm^{-1} (C-N stretching [114]), 1380 cm^{-1} (C-N vibration [123]), 1446 cm^{-1} (attributed to CH3 deformation [124]), 1478 cm-1(aromatic CC stretch [125]), 1600 cm^{-1} (aromatic C=C [126], 1619 cm^{-1} (C=C ring stretching band [127]). The two peaks observed at 1725 cm^{-1} and 1779 cm^{-1} are known as characteristic of PEI and are attributed to symmetric and asymmetric C=O stretching [114] [128]. FTIR results of PEI/CB is shown in the Figure 4.3 with the black line. These results show that PEI chemical structure does not change after incorporation of CB into the composite.

4.1.2 X-Ray Diffraction (XRD) Analysis

Single-crystal XRD data was collected using a model D8 Discover instrument shown in Figure 4.4. The instrument operates at 50 keV and 1000 μA, using a single source copper sealed x-ray source to produce Cu kα radiation using an air-cooled microfocus. The optics filter the $k\beta$ while a beam of $k\alpha 1$ and $k\alpha 2$ at an average wavelength of 1.5419 are emitted. The X-ray source is joint with a parallel beam Montel multi layer mirror which produces a parallel beam of monochromatic x-ray radiation. This enhances the flux density and eliminates background radiation. The diffracted X-ray signal was recorded on an LYNXEYE_XE (1-dimensional mode with 2.263411711 degree opening), scintillation counter with an active area of 14.4 mm by 16 mm. The measurement time was set to be 600 sec with the 0.11^0 angle of incidence. The measurements were auto-repeated for 18 hours and the average signal was prepared to result in the enhancement of the signal to noise ratio of the presented

results. Diffrac EVA V4.0 software was used to analyze the XRD data and background subtracted data are presented and used for phase analysis.

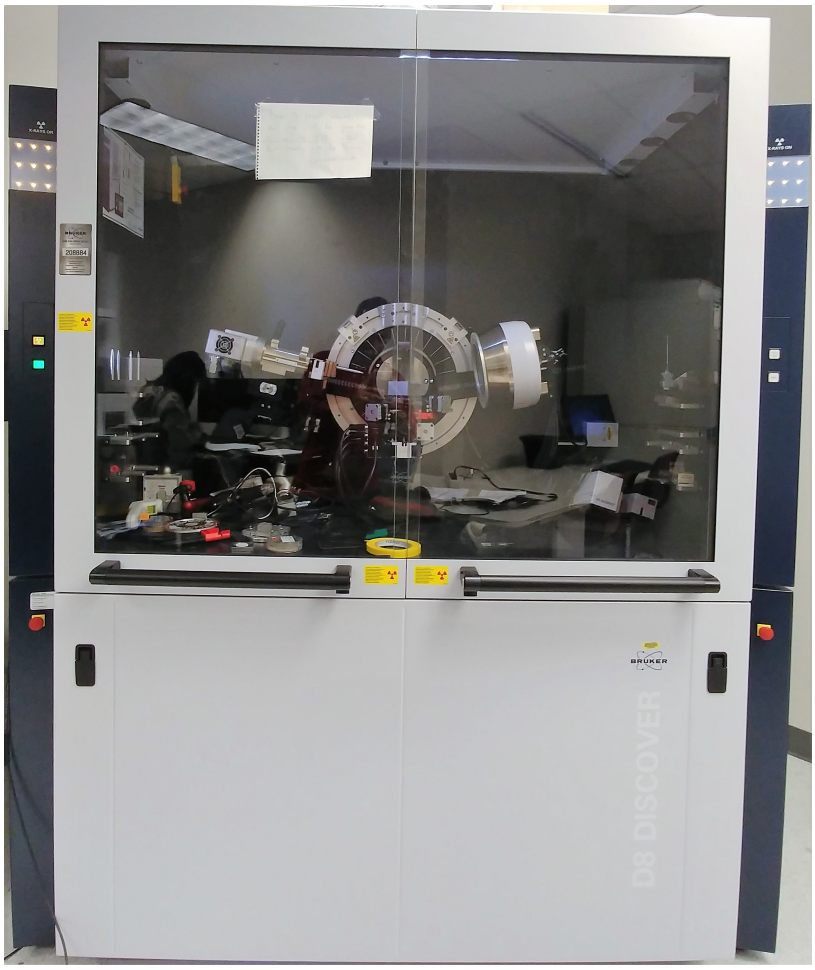

Fig. 4.4. Bruker model D8 Discover X-Ray Diffraction Analysis Instrument

XRD Analysis PEI and PEI/CB

Two samples were prepared to study the difference in the crystal structure of PEI. One sample with PEI/CB solution was prepared on a glass substrate by spin coating method with a speed of 3000 rpm to get a thick PEI film useful for XRD analysis. Another sample was prepared using PEI/NMP solution by spin coating on a glass

substrate with a speed of 3000 rpm. Both the samples were heated at 200^0C after spin coating and dried in a vacuum environment.

The XRD patterns for PEI and PEI/CB composite (2θ = 10 to 60) are presented in Figure 4.5. This analysis illustrates the semi-crystalline property of the PEI, where two peaks are located at 17.2^0 and 23.6^0. The main peak at 17.2^0 (the corresponding d-spacing is 5.15 A^0) shifts to 16.2^0 (the corresponding d-spacing is 5.47 A^0) after the introduction of CB into the composite. This shift of the XRD peak to the left indicates the formation of a larger d-spacing and could be due to planar stress and change in the chemical composition. It demonstrates that the CB has been successfully incorporated into the lattice and altered the unit cell leading to the formation of a polymer composite [129].

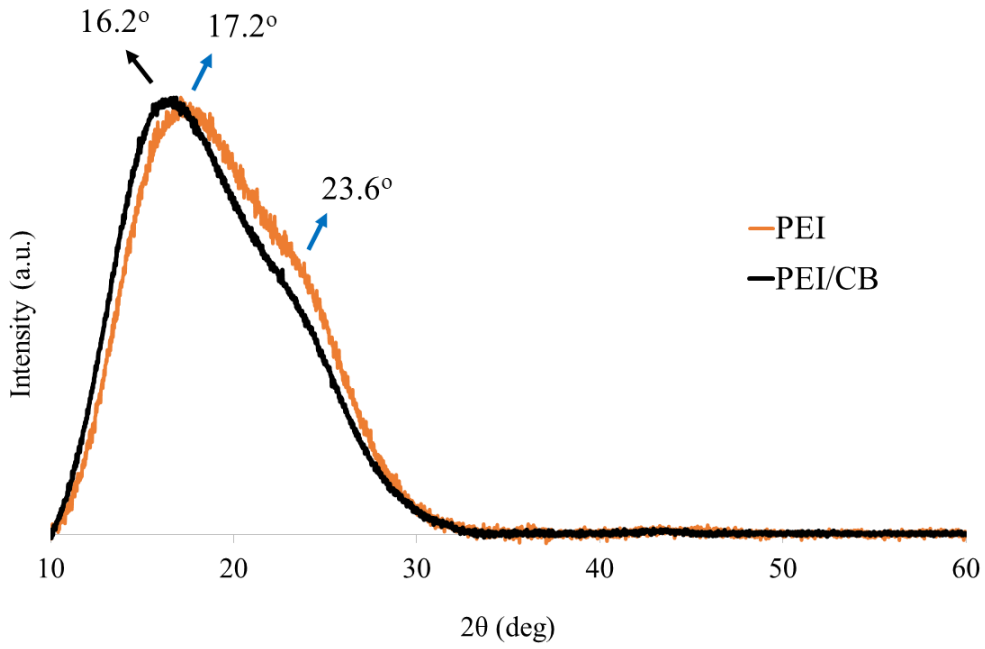

Fig. 4.5. XRD Analysis for PEI and PEI/CB

4.1.3 Field Emission Scanning Electron Microscopy (FESEM) Analysis

A Field Emission Scanning Electron microscope model of JSM-7800F (JEOL USA, Peabody, MA, USA) shown in Figure 4.6 was used to provide images and investigate the morphological properties of the PEI and PEI/CB composite and to estimate the film thickness.

Fig. 4.6. Field Emission Scanning Electron Microscope JSM-7800F

FESEM Analysis of PEI/CB

PEI/CB solution was deposited on a silicon substrate and spin coating method with a speed of 3500 rpm was used to prepare a sample for FESEM analysis. The

PEI/CB film was then heated at 200^0C on a hot plate for 2 hours and then dried in vacuum for 24 hours.

FESEM images of CB and PEI/CB over a silicon substrate are presented in Figures 4.7, 4.8 and 4.9. The FESEM image from the surface of PEI/CB is shown in Figure 4.7. The presenting image shows the unvarying morphology of a porous PEI/CB film. This indicates that the proposed fabrication method has led to the development of a highly uniform film across the electrodes. The porous structure of the fabricated film allows the VOCs to rapidly diffuse through the sensing material, leading to fast response time.

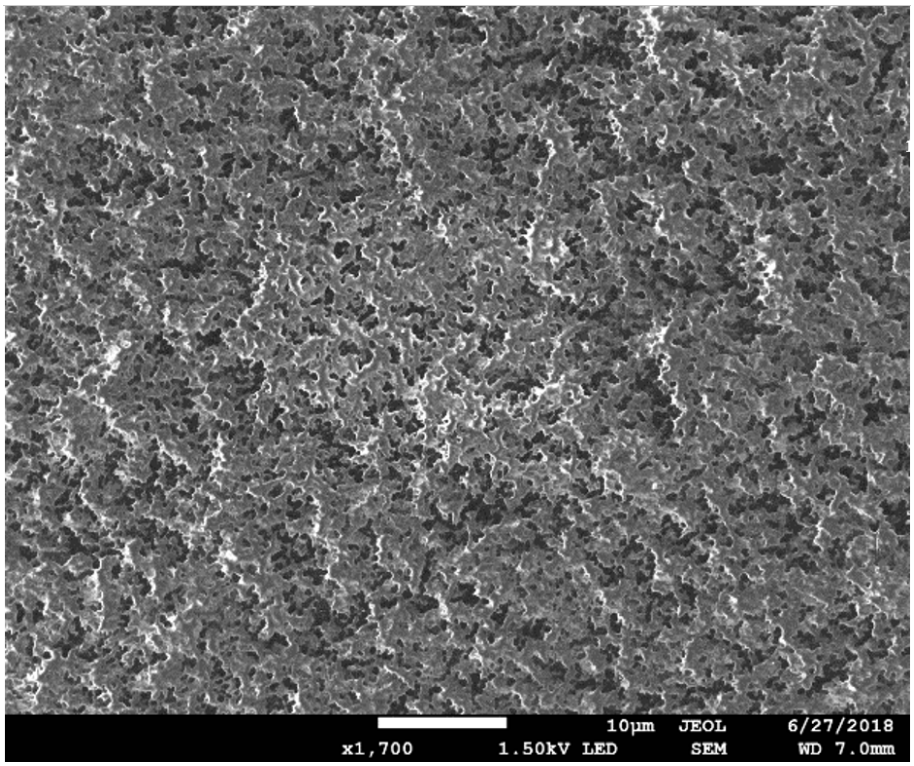

Fig. 4.7. FESEM Image of PEI/CB structure

Cross section image of the PEI/CB film is presented in Figure 4.8. This cross-section image suggests fabrication of a uniform PEI/CB film has been achieved through the proposed method. The cross-section image estimates the average thickness of the fabricated film to be 17μm. More accurate measurement of the film thick-

ness was conducted using Dektak XT profilometer and indicates the film thickness at the electrodes is 15μm.

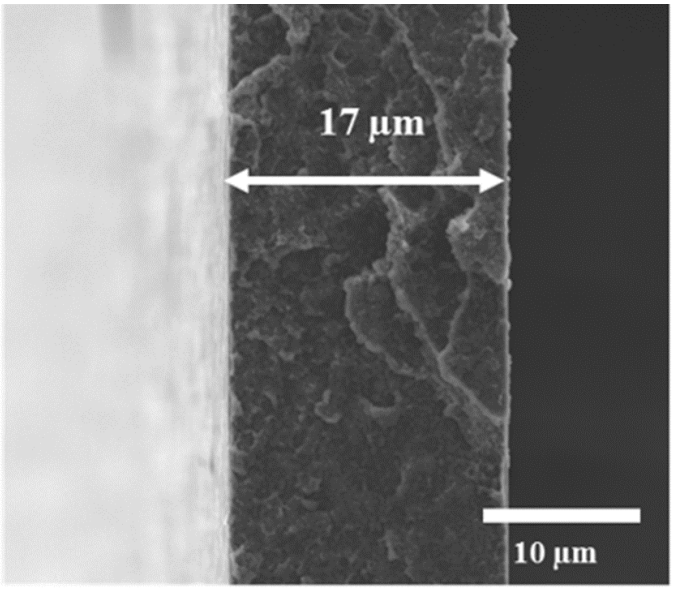

Fig. 4.8. Cross-Sectional FESEM Image of PEI/CB showing its Thickness

FESEM image of the CB structure used in this study has been provided in Figure 4.9 showing a uniform particle size of the carbon black used that helps to get a uniform conductive matrix throughout.

4.1.4 Contact Angle Measurement Analysis

A Rame Hart Goniometer with 1500W optical illuminator shown in Figure 4.10 was used for taking drop images of water on the polymer film. The goniometer connected to the computer with Image Drop software was used to find the contact angle of the drop. Furthermore, the results were further cross-checked by open source ImageJ software by National Institute of Health (NIH).

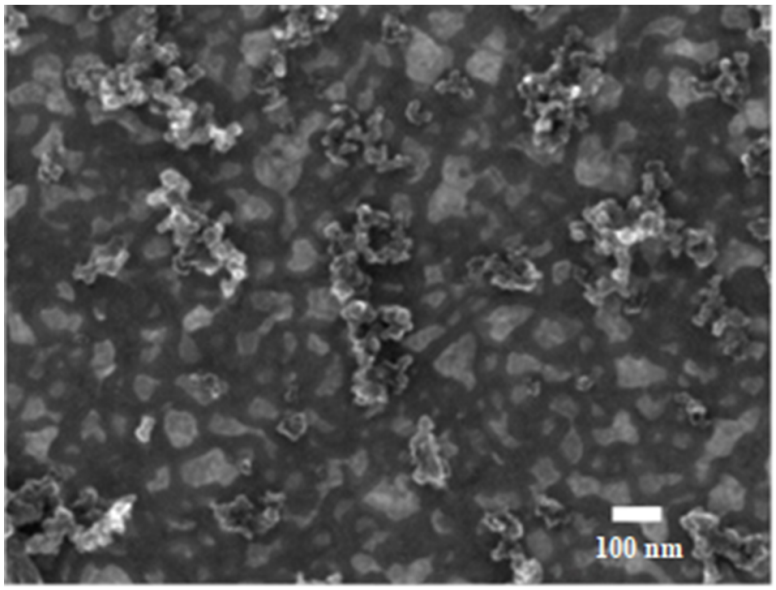

Fig. 4.9. FESEM Image of CB Structure

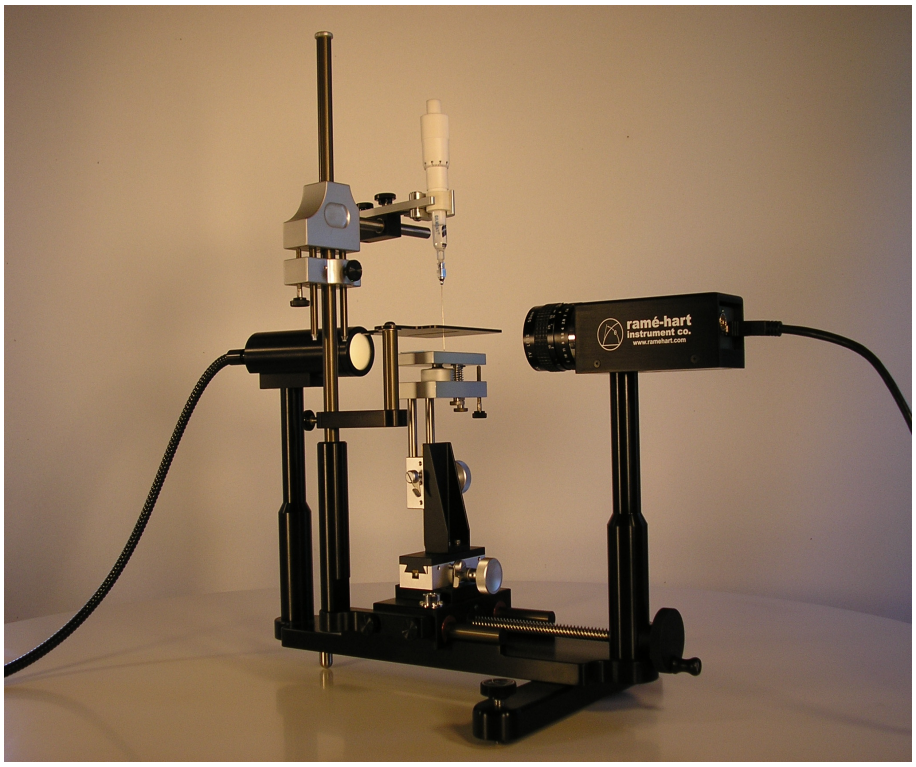

Fig. 4.10. A Standard Goniometer used for Contact Angle Measurement

Contact Angle Measurment Analysis of Heat-Treated and Non-Heat-Treated PEI

Five different samples of PEI film were spin-coated on IDEs with a speed of 5000 rpm and then each substrate was heated at 80^0C for different times being 0 sec, 120 sec, 300 sec, 600 sec, and 3600 sec. To measure the contact angle between the water droplet and PEI film, a small water drop is dropped using a small mouth pipette over the film and the image is taken using the goniometer. Results for the contact angle measurement of each sample is presented in Table 4.1.

Table 4.1. Comparison of Contact Angle Measurement of PEI film.

No.	**Speed**	**Heat Treatment time**	**Left Angle (deg.)**	**Right Angle (deg.)**
1	5000 rpm	0s	58.6^0	59^0
2	5000 rpm	30s	77^0	76.9^0
3	5000 rpm	120s	83.8^0	83^0
4	5000 rpm	300s	84.2^0	83.6^0
5	5000 rpm	600s	84.1^0	84^0

Figure 4.11 shows the contact angle measurements between spin coated PEI film and the water droplet. Figure 4.11 a) proves that without heat treatment of the PEI film, the film is more hydrophilic which will allow it to interact with water molecules because the contact angle shown was much smaller than the heat-treated film. This is due to entrapped NMP solvent in the PEI film which is a polar solvent that absorbs moisture and increases its affinity to water. On the other hand, it was noticed that speed does not affect the contact angle measurement because only the thickness of the film changes with the speed, the crystal structure depends on the fabrication process of the film. Figures 4.11 b) c) d) and e) show the contact angle for the heat treated PEI layer for 2, 5, 10 and 60 min respectively. These images prove that heat treatment of PEI film improves the hydrophobicity of the film by showing a higher

contact angle between the water droplet and the PEI surface. The angle significantly increases without heat-treated PEI film from 59^0 to 84^0 for a film heat treated for 10 minutes or more.

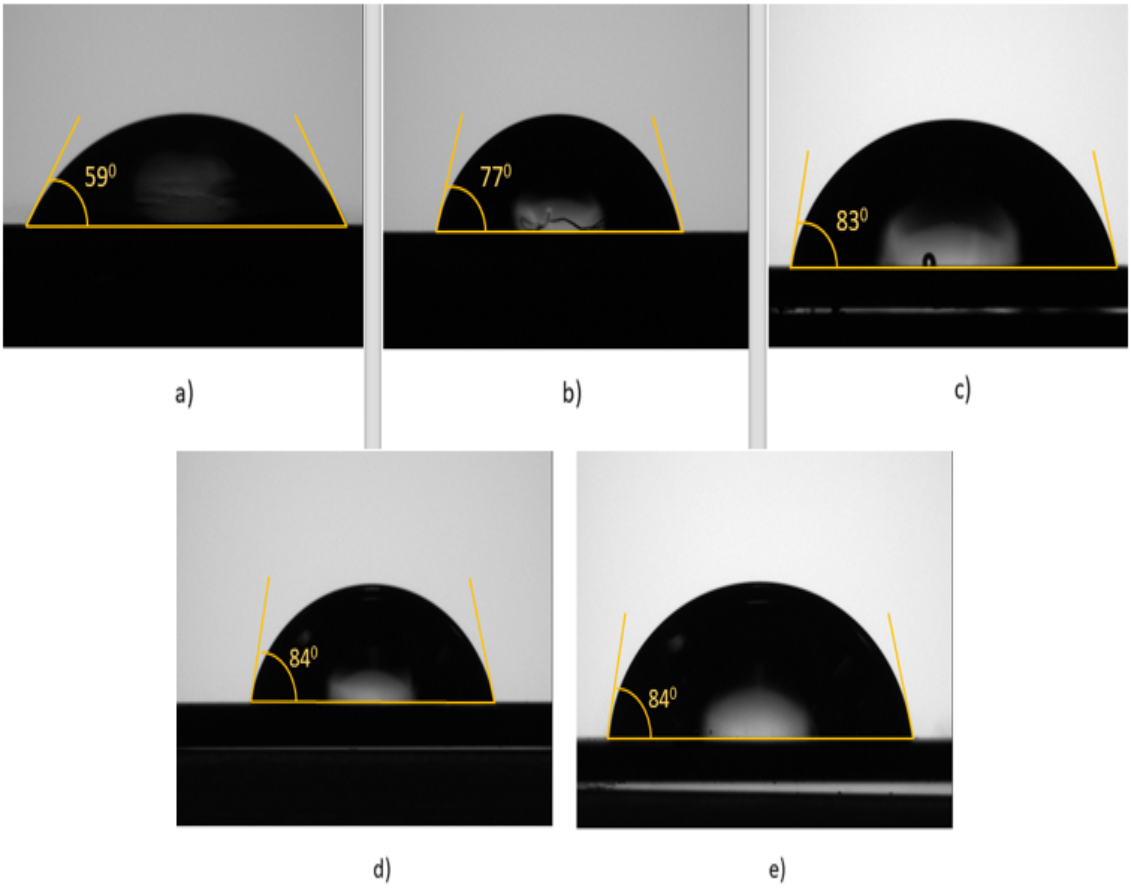

Fig. 4.11. Contact Angle Measurement for PEI film at 5000 rpm for Different Heat Treatment Time a) 0 sec, b) 120 sec c) 300 sec, d) 600 sec, and e) 3600 sec

Contact Angle Measurement analysis of PEI/CB

Six different samples of PEI/CB were fabricated for CAM. Five of these substrates were spin-coated at different speeds being 3000 rpm, 4000 rpm, 5000 rpm, 6000 rpm, 7000 rpm, and then heated at 200^0C and the other substrate was spin-coated at 4000

rpm and allowed to dry without any heat in the room environment. This gives a series of data, which is presented in Table 4.2.

Table 4.2. Comparison of Contact Angle Measurements of PEI/CB Film at Different Spin Coating Speeds.

No.	**Speed**	**Left Angle (deg.)**	**Right Angle (deg.)**
1	4000 rpm (Non-Heat-treated)	54.9^0	55.5^0
2	3000 rpm (Heat-treated)	79.2^0	79.3^0
3	4000 rpm (Heat-treated)	79^0	79.5^0
4	5000 rpm (Heat-treated)	80.1^0	80^0
5	6000 rpm (Heat-treated)	80.3^0	80.5^0
6	7000 rpm (Heat-treated)	80.3^0	80.3^0

Figure 4.12 shows the contact angle measurement for PEI/CB film at different speeds and it is determined that the film which is not heated gives a relatively lower contact angle between the water droplet and the PEI/CB film. The lower contact angle between the surface and the drop means the high absorption of water on the surface showing the hydrophilic nature of the film. Another thing that is observed with the measurements is that the heat treatment increases the contact angle significantly from 55^0 to 80^0 and the study shows that the contact angle measurement is not affected by the spin coating speed of film fabrication.

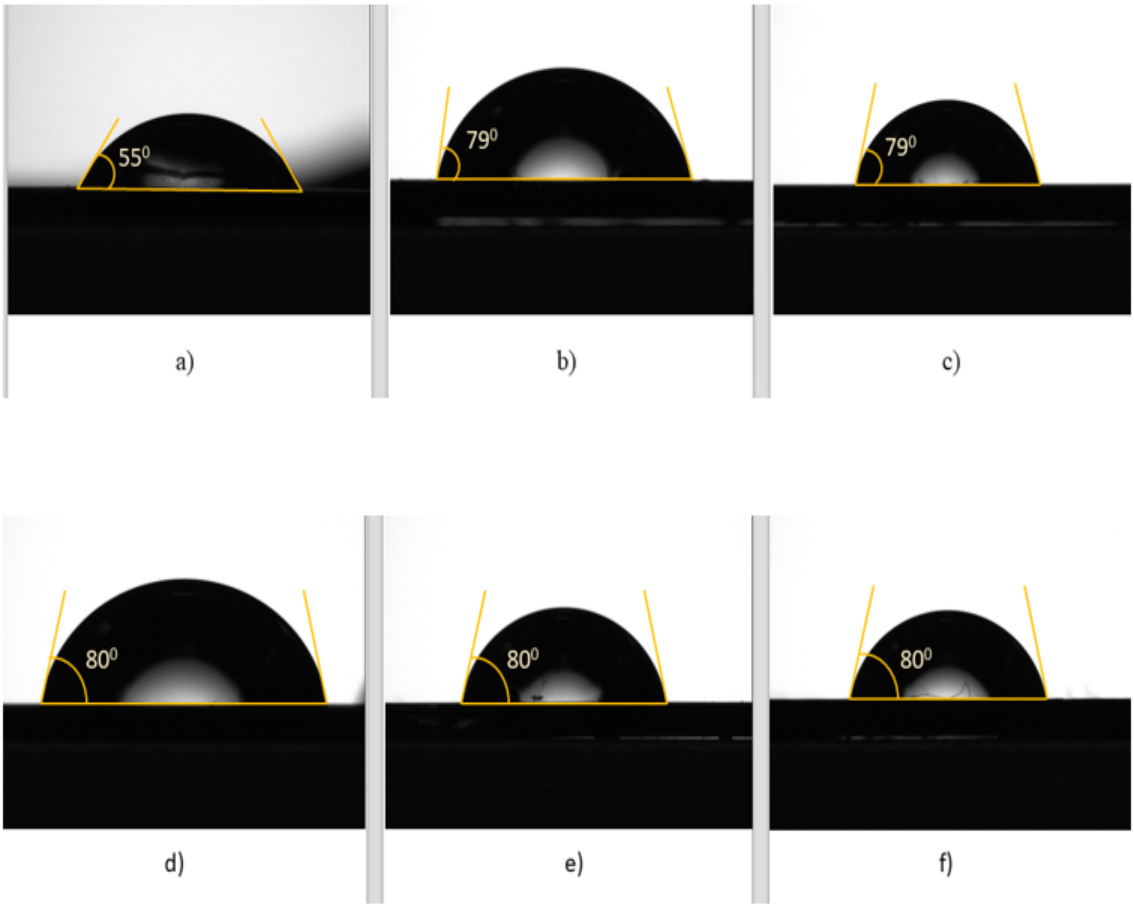

Fig. 4.12. a) Contact Angle of Water Drop on PEI/CB film 4000 rpm without heat treatment b), c), d), e), f) Contact Angle of Heat Treated PEI/CB at speed 3000 rpm, 4000 rpm, 5000 rpm, 6000 rpm, and 7000 rpm respectively.

4.1.5 Profilometer Measurements

The Dectak XT profilometer (Brucker, Billerica, MA, USA) was used to measure the film thickness as shown in Figure 4.13. The films were fabricated by different speeds and different heat treatment times, described in detail in Section 3.2.2 and 3.2.3. The fabrication technique of the film was discussed in detail in Section 3.2.1.

Fig. 4.13. Bruker Dektak XT profilometer for film thickness measurement

Thickness measurement of Heat-Treated and Non Heat-Treated PEI films

The results at each spin coating speed of 3000 rpm, 5000 rpm and 7000 rpm with various heat treatment times of 0 sec, 30 sec, 120 sec, 300 sec and 600 sec at heat treatment temperature of 80^0C were presented in Figure 4.14 using the calibration curve. The curve shows that heat treatment steps in fabricating the PEI film reduces the film thickness drastically and a steady state in thickness reduction is reached at

10 min. After 10 min, the change in thickness is in the range of few nanometers and the surface starts becoming rough. The constraint in heat treatment temperature was due to the fact that f-GNPs merge to form bigger particles making IDEs conductive in the range of $100's$ of ohms. Hence this study was done at 80^0C with a varying time to prevent the f-GNPs from coagulating into bigger particles.

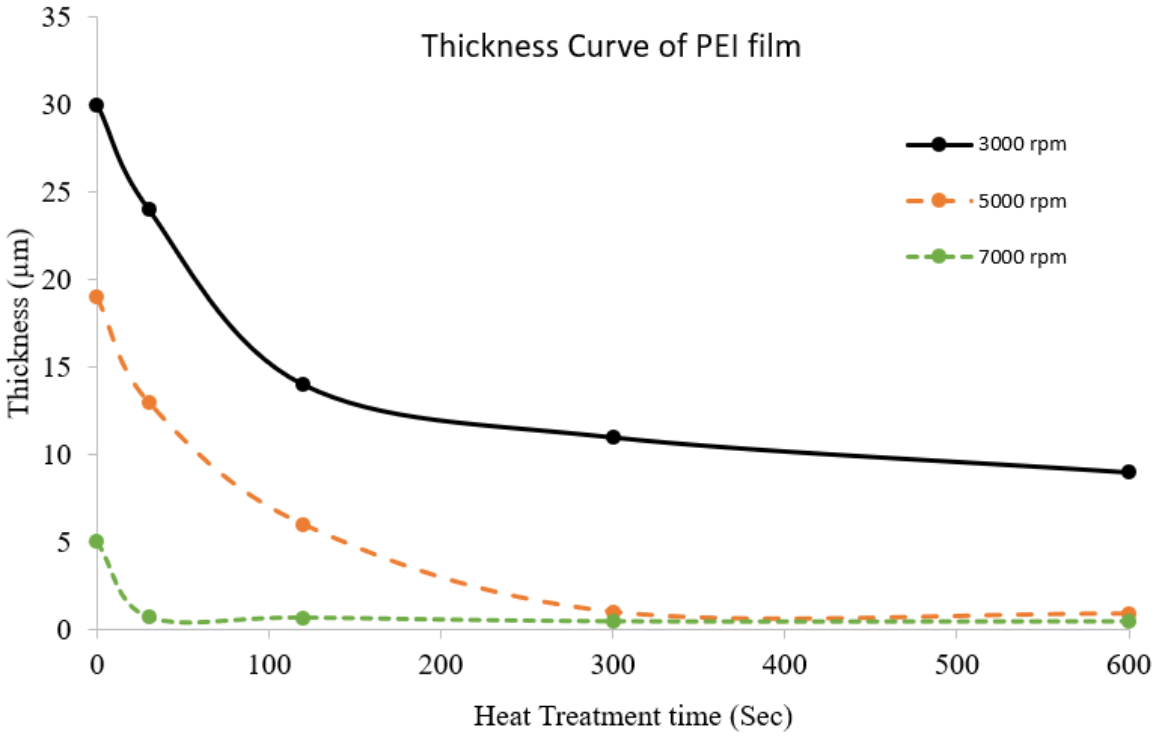

Fig. 4.14. Thickness Curve of PEI film

Thickness measurement of PEI/CB films

The fabrication technique for the film was discussed in detail in Section 3.2.3. The result shown in Figure 4.15 shows that a uniform film with a low surface roughness was achieved by spin coating at various spin coating speeds. The thickness curve shows that the thickness varies from 39μm to 5μm for the spin coating speed of 1000 rpm and 7000 rpm respectively. This calibration curve can give an approximation of thickness at a different speed. The variation in thickness depends on various factors

such as spin coating speed, concentration and the viscosity of the material, heat treatment time and temperature. From the calibration curve, it can be seen that the film thickness is inversely proportional to spin coating speed. The thickness of the film will be directly proportional to concentration, and viscosity of the material and inversely proportional to heat treatment time and temperature. This study has been done using variable speed only because the temperature was chosen above the glass transition temperature of PEI which is 217^0C and there was no time constraint in heating to achieve the thinnest layer possible at a specific speed.

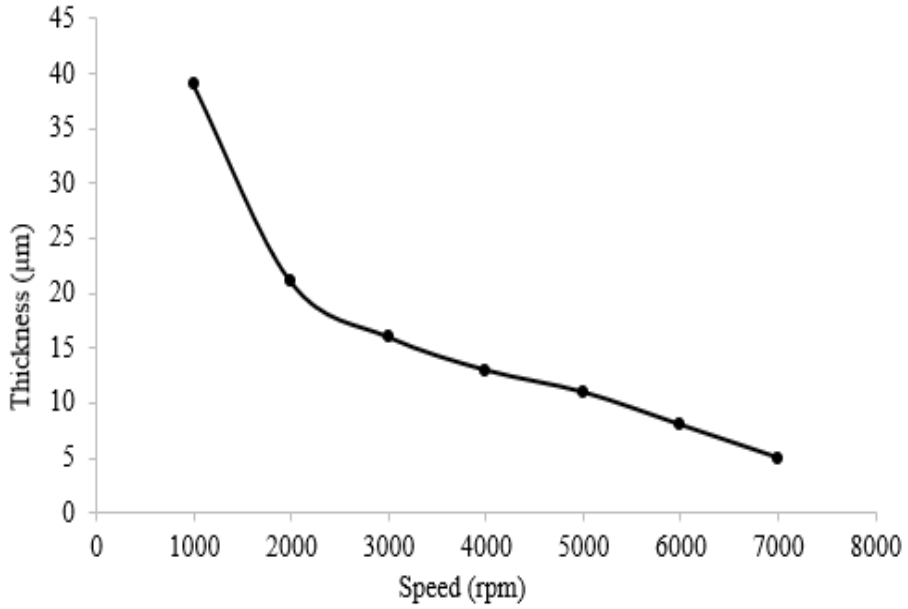

Fig. 4.15. Thickness Curve for PEI/CB film from 1000 rpm to 7000 rpm

4.2 Sensor Results

4.2.1 PEI/Carbon Black (CB) Sensor

PEI/CB sensors were fabricated with the method described in Section 3.2.3 and tested with the experimental set-up presented in Section 3.3. The results of the sensor$'s$ response with interaction with the VOCs are presented in terms of relative response (RR) using the following formula:

$$Relative Response(RR)_{VOC} = \frac{R_{VOC} - R_{AIR}}{R_{AIR}} X100 \tag{4.1}$$

The presented results show the average of five devices and the error bar describes the standard deviations of the sensors.

PEI/CB Sensor Relative Response to Nonanal

PEI/CB sensors fabricated on one substrate were exposed to 50 ppm of nonanal for three cycles and results are presented in Figure 4.16. The sensors are first stabilized in dry air inside the experimental test setup and then the flow of nonanal is allowed. The presented results show that the initial resistance of the sensors has increased by 1.1% $\pm$ 0.01% in each cycle after introducing to 50 ppm of nonanal. The percentage of resistance change was similar in all sensors independent of their initial value. This indicates successful fabrication of similar sensors across the electrodes. The spin casting method followed by the proposed heat treatment is necessary to develop such a uniform thin film across the IDEs. It should be noted that this reproducibility was not possible without the proposed heat treatment method. The results in Figure 4.20 also show that the sensors present a similar response at each cycle. The standard deviation of the sensor$'s$ relative response to nonanal was measured to be smaller than 0.005% of sensor$'s$ initial resistance. This shows the fabricated sensors present a repeatable response to nonanal and will work properly for multiple cycles. The sensors reach the steady state in a short time period and the sensors response time

is estimated to be about 280s for reaching up to 90% of the resistance change. These results show that the proposed fabrication method leads to the development of similar PEI/CB sensors over the IDE. The fabricated sensors present a fast and repeatable response in interaction with nonanal. The increase in resistance of the sensors is explained by swelling of the polymer due to physical absorption of VOC molecules on the PEI/CB sensing layer and the resistance of CB is affected by the method of percolation theory.

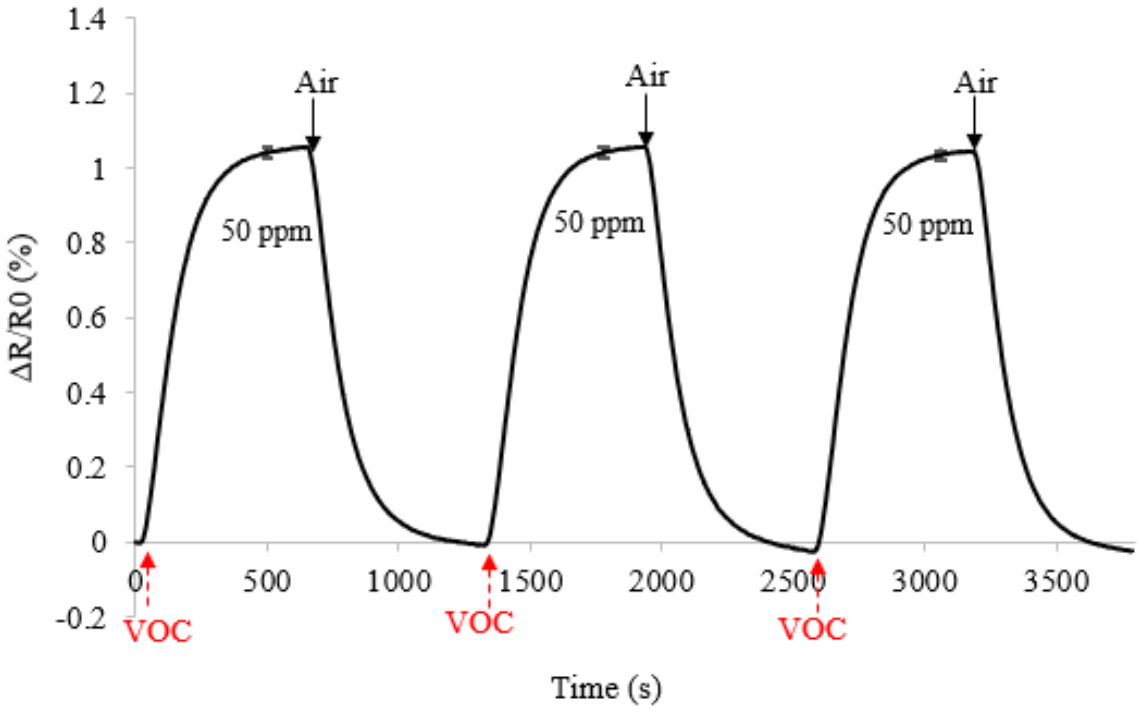

Fig. 4.16. PEI/CB Sensors Response to a fix concentration of Nonanal (50 ppm) for three cycles

In order to determine the sensing capability of the fabricated sensor towards nonanal, the sensors were tested from a lower concentration (1 ppm 4 ppm) to higher concentrations (5 ppm - 20 ppm) of nonanal and the results are illustrated in Figure 4.17 and Figure 4.18. The presenting results show that PEI/CB resistance increases by 0.02%, 0.05%, 0.08%, 0.10%, 0.20%, 0.32%, 0.42% for 1, 2, 4, 5, 10, 15,

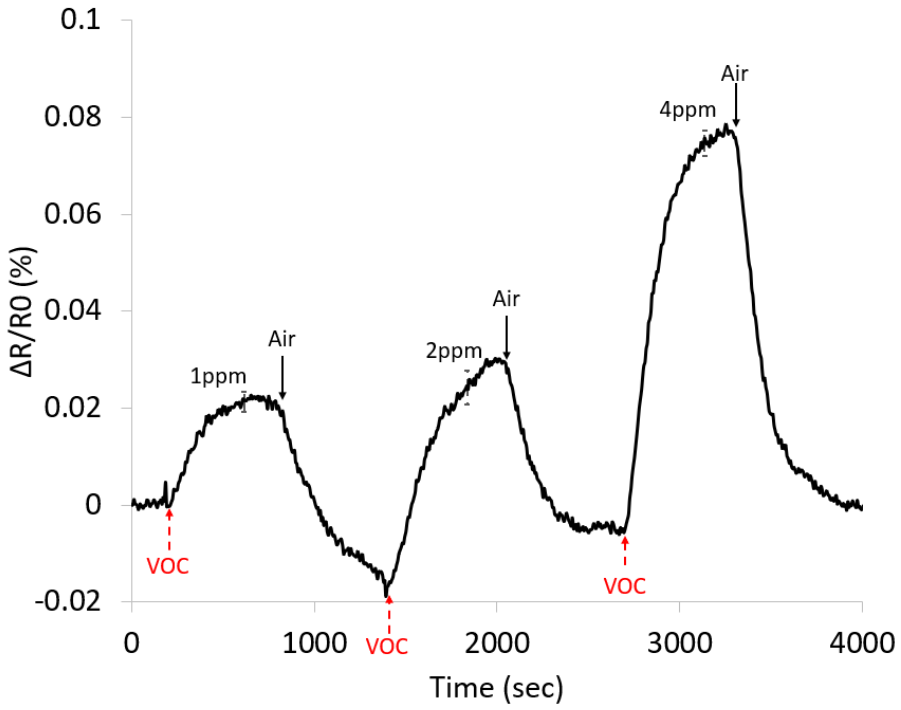

Fig. 4.17. PEI/CB Sensor Response to Nonanal at 1 ppm, 2 ppm, and 4 ppm

and 20 ppm of nonanal. The sensors′*s* average relative response to higher concentrations of nonanal is greater than lower concentrations of the VOC. This behavior of the proposed PEI/CB sensors could be used to determine sensitivity at different concentrations of nonanal. Interaction of nonanal with the composite leads to swelling of the PEI which increases the separation between CB structures thus increasing the resistance of the sensors. The sensors fast response time and small standard deviation make the proposed PEI/CB suitable for detecting different concentrations of nonanal.

The calibration curves of the fabricated sensors in response to nonanal are presented in Figure 4.19. The calibration curve for a wider range of 1 ppm to 80 ppm is provided with the calibration curve for a smaller range of 1 ppm to 10 ppm within.

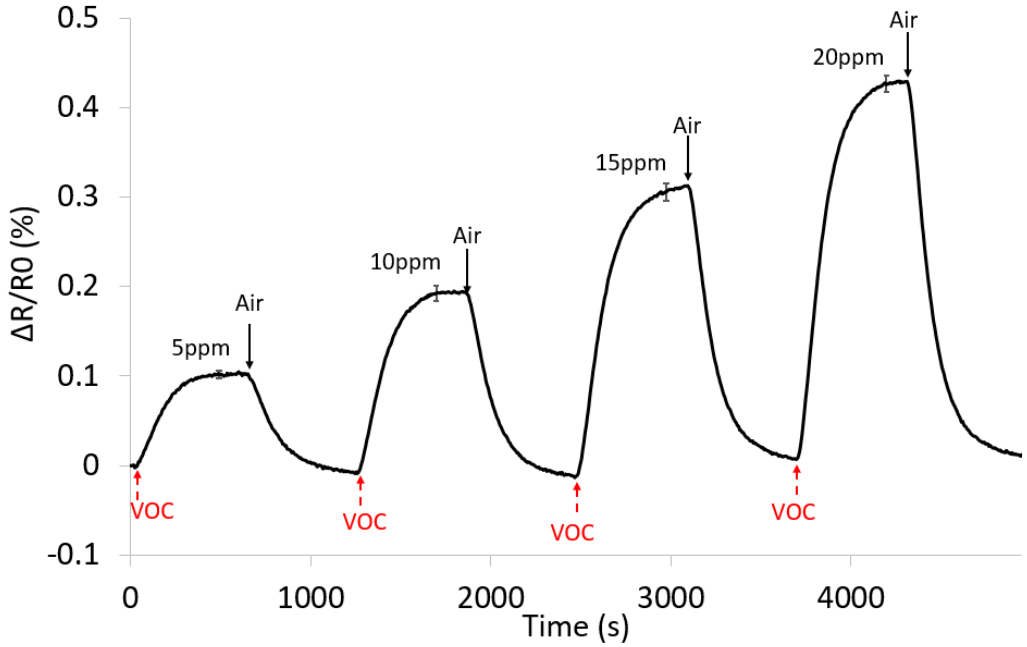

Fig. 4.18. PEI/CB Sensors Response to different concentration of Nonanal (5 ppm to 20 ppm)

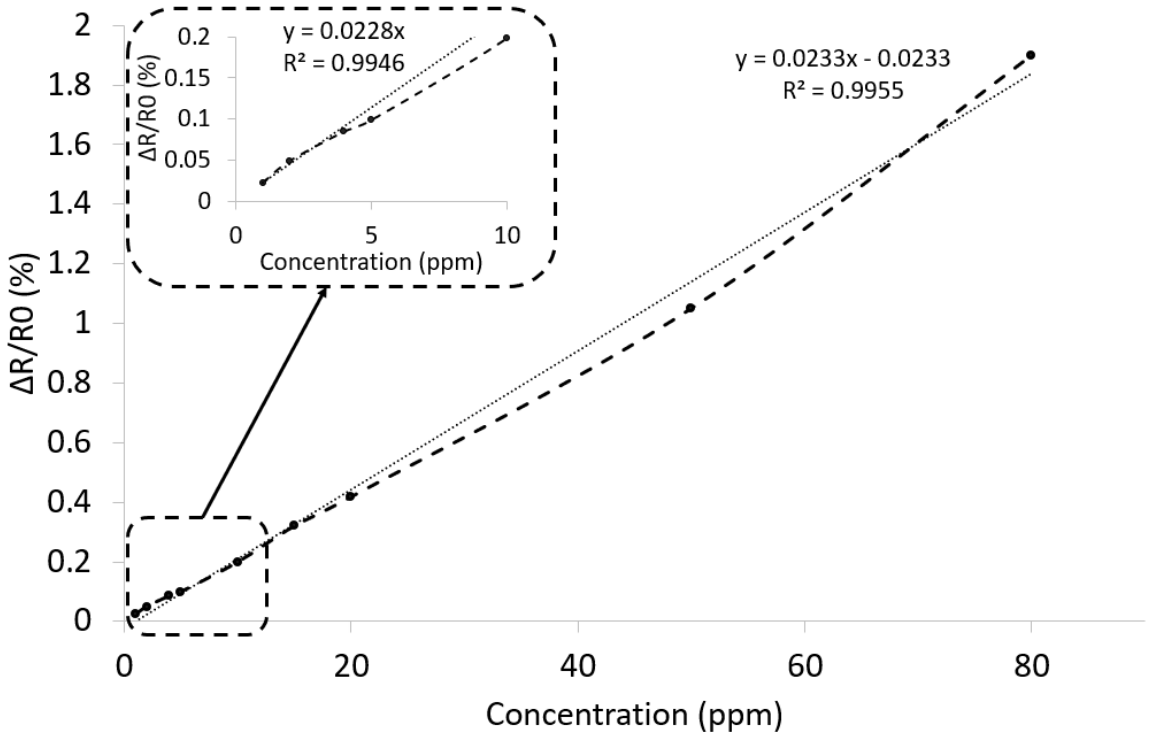

Fig. 4.19. PEI/CB Sensors Calibration Curve for Nonanal (1 ppm to 80 ppm)

The presenting results show that the proposed PEI/CB sensor can be used to detect a wide range of nonanal (1-80 ppm). Linear regression shows nearly a linear relation between the sensor′*s* resistance change and concentration of the VOC. This linear behavior is favorable and makes it possible to predict the concentration of the targeting VOC accurately via such a calibration curve.

PEI/CB Sensor Sensitivity

Sensitivity is defined as the slope of the calibration curve of the VOC and the unit of sensitivity is %/ppm. The sensitivity of the fabricated PEI/CB sensors has been investigated by introducing them to different concentrations of dodecane (hydrocarbon), 2-nonanone (ketone), 1-octanol (alcohol) and nonanal (aldehyde). The sensor′s response to higher concentrations of dodecane (50-130 ppm), 1-octanol (16-60 ppm)

were less than 0.04% and 0.07% respectively. The sensor′*s* resistance change per ppm of the targeting VOCs is presented in Figure 4.20. The presenting results show that the sensors were not sensitive toward dodecane, 2-nonanone and 1-octanol which are important VOCs linked to different metabolic pathways and are potential biomarkers to different diseases.

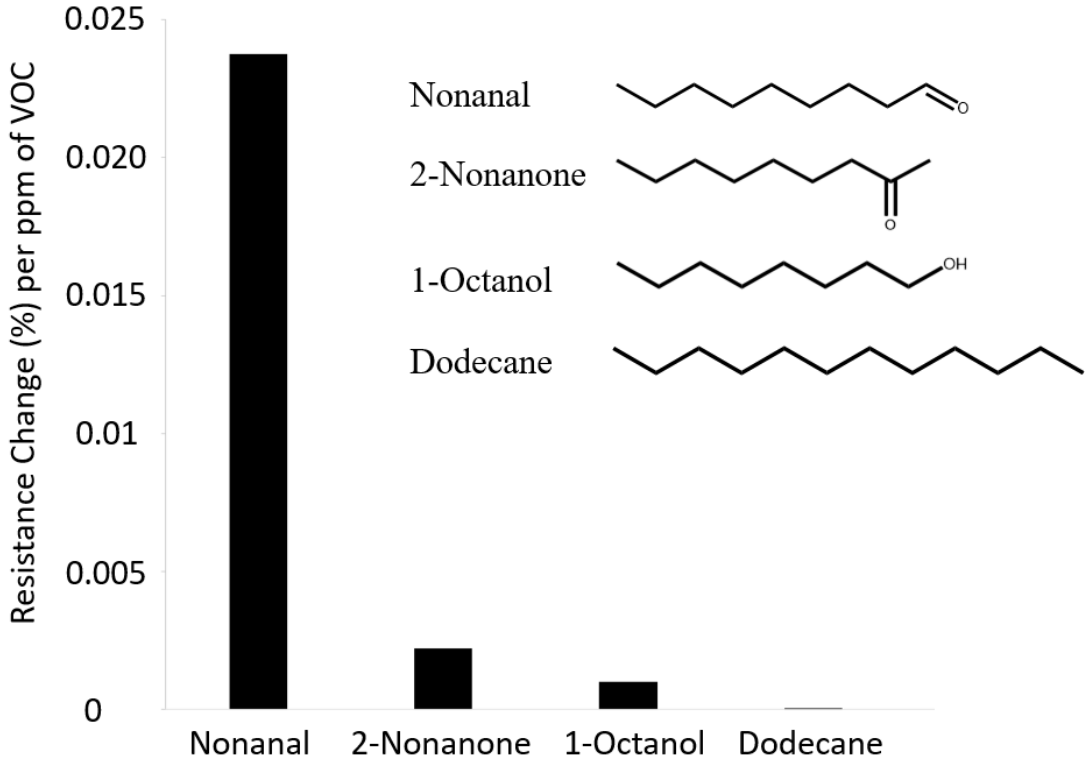

Fig. 4.20. Resistance Change per ppm of VOC calculated from the Calibration Curve

The sensor′*s* resistance change per ppm of VOC has been estimated from the calibration curve of the sensors for nonanal, 1-octanol, dodecane, and acetone. The presented result indicates the high selectivity of the PEI/CB sensors toward nonanal against other VOCs. This would make the proposed sensors a potential solution for detecting diseases linked to aldehydes.

PEI/CB Sensor Response to Water Vapor

PEI/CB sensor response was evaluated to humidity by exposing the fabricated sensors to water vapor at R.H of 50%, 75%, and 85%. The sensors response to water vapor is presented in Figure 4.21. The sensors were exposed to humidity in cycles of 10 min each and the presenting results show that the prolonged exposure to water vapor can be tolerated without any damage to the sensors. The sensors also presented a limited and fixed change in response to water vapor. The sensors relative response to water vapor at R.H of 50%, 70%, and 85% were 2%, 3.7%, and 4% respectively. These results agree with characterization results from contact angle measurements and show that the proposed sensors would not be highly sensitive to interfering water vapor in the air.

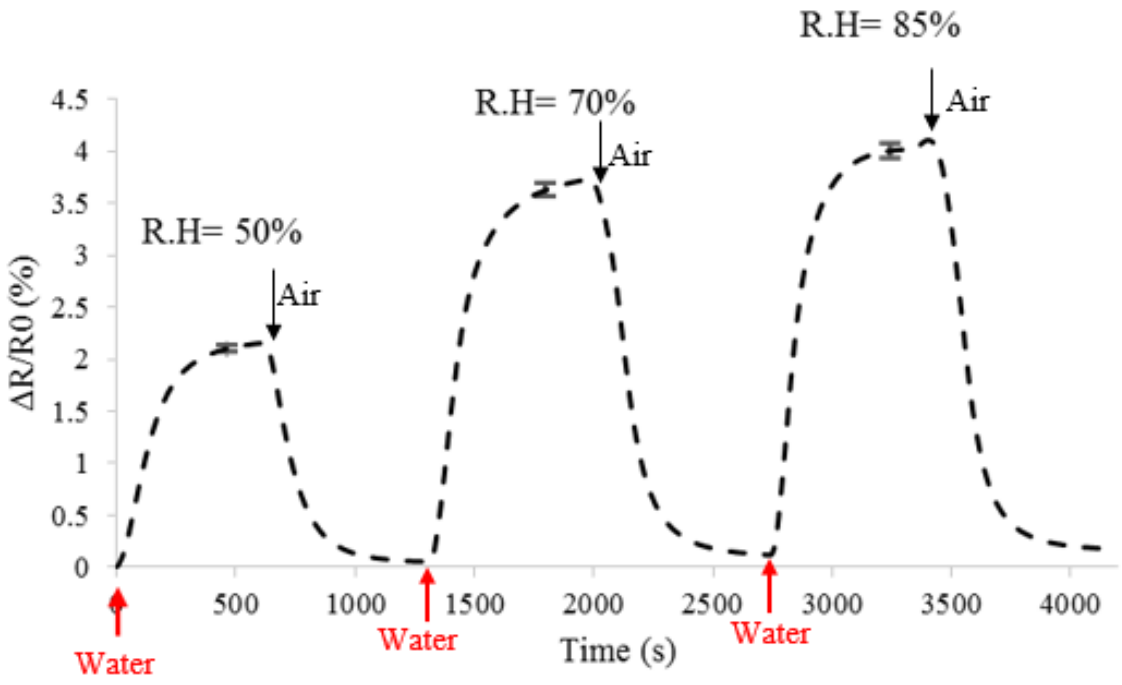

Fig. 4.21. PEI/CB Sensors Response to Water Vapor (R.H = 50%, 75%, and 85%)

The effect of humidity to PEI/CB sensor$'s$ sensitivity was further investigated by exposing the sensor to nonanal at higher humidity concentrations. The sensors have

been stabilized in an environment with R.H 50% and 85%. The relative response of PEI/CB sensor to 5 ppm of nonanal at R.H of 0%, 50%, and 85% are presented in Figure 4.22. The presenting results show that the sensor sensitivity decreased by less than 14% at 50% RH and decreased less than 34% at 85% RH as compared to in dry air. This can be explained by the reason that water vapors have been diffused into the PEI/CB film at high humidity concentrations and that limits the expansion of the polymers. Diffusion of water vapor into the sensing film lowers the surface area for interaction of vapor analytes of nonanal to sensing film with results in lower resistance change of the fabricated sensors as compared to sensors in dry air.

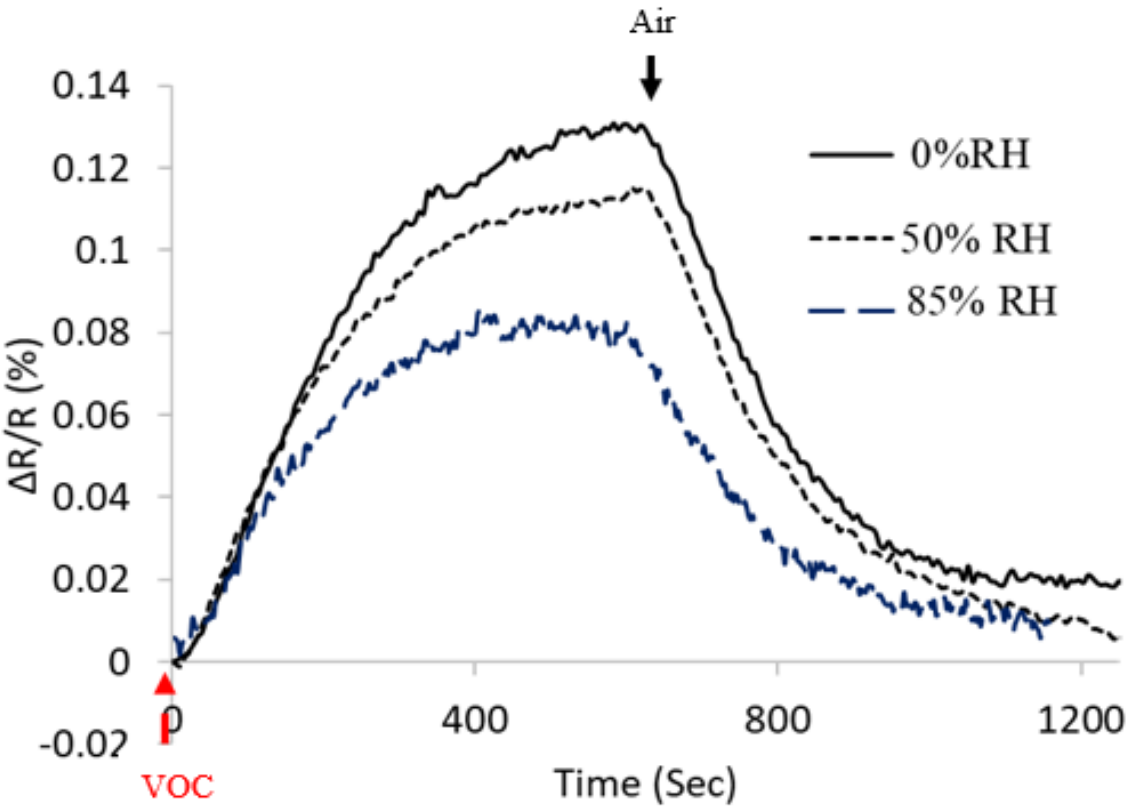

Fig. 4.22. PEI/CB Sensors Response to Nonanal in the present of Water Vapor (R.H = 0%, 50% and 85%)

PEI/CB Sensor Degradation

In order to investigate the drop in resistance change ($\Delta R/R_0$) for the response of nonanal, the sensor has been tested for the period of 36 days starting from day 1 and testing after every seven days in the presence of 5 ppm of nonanal at 0% RH. The result for PEI/CB sensor degradation has been presented in Figure 4.23 showing resistance change drop of less than 5% over time. This shows that the fabricated sensor is not susceptible to degradation making it useful for long term use for sensing applications. This high stability of the sensors could be due to the intrinsic properties of the PEI that makes it chemically stable and the impact of the heat treatment in developing a more hydrophobic composite which reduces the adhesion of water moisture into the film. This prevents the sensing layer from degrading over time.

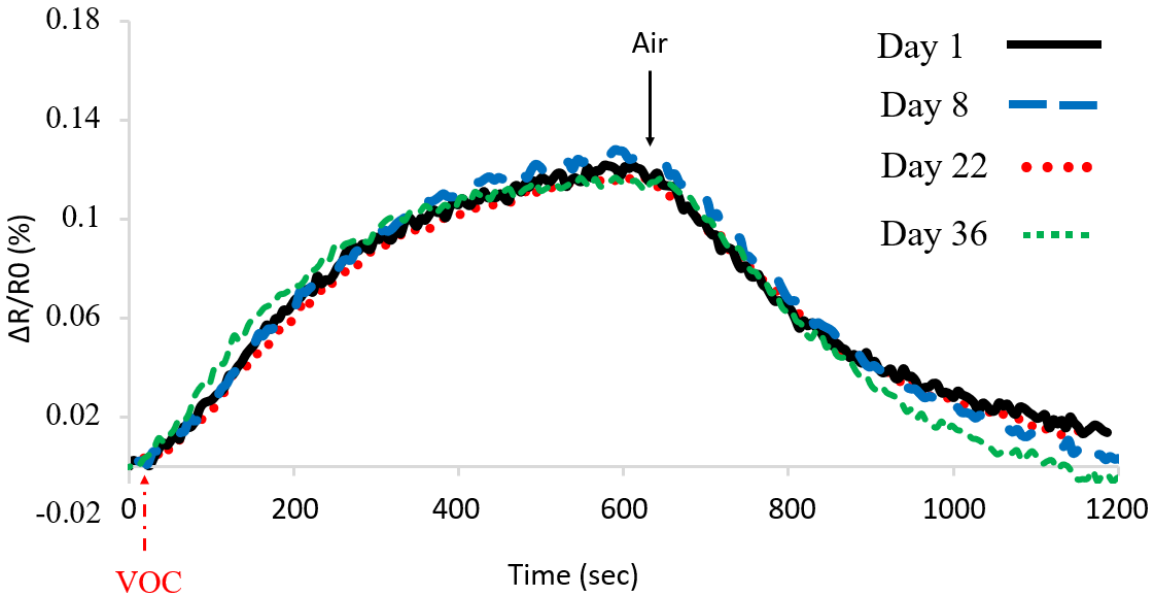

Fig. 4.23. Degradation study of PEI/CB Sensor at 5 ppm of Nonanal

4.2.2 F-GNP Sensor

Sensors of 1-Mercapto-(triethylene glycol) methyl ether functionalized GNPs were fabricated with the method described in Section 3.2.4 and tested with the experimental set-up presented in Section 3.3. The results of the response of the sensors with interaction to the VOCs are presented in terms of relative response (RR) using Formula 4.1. The presented results show the average of four devices and the error bar describes the standard deviations of the sensors.

Relative Response of f-GNPs to Nonanal

Sensors of 1-Mercapto-(triethylene glycol) methyl ether functionalized GNPs fabricated on one substrate were exposed to 5, 10 and 15 ppm of nonanal for one cycle in a stable environment at 0% RH and results are presented in Figure 4.28. The presenting results show that the resistance of the sensors has increased by 1.43%±0.15%, 2.3%±0.23% and 3.45%±0.35% for 5, 10 and 15 ppm of nonanal respectively. The percentage of resistance change was similar in all sensors independent of their initial value. Higher standard deviation is noticed compared to PEI/CB sensors because the sensors are fabricated using drop casting method which provides a random network of GNPs and reproducibility depends on the amount of the material drop-casted on IDEs. This indicates successful fabrication of similar sensors across the electrodes. The drop casting method gives non-uniformly distributed GNP's which can only be achieved by the drop casting method giving more sensitivity to various VOCs. This method has been shown to fabricate a more sensitive sensor than the sensors fabricated using a layer-by-layer method. The result in Figure 4.24 shows that the response of the sensors does not come back at the same base level but becomes stable before coming to the same initial value of resistance. This could be due to the fact that some molecules of nonanal undergo chemisorption and are embedded into the GNP network, changing the initial resistance of the sensors by a small value. The sensors reach a steady state in a short time period. The sensor′s response time is estimated to

be about 180 sec for reaching up to 90% of the resistance change. These results show that the proposed fabrication method leads to the development of a highly sensitive sensor over IDEs. The fabricated sensors present a linear response in interaction with nonanal.

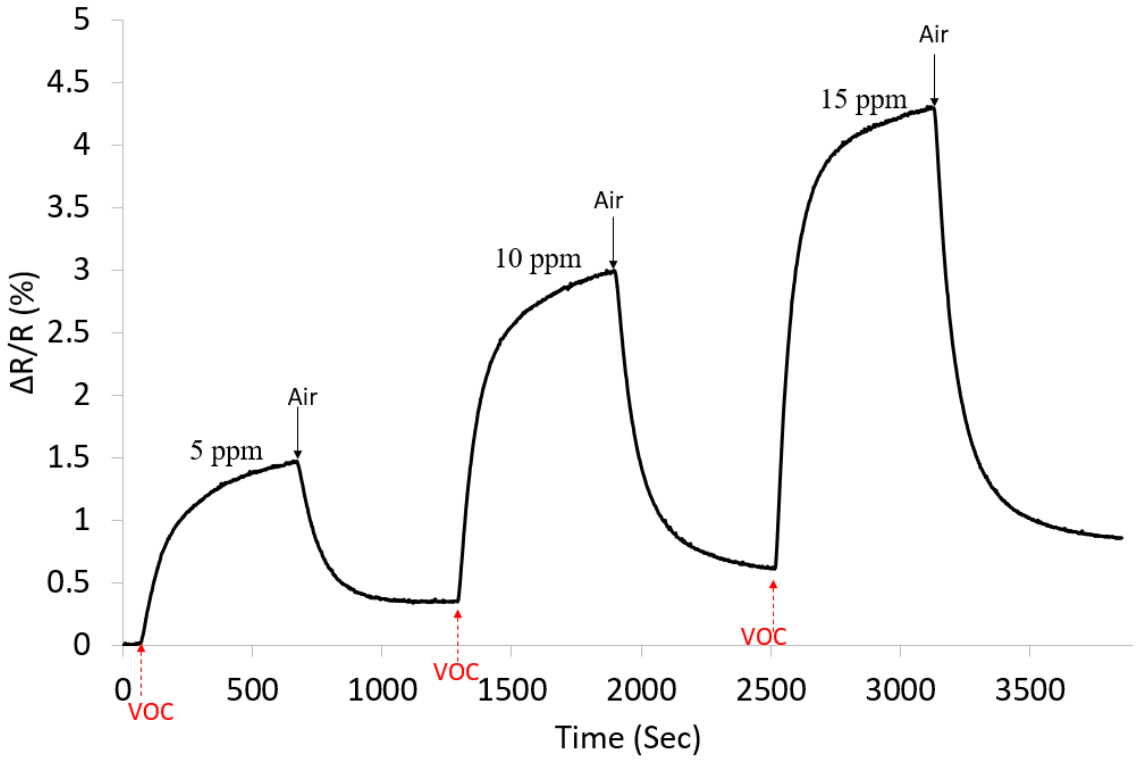

Fig. 4.24. Response of f-GNP Sensor to Nonanal at a concentration of 5 ppm, 10 ppm, and 15 ppm

The sensor results for smaller concentration (400 ppb 3 ppm) are also presented in Figure 4.25. A resistance change of 0.20%, 0.32%, 0.5% and 0.9% for 400 ppb, 1 ppm, 2 ppm and 3 ppm respectively were observed for the fabricated sensors. A slight increase in the baseline resistance after each cycle is observed and this is due to the fact that nonanal can stay among the f-GNPs network even after the flow is stopped, as a result increasing the resistance by a small amount.

The calibration curve of the fabricated sensors in response to nonanal is presented in Figure 4.26. The presenting results show that the proposed f-GNP sensors can be

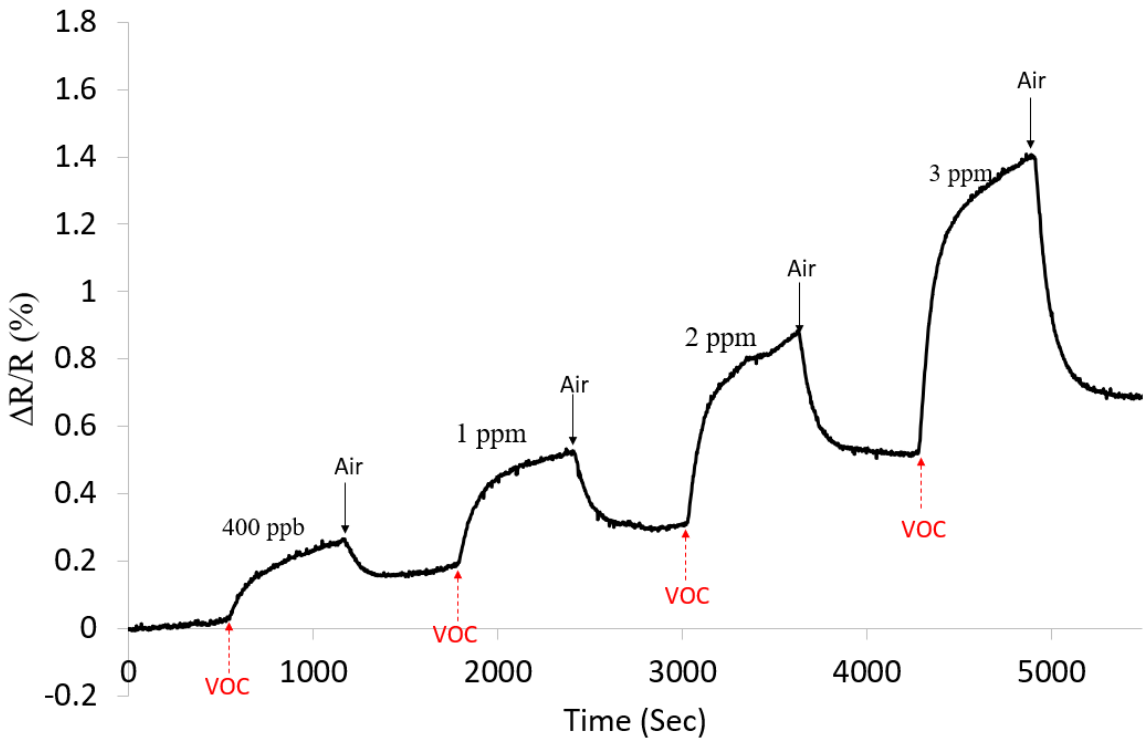

Fig. 4.25. f-GNP Sensor Response to Nonanal at 400 ppb, 1 ppm, 2 ppm, and 3 ppm concentration

used to detect a wide range of nonanal (400 ppb to 15 ppm) and can even detect smaller concentrations. The calibration curve is provided with the calibration curve for a smaller range of 400 ppb to 3 ppm within. The calibration curve shows a nearly linear relation between the sensor$'s$ resistance change and the concentration of the VOC. This linear behavior is favorable and makes it possible to predict the concentration of the targeting VOC accurately via such a calibration curve.

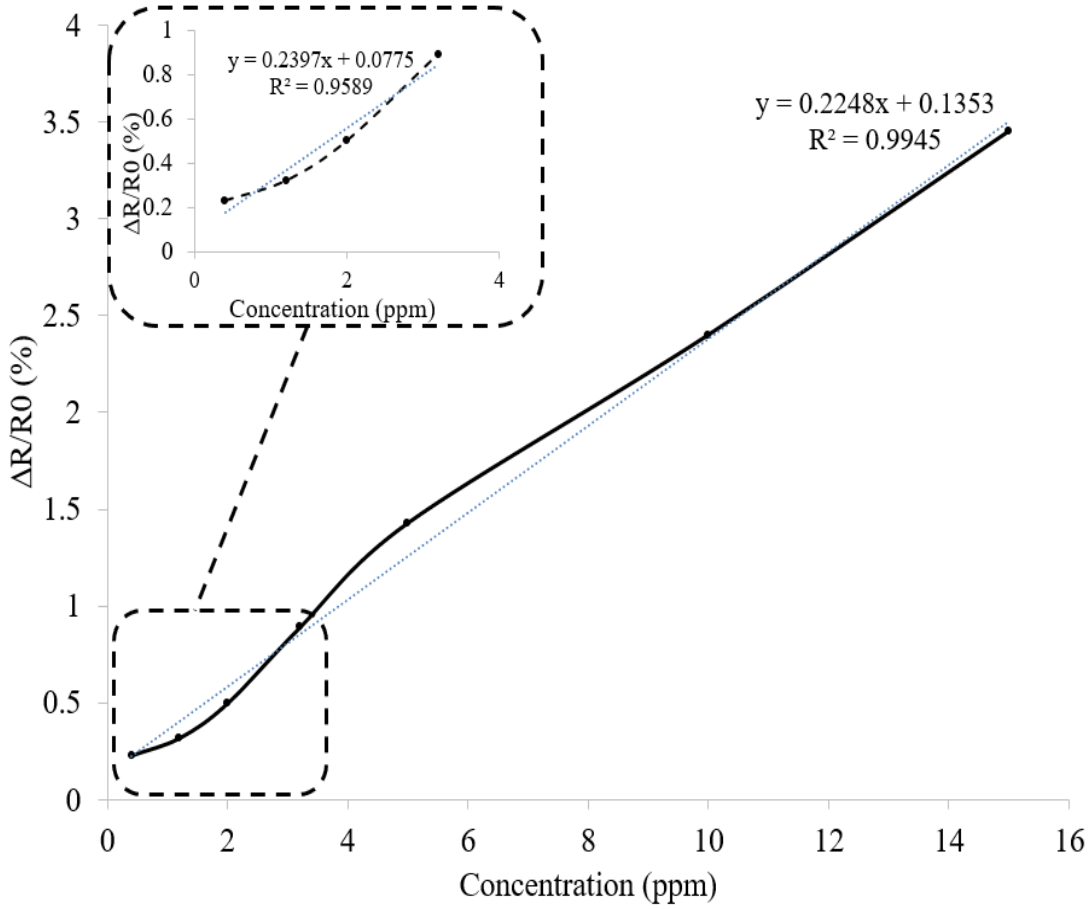

Fig. 4.26. Calibration Curve of f-GNP Sensor towards Nonanal from 400 ppb-15 ppm

Sensitivity and Selectivity of f-GNP Sensor

The sensitivity of the fabricated sensor can be described as the slope of the calibration curve for the VOC. The sensitivity of the f-GNP sensor has been investigated thoroughly by introducing them to different concentrations of nonanal (5 - 15 ppm), dodecane (5- 15 ppm), 2-nonanone (5 - 15 ppm) and 1-octanol(5 - 15 ppm). The sensors response to concentrations of at 5 ppm of nonanal, 2-nonanone, dodecane, and 1-octanol was 1.43%±0.155%, 0.45%±0.05%, 0.43%±0.048%, and 1.68%±0.19%. At 10 ppm the sensor$'s$ response to nonanal, dodecane, 2-nonanone, and 1-octanol was 2.65%±0.29%, 0.62%±0.07%, 1.2%±0.135% and 2.70%±0.30% respectively and at 15 ppm the change observed is 3.6%±0.395%, 1.25%±0.14%, 2.25%±0.25%, and 3.6%±0.4% respectively. The actual sensor results for 1-octanol, 2-nonanone and dodecane is presented in Figures 4.27, 4.28 and 4.29. The presenting results show that the sensors are sensitive toward dodecane, 2-nonanone and 1-octanol which are important VOCs linked to different metabolic pathways. Figure 4.27 shows the f-GNP sensor response towards 1-octanol showing a fast response time of 100 sec to reach 90% of the resistance change. Figure 4.28 and 4.29 shows the sensor response to 2-nonanone and dodecane respectively and it is observed that the sensor does not get stable in the presence of VOC in 10 minutes which shows that the sensor has a higher response time for 2-nonanone and dodecane.. The reason for such high sensitivity for the fabricated 1-Mercapto-(triethylene glycol) methyl ether functionalized GNP sensors is because of multiple double bonded oxygen atoms connected to alkyl chain connected to the gold core. Each double bonded oxygen atom has two lone pair which makes hydrogen bonds with hydrogen donor VOCs. This makes it highly reactive to hydrocarbon VOC analytes. The calibration curve for the VOCs has been presented in Figure 4.30 that helps find the sensitivity of the f-GNP sensor to each VOC. This calibration curve helps to compare the sensitivity of the f-GNP sensor towards various VOCs over a wide range of concentration.

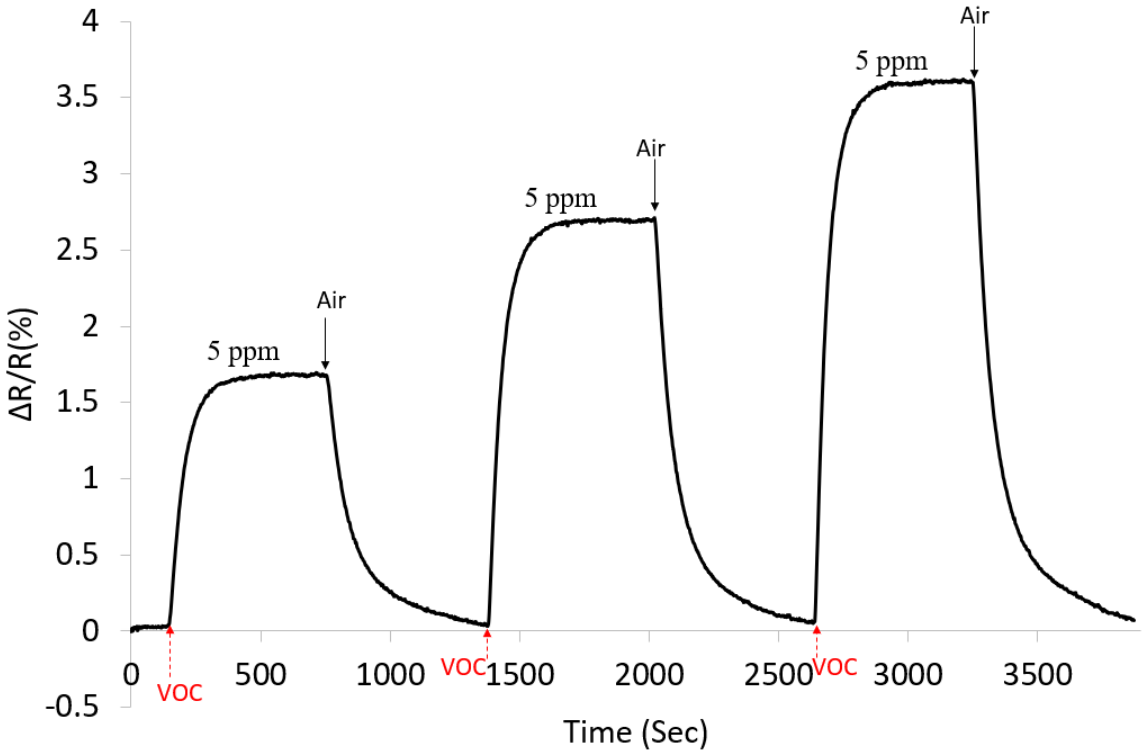

Fig. 4.27. Response of f-GNP Sensor to 1-octanol at a concentration of 5 ppm, 10 ppm and 15 ppm

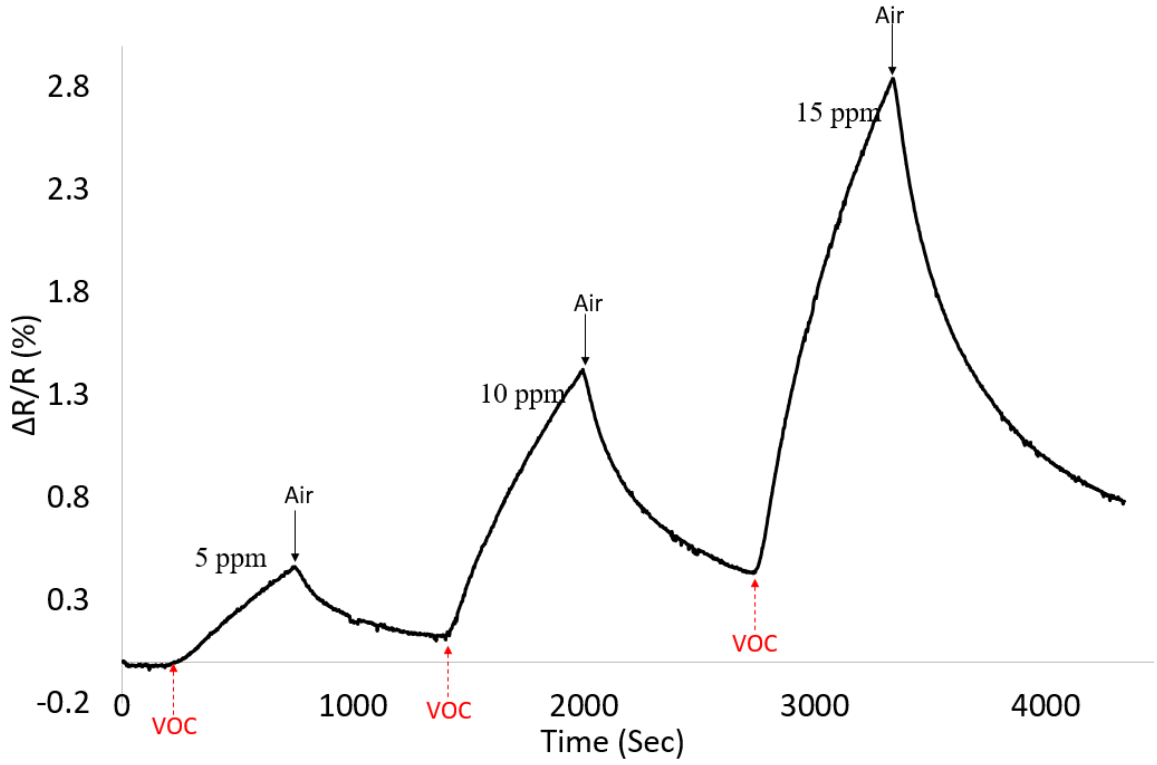

Fig. 4.28. Response of f-GNP Sensor to 2-nonanone at a concentration of 5 ppm, 10 ppm and 15 ppm

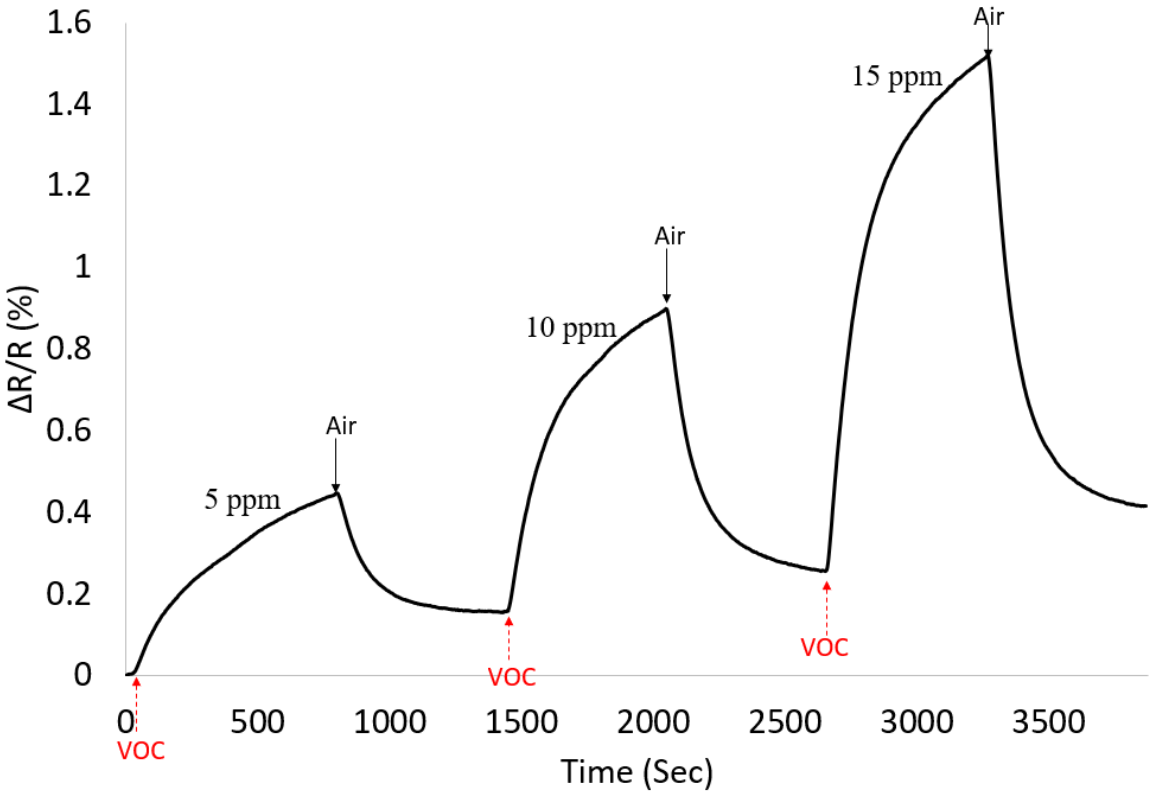

Fig. 4.29. Response of f-GNP Sensor to Dodecane at a concentration of 5 ppm, 10 ppm, and 15 ppm

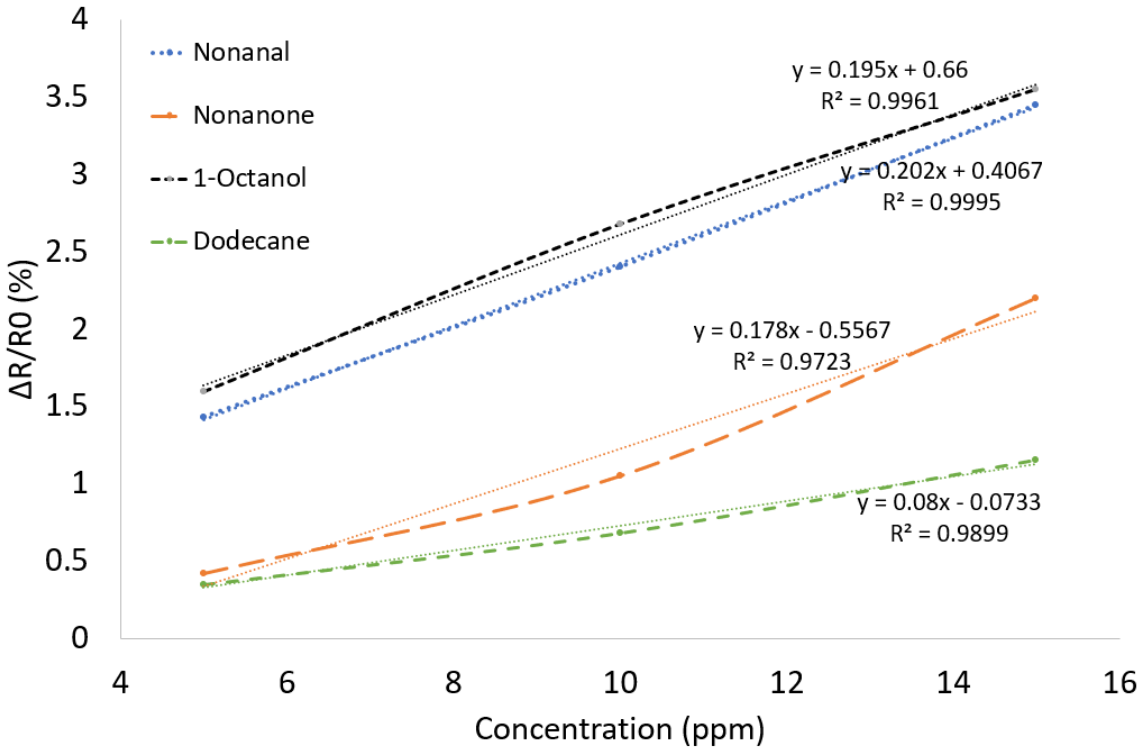

Fig. 4.30. Calibration Curve for f-GNP Sensor towards Nonanal, 1-Octanol, 2-Nonanone and Dodecane from 5 ppm to 15 ppm

The sensitivity of f-GNP sensors towards VOCs is calculated using a calibration curve by determining the slope of the curve for each VOC. From the calibration curve, the sensitivity for different VOCs is found to be 0.202% per ppm for nonanal, 0.195% per ppm for 1-octanol, 0.182% per ppm for 2-nonanone and 0.08% per ppm for dodecane. The sensitivity bar graph of the fabricated sensor towards different VOCs has been presented in Figure 4.31. The presented result indicates the high sensitivity of the f-GNP sensors toward nonanal as well as other VOCs too. This is due to an ether functional group that does not have any O-H bond, hence cannot act as hydrogen bond donors but compounds with hydrogen bonding capacity can be dissolved in ether by making bonds to free electron pairs on each side of ether oxygen atoms.

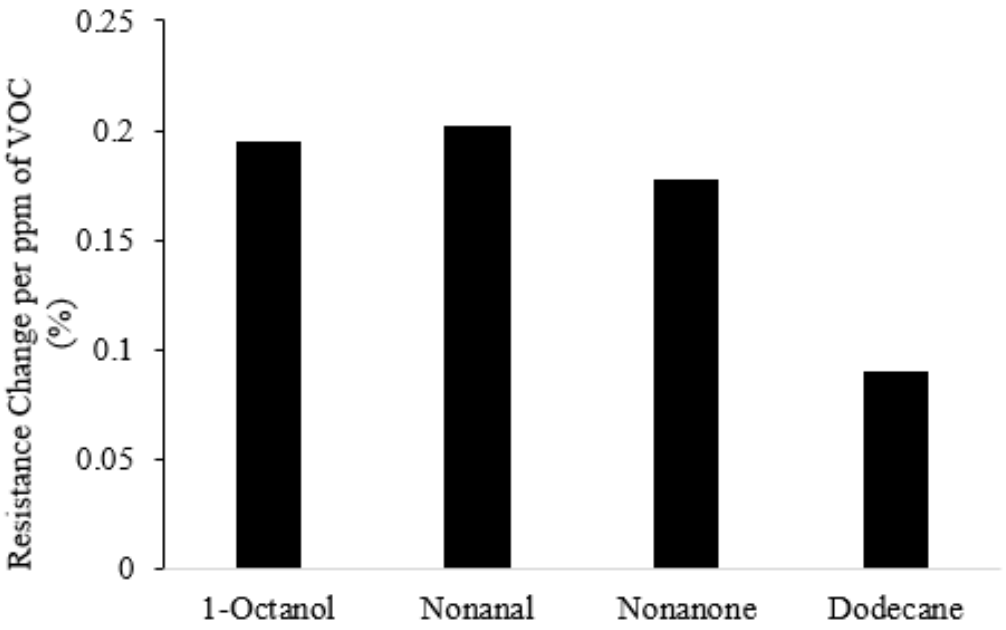

Fig. 4.31. Sensitivity of f-GNP Sensor towards different VOCs per ppm

Further, the selectivity of the fabricated sensor towards nonanal is calculated using Formula 4.2.

$$SensorSelectivity(Nonanal) = \frac{Sensitivity_{Nonanal}}{Sensitivity_{VOC}} \tag{4.2}$$

For the f-GNP sensors, the sensor$'s$ selectivity towards nonanal is 2.25 times with respect to dodecane and approximately 1.03- and 1.13-times w.r.t 1-octanol and 2-nonanone respectively. The selectivity bar graph for the f-GNP sensor is presented in Figure 4.32 and the results show that the sensor is not very selective towards nonanal. The reason for low selectivity is high sensitivity to each of the targeting VOCs.

Response of f-GNP Sensor to Water Vapor

In order to evaluate f-GNP sensor$'$s response to humidity, the fabricated sensors were exposed to R.H of 25% and 45% for a time duration of 10 min each. The sensors response to water vapor is presented in Figure 4.33.

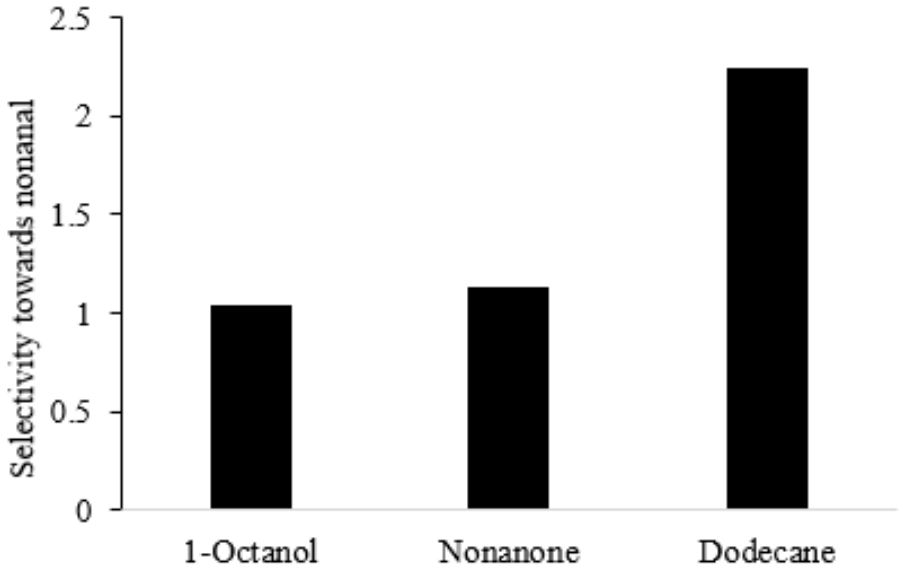

Fig. 4.32. Selectivity of f-GNP Sensor towards Nonanal compared to 1-Octanol, Nonanone and Dodecane

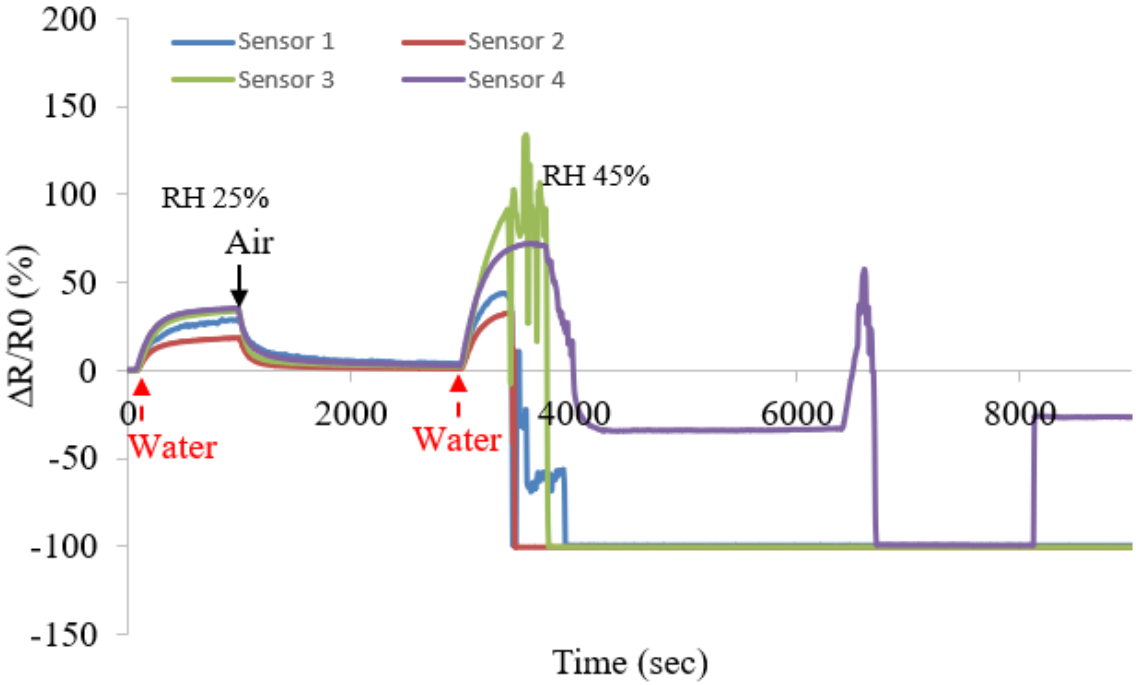

Fig. 4.33. GNP Sensor Response at RH of 25% and 45%

At 25% RH, the f-GNP sensor shows an average resistance change of approximately 30% showing high affinity to water. The presenting results also show that the fabricated sensors could not tolerate RH of 45% and gets damaged showing resistance of the only 100 ohm. This is due to the reason because water is one of the solvents for f-GNP and coagulate the GNPs cores particles into a bigger particle which makes the initial resistance to drop in the range of a hundred ohms. This high affinity for water for f-GNPs is due to the fact that water is a solvent for these f-GNPs. 1-Mercapto-(triethylene glycol) methyl ether functionalized GNPs are soluble in water because ether has two polar C-O bonds which create a dipole moment resulting in its high affinity to water.

4.2.3 F-GNP/PEI Sensor

Sensors were fabricated with the method described in Section 3.2.4 and 3.2.5 and tested with the experimental set-up presented in Section 3.3. The results of the response of the sensor with interaction to the VOCs are presented in terms of relative response (RR) using Formula 4.1. The presented results show the average of four devices and the error bar describes the standard deviations of the sensors.

Relative Response of f-GNP/PEI Sensor to Nonanal

F-GNP/PEI sensors fabricated on one substrate were exposed to 5, 10, and 15 ppm of nonanal for one cycle each and results are presented in Figure 4.34. The presenting results show that the resistance of the sensors has increased by 1.15%±0.115%, 2.2%±0.22% and 3.25%±0.325% for 5 ppm, 10 ppm and 15 ppm of nonanal respectively. The percentage of resistance change was similar in all sensors independent of their initial value. Higher standard deviations were noticed because the f-GNP material was drop casted which provide a random network of GNPs. Spin coating of PEI on top of fabricated f-GNP gives a highly uniform film and due high affinity of PEI to nonanal, there is less than 8% drop in resistance change of the sensor towards

nonanal at 15 ppm compared to the f-GNP sensor without a PEI layer. The result in Figure 4.34 shows that the response of the sensor comes back at the same resistance level indicating that the PEI layer improves absorption and desorption of the VOC molecules. The sensors reach the steady state in a short time period and the response time is estimated to be about 160 sec for reaching up to 90% of the resistance change. Both the materials used to fabricate the f-GNP/PEI sensor show high affinity to aldehydes such as nonanal. F-GNP has lone pair of electrons at each double bonded oxygen site which makes it sensitive to nonanal and while PEI has closed bonded structure to achieve chemical stability, but still nonanal acts as one of the solvents for PEI. The sensitivity of both the materials towards nonanal gives such high resistance change at lower concentration even after having thicker sensing layer as compared to f-GNP sensors. These results show that the proposed fabrication method leads to the development of a highly sensitive sensor over IDE. The fabricated sensors present a linear response in interaction with nonanal.

The sensor results for smaller concentration (400 ppb to 3 ppm) are presented in Figure 4.35. The sensor results show a resistance change of 0.08%, 0.19%, 0.32% and 0.8% at 400 ppb, 1 ppm, 2 ppm and 3 ppm respectively. The resistance value goes below than initial resistance value and this can be explained by the reason that some VOC molecules from previous experiments come off the PEI layer when the flow of nonanal is stopped. These results show that f-GNP with PEI is able to detect nonanal even in the range of ppb due to their high sensing ability for nonanal.

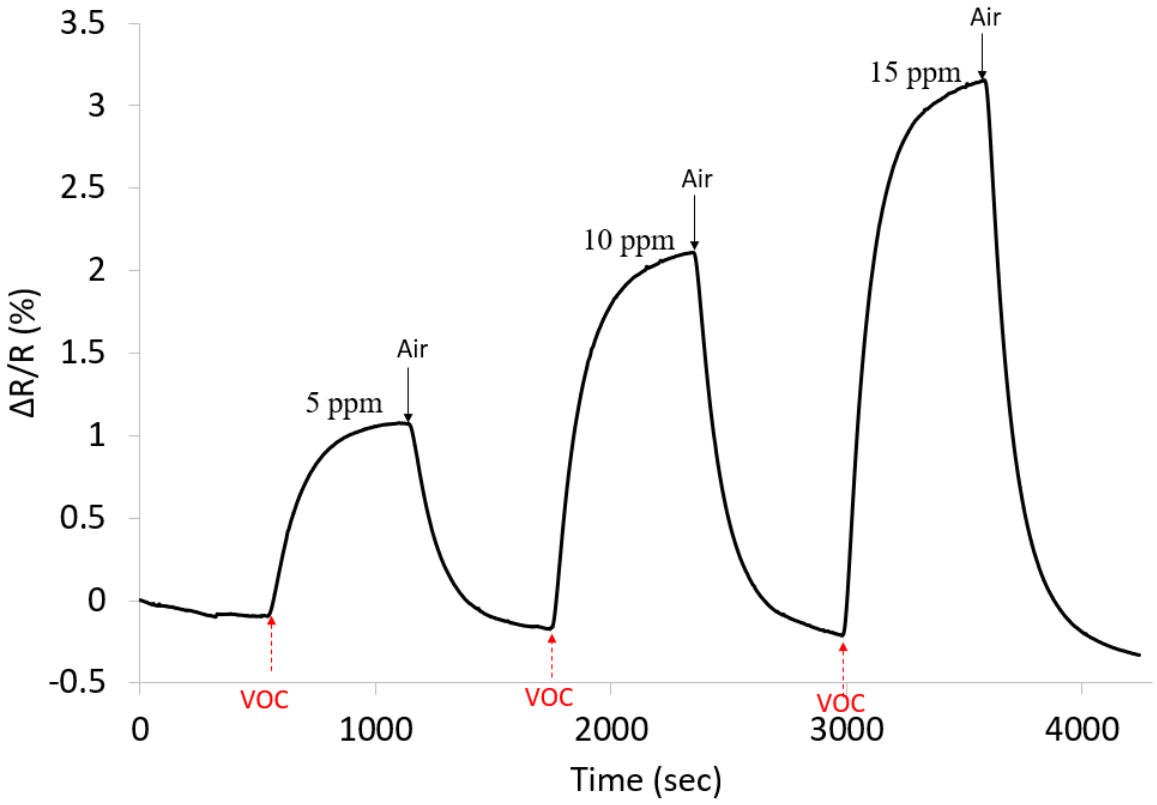

Fig. 4.34. Response of f-GNP/PEI Sensor to 5 ppm, 10 ppm, and 15 ppm of nonanal

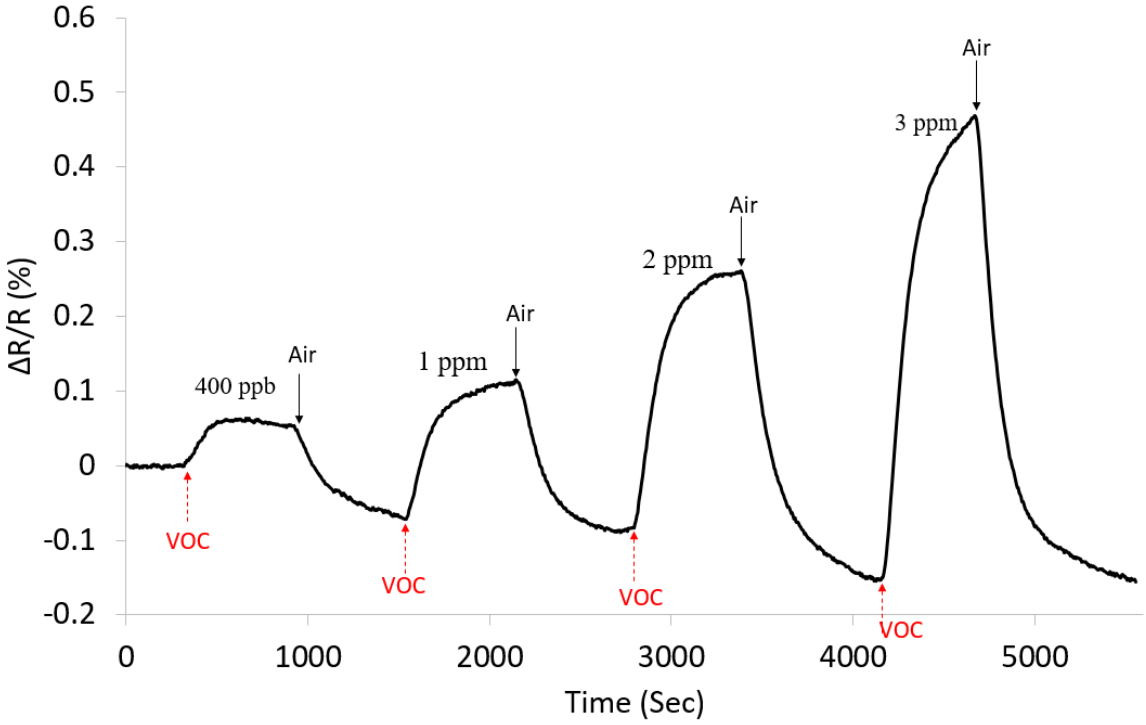

Fig. 4.35. Response of f-GNP/PEI Sensor to Nonanal at Smaller Concentrations (400 ppb to 3 ppm)

The calibration curve of the fabricated sensors in response to nonanal is presented in Figure 4.36. The calibration curve for a wider range of 400 ppb to 15 ppm is provided with the calibration curve for a smaller range of 400 ppm to 3 ppm within. The presenting results show that the proposed f-GNP/PEI sensor can be used to detect a wide range of nonanal and can even detect smaller concentrations. Linear regression shows a nearly linear relationship between the sensor$'s$ resistance change and concentration of the VOC. This linear behavior is favorable and makes it possible to predict the concentration of the targeting VOC accurately via such a calibration curve.

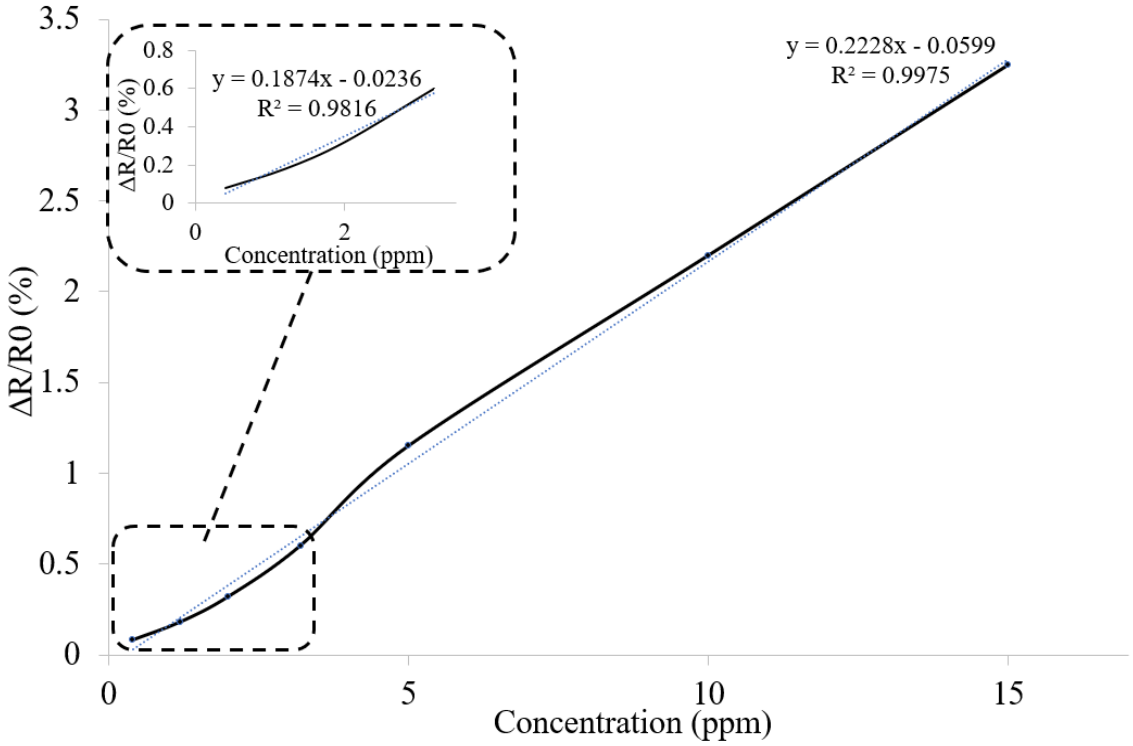

Fig. 4.36. Calibration Curve for f-GNP/PEI Sensor towards Nonanal from 400 ppb to 15 ppm

Sensitivity and Selectivity of f-GNP/PEI Sensor

The sensitivity of the fabricated sensor can be described as the slope of the calibration curve for the VOC. The sensitivity of the f-GNP/PEI sensor has been investigated by introducing them to different concentrations of dodecane (hydrocarbon), 2-nonanone (ketone), and 1-octanol (alcohol). The sensor′s response to concentrations of 15 ppm nonanal, 2-nonanone, dodecane, 1-octanol was 3.25%±0.325%, 0.7%±0.07%, 0.24%±0.024%, and 1.05%±0.105% respectively. The actual sensor results for 1-octanol, 2-nonanone and dodecane are presented in Figures 4.37, 4.38 and 4.39. Figure 4.37 shows the sensor results with 1-octanol and resistance change of 0.4%, 0.7%, and 1.05% was observed for 5, 10 and 15 ppm respectively. Short re-

sponse time of 110 sec was observed to reach 90% of the resistance change. Figure 4.38 shows a resistance change of 0.35%, 0.58% and 0.7% with 100, 150 and 200 ppm of 2-nonanone respectively. Response time of 110 sec was observed at each concentration of nonanone. This also shows that the fabricated f-GNP/PEI sensor does not detect 2-nonanone at 15 ppm and presents a limit of detection of 50 ppm. Figure 4.39 shows a resistance change of 0.07%, 0.16% and 0.24% with 5, 10 and 15 ppm of dodecane respectively. The approximate response time is about 130 sec to reach 90% of the resistance change. The sensor response to 2-nonanone and dodecane shows that after adding the PEI layer on top of f-GNP, it improves the absorption and desorption of VOCs from the PEI film.

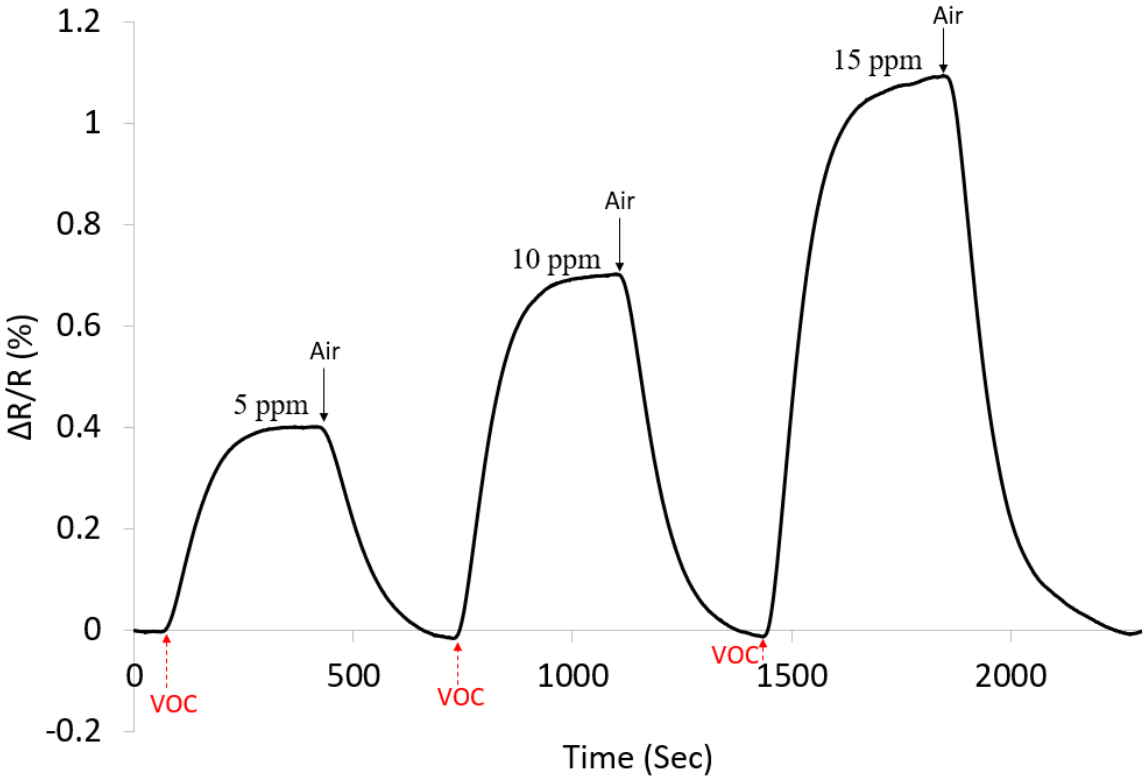

Fig. 4.37. Response of f-GNP/PEI Sensor to 1-Octanol at 5, 10, and 15 ppm

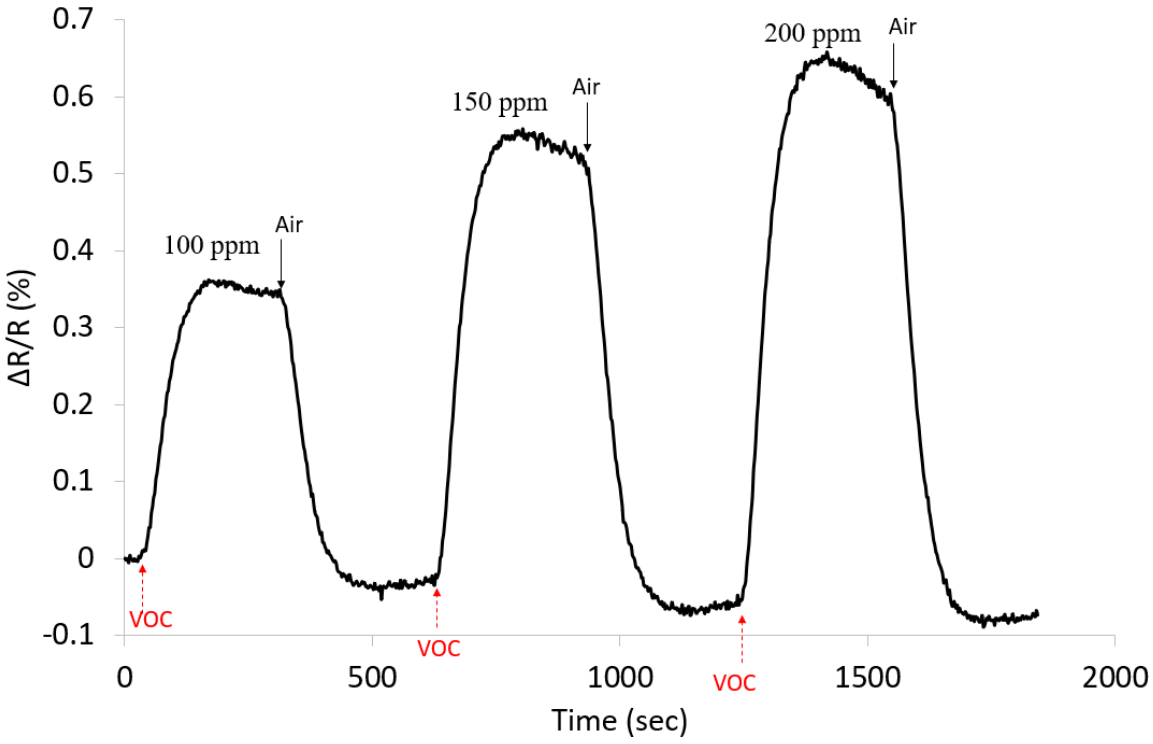

Fig. 4.38. Response of f-GNP/PEI Sensor to 2-Nonanone at 100, 150, and 200 ppm

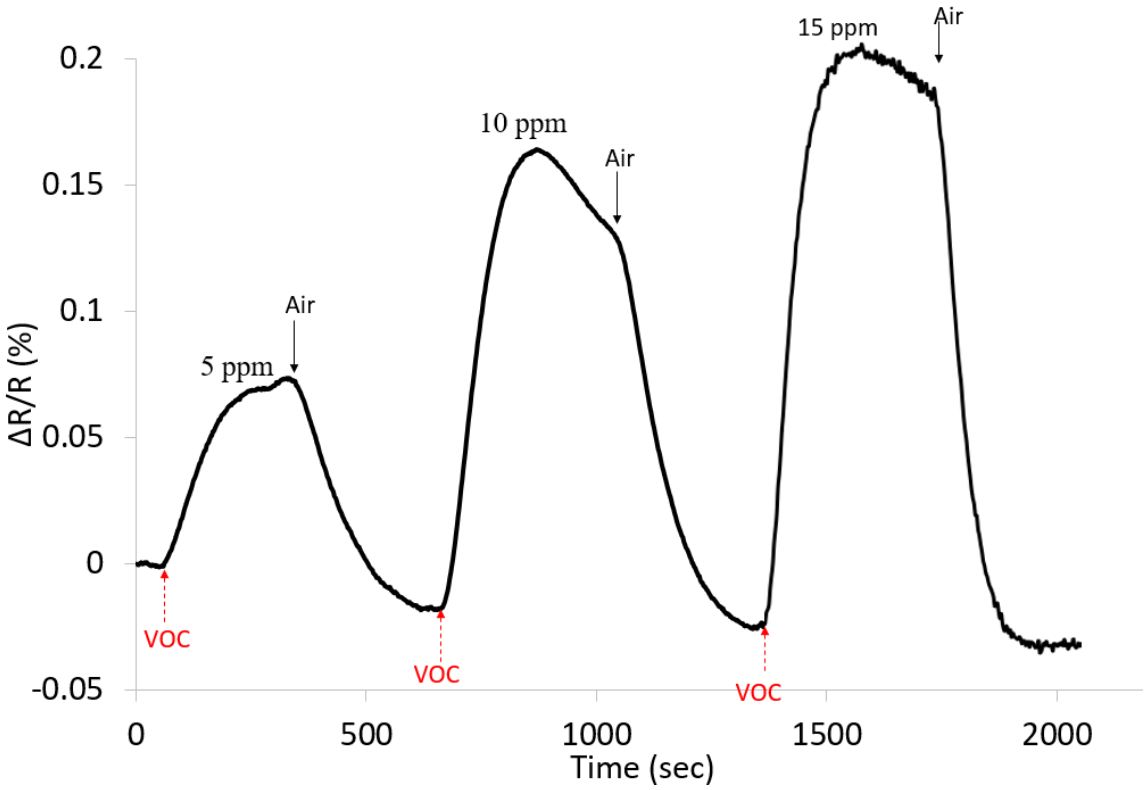

Fig. 4.39. Response of f-GNP/PEI Sensor to Dodecane at 5, 10, and 15 ppm

The calibration curve for the VOCs has been presented in Figure 4.40. The presenting results show that the fabricated sensors are highly sensitive towards nonanal than other targeting VOCs.

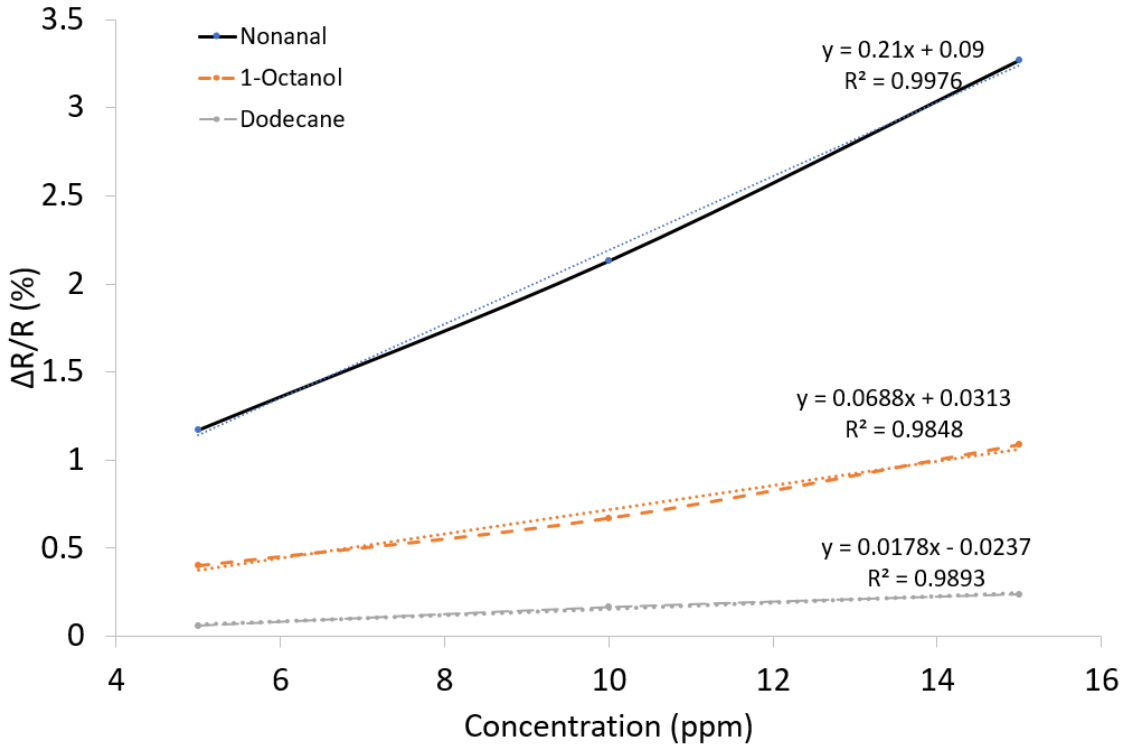

Fig. 4.40. Calibration Curve for f-GNP/PEI Sensor towards Nonanal, 1-Octanol and Dodecane

The sensitivity of the sensor which is defined as the calibration curve of the VOC is presented in Figure 4.41 in the form of a bar chart showing the sensitivity of 0.21%, 0.043%, 0.017% and 0.0035% per ppm of nonanal, 1-octanol, dodecane, and 2-nonanone respectively. This high sensitivity towards nonanal is observed because aldehydes such as nonanal are a solvent for PEI and closed bonded structure of PEI prevents reacting to another hydrocarbon VOCs. This in combination with sensing capabilities of f-GNP which shows high sensitivity towards nonanal is the reason for such high sensitivity for f-GNP/PEI sensors.

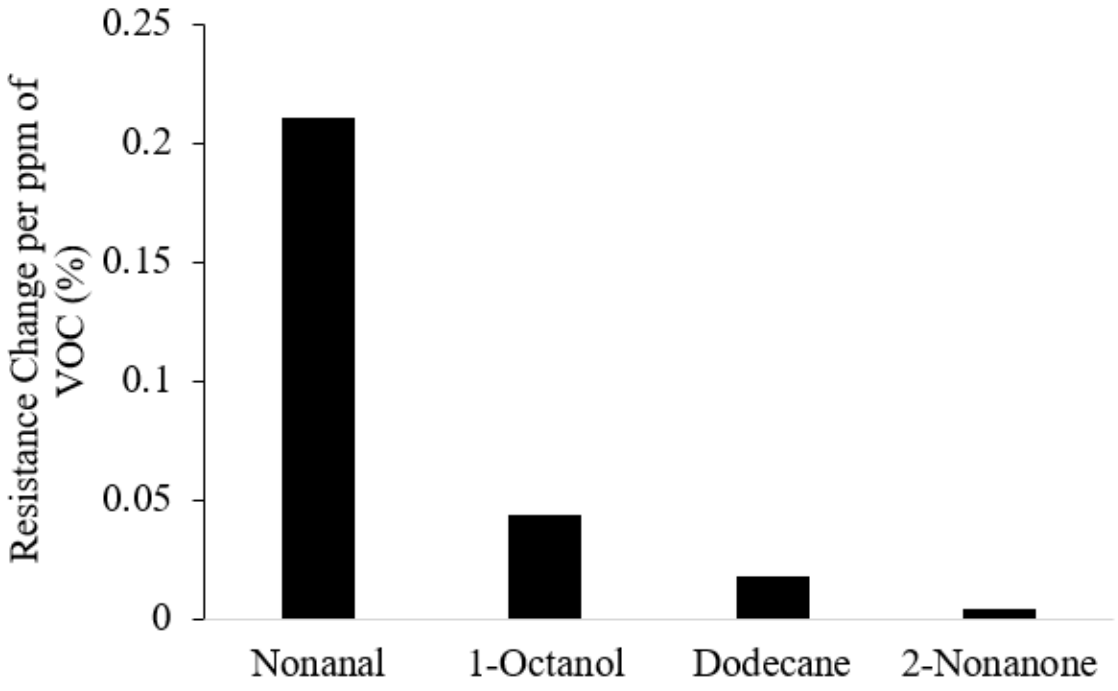

Fig. 4.41. Sensitivity of f-GNP/PEI Sensor towards various VOCs per ppm

Further, the selectivity of the fabricated sensor towards nonanal is calculated using Formula 4.2. For f-GNP/PEI sensor, the sensor′s selectivity towards nonanal is 12.5 times with respect to dodecane, 5 times w.r.t 1-octanol and 60 times w.r.t 2-nonanone. The selectivity bar graph for the f-GNP/PEI sensor is presented in Figure 4.42 and the results show that the sensor is highly selective towards nonanal. A comparison between the selectivity of f-GNP and f-GNP/PEI sensor has been made in Figure 4.43 showing the improved selectivity of the sensor on the incorporation of PEI as a sensing layer. It is observed that the f-GNP/PEI sensor is highly sensitive towards nonanal as compared to f-GNP sensor because of incorporating PEI on top of f-GNP by the spin coating method which lowers the sensing of f-GNP towards other VOC molecules except nonanal. This is because PEI is formed by internal bonding and does not have any loose electrons to bond with other molecules but nonanal. This helps maintain the sensing f-GNP/PEI sensor towards nonanal.

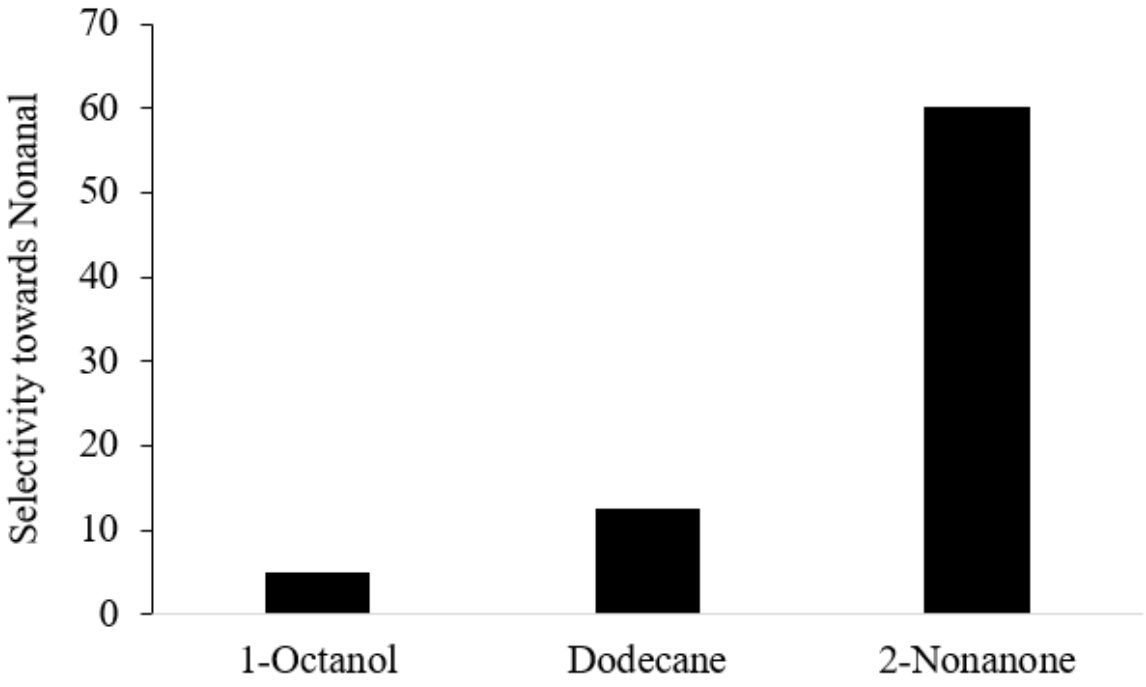

Fig. 4.42. Selectivity of f-GNP/PEI Sensor towards Nonanal

GNP/PEI Sensor Response to Water Vapor

In order to evaluate f-GNP/PEI sensor′s response to humidity, the fabricated sensors were exposed to different concentrations of nonanal at 50% and 85% RH environment. The reason for testing at such high humidity is to determine if the f-GNP/PEI sensor can tolerate harsh environment conditions and also the working humidity range for industries and homes is from 30 - 70%. The sensors were stabilized in an environment with R.H 50% and 85%. The relative response of f-GNP/PEI sensor to 5, 10 and 15 ppm of nonanal at R.H of 50% and RH of 85% are presented in Figure 4.44 and Figure 4.45. The presenting results show that the sensor′s sensitivity increased at 50% and 85% RH as compared to in dry air. The sensors showed increased resistance change of 1.75%, 3.87% and 6.3% at 5 ppm, 10 ppm and 15 ppm respectively in 50% RH conditions and increased resistance change of 9.14%, 19.6% and 34.9%

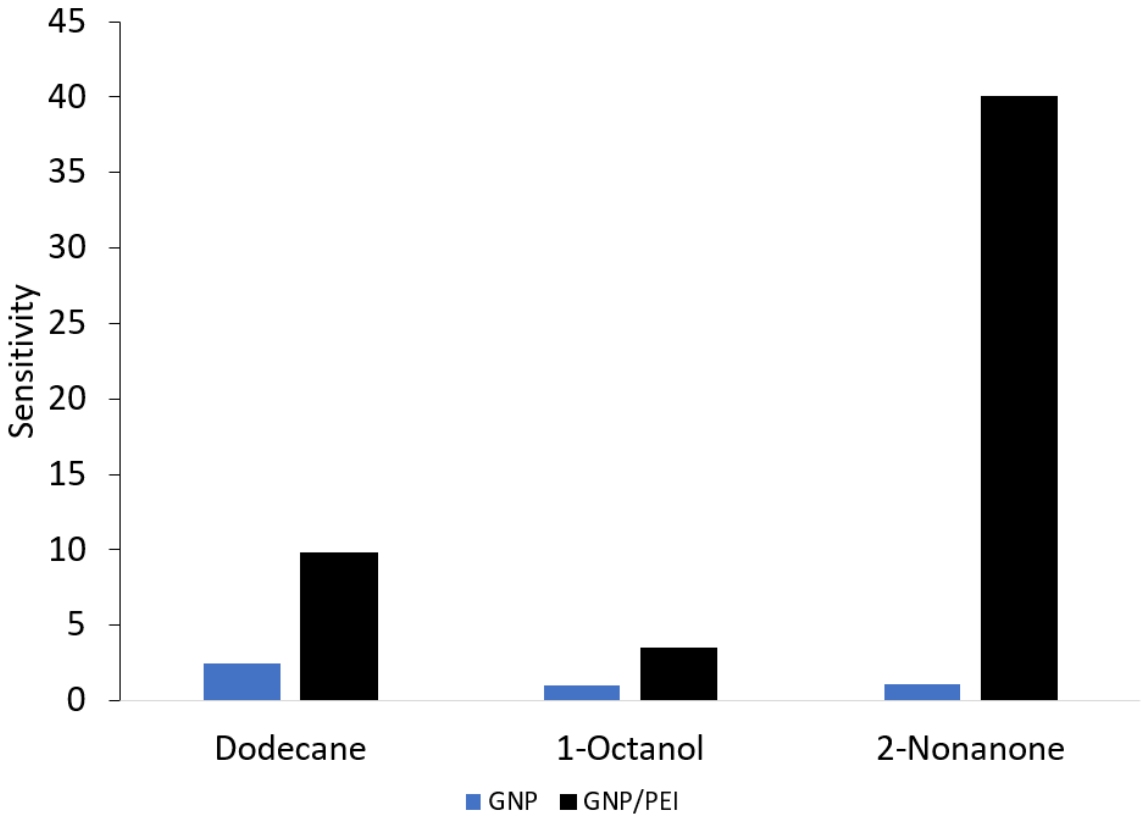

Fig. 4.43. Selectivity Comparison between f-GNP and f-GNP/PEI Sensor

at 5 ppm, 10 ppm and 15 ppm of nonanal respectively in 85% RH condition. The presenting results show that the fabricated sensors could tolerate prolonged exposure to water vapor. No sensor was damaged after exposure to water vapor with R.H of up to 85% for 10 min. These results agree with characterization results from contact angle measurements and show that the proposed sensors would not be highly sensitive to interfering water vapor in the air. This also proves the importance of heat treatment of spin coated PEI to achieve a hydrophobic PEI layer for the sensor.

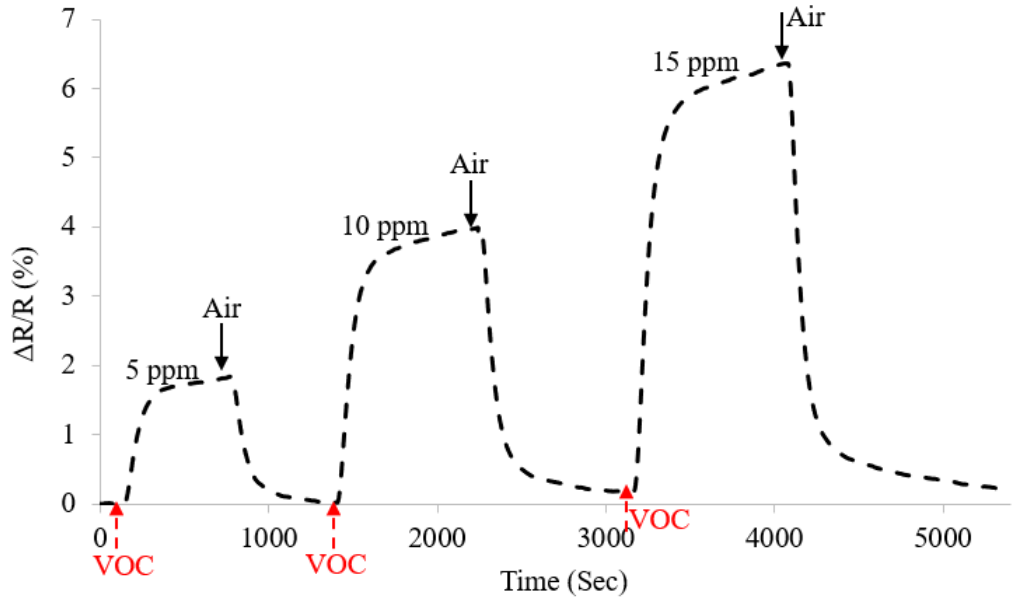

Fig. 4.44. Response of f-GNP/PEI Sensor to Nonanal from 5 - 15 ppm at 50% RH

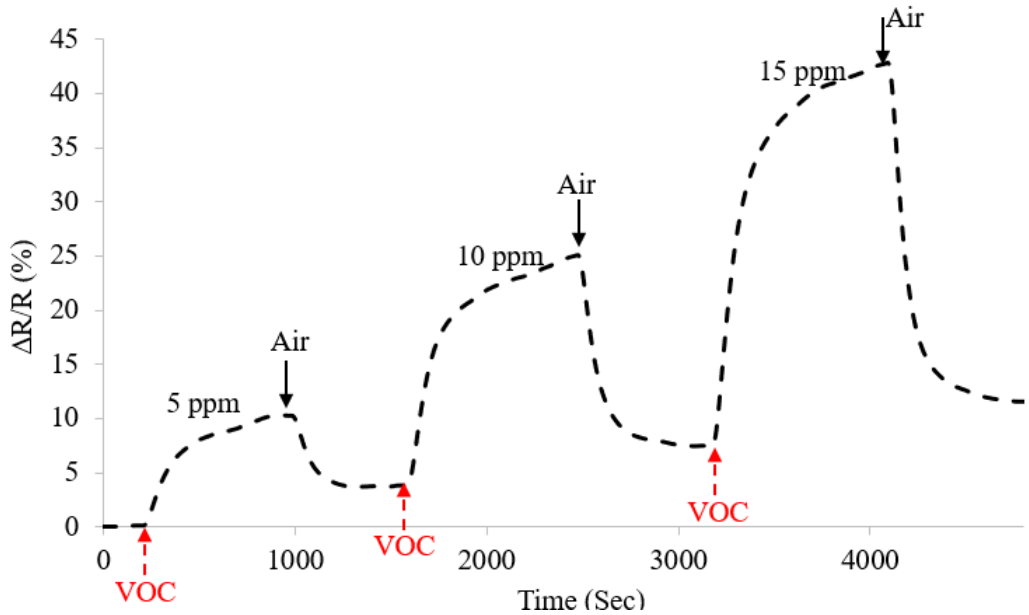

Fig. 4.45. Response of f-GNP/PEI Sensor to Nonanal from 5 - 15 ppm at 85% RH

Comparison of Fabricated Sensors to Related Work

In order to determine the effectiveness of our fabricated sensors, the sensitivity of the sensors is compared with other related work and make comparison whether the sensors work in similar range or better than the previously fabricated sensors by other researchers. Kahn et al. present one of the very few research articles that present a GNP based sensor that has nonanal as one of the VOCs among others such as styrene, ethanols and propionitrile [10]. Five different thiol protected GNP sensors are presented in this paper which are 2-nitro 4-trifluormethylbenzenethiol (NTMBT) GNP, 4-chlorobenzene methanethiol (CBMT) GNP, 3-ethoxythiophenol (ETP) GNP, 4-tertButylbenzenethiol (tBBT) GNP and 2-Naphthalenethiol (NT) GNP sensor. Each sensor is tested at different concentration but to make a comparison, 1 ppm VOC concentration is chosen. A comparison bar graph between our work and Kahn et. al work is presented in Figure 4.46. The results in the presented figure show the resistance change (%) of the sensor with 1 ppm of nonanal and observed that our work is comparable to other work that has been already published. Not much work has been done on detecting nonanal but other aldehydes such as formaldehyde have been presented in other papers. Hosono et al. presented 4-ethylbenzenesulphonic acid doped polypyrrole polymer film to report a 40% resistance change to 500 ppm of formaldehyde [130]. Zheng et al. reported a frequency change of 100Hz with 150 ppm of formaldehyde using Polyaniline/TiO_2 polymer composite QCM sensor [131].

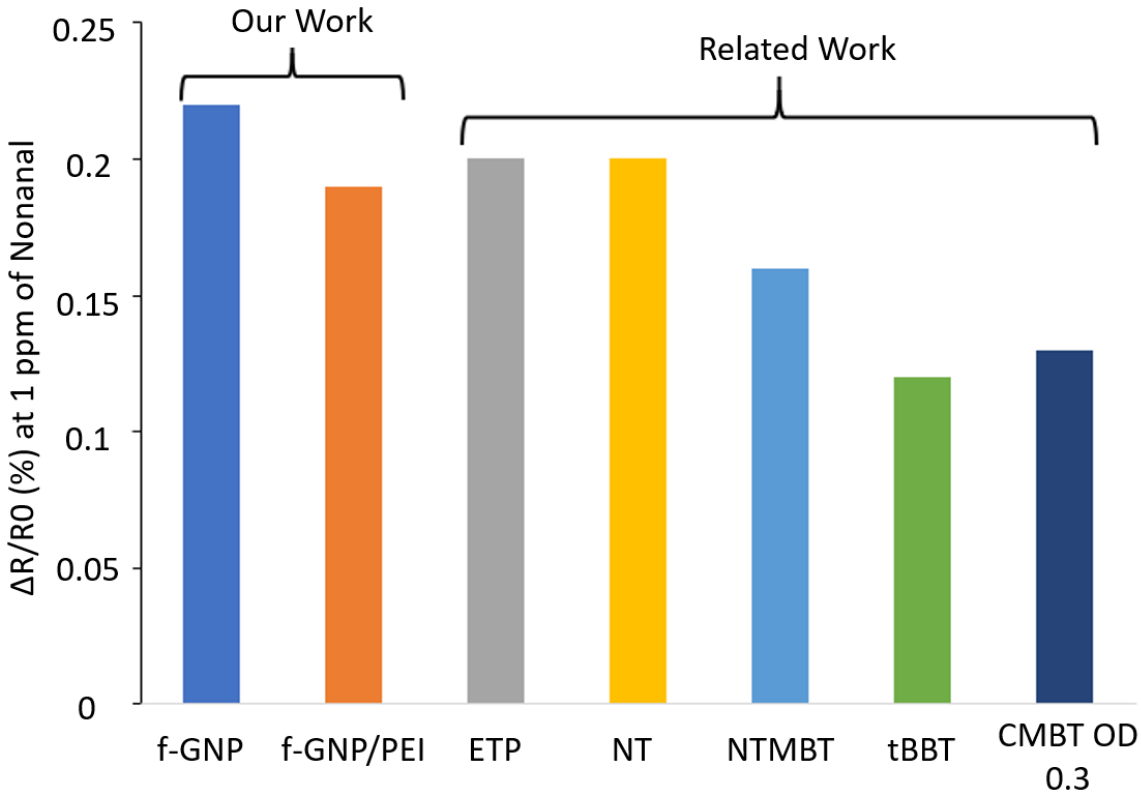

Fig. 4.46. Comparison of presented work to other Related work

Fabrication challenges for f-GNP and f-GNP/PEI sensor

Formation of the conducting network of 1-Mercapto-(triethylene glycol) methyl ether functionalized GNPs is achieved after the evaporation of the solvent (ethanol) by drop casting method. Drop casting is not known as a reproducible fabrication method because it forms a non-uniform random network of f-GNPs. The surface properties of the substrate (IDEs) and the concentration of f-GNPs in the ethanol plays an important role in the development of the proposed sensor. It should be noted that fabrication the f-GNPs on the IDEs with different surface properties than the one used in this study could result in the development of less sensitive sensors. Also, surface chemistry while fabricating the f-GNP and f-GNP/PEI sensor is very important. Change in the fabrication steps would also change the surface chemistry between the substrate and f-GNPs, between f-GNPs and environment, and between f-GNPs and PEI. This would result in different sensor results than presented here. For example, the attempts on the development of the sensors on a more hydrophilic substrate or altering the fabrication steps would result resulted in less sensitive sensors. It is also important to consider that sonicating the f-GNPs for a long period of time and degradation of the material over time can also lead in the development of f-GNP and f-GNP/PEI sensors with lower sensing properties.

5. CONCLUSION AND FUTURE WORK

In this chapter, conclusion if given for the fabricated sensors in Section 5.1 describing what work has been achieved. Section 5.2 gives an insight into the future work that can be performed using these sensors and develop a real-time breath sensor monitoring system.

5.1 Conclusion

The major goal for this project was to develop a resistive based sensor that can detect nonanal which presents the lowest p-value among other important VOCs among lung and breast cancer patients. To develop a chemiresistive based sensor using conductive polymer composite, a polymer PEI was chosen after intensive literature review because PEI has aldehydes as a solvent while it is chemically stable to other chemicals such as alcohols, alkane, and ketones. After careful study for the fabrication method, the spin coating method was used to fabricate the sensors because it can provide highly uniform thin film with high repeatability. Heat treatment step was incorporated in the fabrication of sensors because it increases the hydrophobicity of the PEI/CB film. The fabricated PEI/CB sensor shows 0.021% resistance change per ppm of nonanal which is 10 times more than the next VOC the sensor is sensitive to. This indicated that the PEI/CB can detect nonanal with high selectivity in the presence of other VOCs. this CPC based sensor can work in high humidity concentration, although a 34% reduction in resistance change is noticed at 85% RH.

For 1-Mercapto-(triethylene glycol) methyl ether functionalized GNP, it was concluded that the fabricated sensors are highly sensitive to all the VOCs presenting similar percentage change per ppm of VOC signifying that the sensor is not very selective. Also, the results indicate that the sensor cannot work at humidity concen-

tration of 45% which hinder its application for breath sensing application because the exhaled breath has 70% moisture content. The proposed method of incorporating a PEI layer on top of the fabricated f-GNP sensor gives better results that bare f-GNP sensor. Spin coating PEI on top of GNP sensor gives a uniform film of 2.5μm and heat treatment at 80^0C increases the hydrophobicity from 59^0 to 84^0 making the film resistance to water. The fabricated f-GNP/PEI sensor presents high sensitivity (0.21% per ppm of nonanal) with better cross selectivity with other VOCs as compared to GNP sensor. The results with water show that the sensor can tolerate high relative humidity of 70% showing only 4% resistance change. Two sensors have been presented with high sensitivity and cross selectivity towards nonanal with respect to other VOCs that can work in RH of 85%.

5.2 Future Work

This work can be continued for making the fabricated sensors more hydrophobic so that resistance change at higher humidity concentration is lower than presented values. This can increase the sensitivity of the sensor at high humidity concentration.

In this project, the fabricated sensors on the substrate are of similar material that can give high selectivity detection of a limited number of VOCs. This can be changed by using different materials selective to different chemical classes of VOCs and incorporating those material on to the same substrate giving an array of sensor. This work can help detect various VOCs simultaneously with high sensitivity and selectivity and can help in disease monitoring through the development of the system. This system could be a hand-held portable system for breath monitoring using a sensor array, micro-controller, and other electronics. This handheld device can send data directly to your smartphone for better interaction with the user.

REFERENCES

REFERENCES

[1] M. S. Pepe, R. Etzioni, Z. Feng, J. D. Potter, M. L. Thompson, M. Thornquist, M. Winget, and Y. Yasui, "Phases of biomarker development for early detection of cancer," *Journal of the National Cancer Institute*, vol. 93, no. 14, pp. 1054–1061, 2001.

[2] I. J. Jacobs and U. Menon, "Progress and challenges in screening for early detection of ovarian cancer," *Molecular & Cellular Proteomics*, vol. 3, no. 4, pp. 355–366, 2004.

[3] A. Amann and D. Smith, *Volatile biomarkers: non-invasive diagnosis in physiology and medicine*. Newnes, 2013.

[4] M. Basanta, R. M. Jarvis, Y. Xu, G. Blackburn, R. Tal-Singer, A. Woodcock, D. Singh, R. Goodacre, C. P. Thomas, and S. J. Fowler, "Non-invasive metabolomic analysis of breath using differential mobility spectrometry in patients with chronic obstructive pulmonary disease and healthy smokers," *Analyst*, vol. 135, no. 2, pp. 315–320, 2010.

[5] S. Nag, "Development of conductive nanocomposite sensors for anticipated diagnostic of diseases," Ph.D. dissertation, Université de Bretagne Sud, 2014.

[6] K. A. Kouremenos, M. Johansson, and P. J. Marriott, "Advances in gas chromatographic methods for the identification of biomarkers in cancer," *Journal of Cancer*, vol. 3, p. 404, 2012.

[7] K. Hackner, P. Errhalt, M. R. Mueller, M. Speiser, B. A. Marzluf, A. Schulheim, P. Schenk, J. Bilek, and T. Doll, "Canine scent detection for the diagnosis of lung cancer in a screening-like situation," *Journal of breath research*, vol. 10, no. 4, p. 046003, 2016.

[8] F. Pirrone and M. Albertini, "Olfactory detection of cancer by trained sniffer dogs: a systematic review of the literature," *Journal of Veterinary Behavior: Clinical Applications and Research*, vol. 19, pp. 105–117, 2017.

[9] G. Konvalina and H. Haick, "Sensors for breath testing: from nanomaterials to comprehensive disease detection," *Accounts of chemical research*, vol. 47, no. 1, pp. 66–76, 2013.

[10] N. Kahn, O. Lavie, M. Paz, Y. Segev, and H. Haick, "Dynamic nanoparticle-based flexible sensors: Diagnosis of ovarian carcinoma from exhaled breath," *Nano letters*, vol. 15, no. 10, pp. 7023–7028, 2015.

[11] S. N. Kim, J. F. Rusling, and F. Papadimitrakopoulos, "Carbon nanotubes for electronic and electrochemical detection of biomolecules," *Advanced materials*, vol. 19, no. 20, pp. 3214–3228, 2007.

[12] M. K. Nakhleh, Y. Y. Broza, and H. Haick, "Monolayer-capped gold nanoparticles for disease detection from breath," *Nanomedicine*, vol. 9, no. 13, pp. 1991–2002, 2014.

[13] R. Ionescu, U. Cindemir, T. G. Welearegay, R. Calavia, Z. Haddi, Z. Topalian, C.-G. Granqvist, and E. Llobet, "Fabrication of ultra-pure gold nanoparticles capped with dodecanethiol for schottky-diode chemical gas sensing devices," *Sensors and Actuators B: Chemical*, vol. 239, pp. 455–461, 2017.

[14] H. Deng, L. Lin, M. Ji, S. Zhang, M. Yang, and Q. Fu, "Progress on the morphological control of conductive network in conductive polymer composites and the use as electroactive multifunctional materials," *Progress in Polymer Science*, vol. 39, no. 4, pp. 627–655, 2014.

[15] A. Jemal, R. Siegel, E. Ward, Y. Hao, J. Xu, T. Murray, and M. J. Thun, "Cancer statistics, 2008," *CA: a cancer journal for clinicians*, vol. 58, no. 2, pp. 71–96, 2008.

[16] G. Peng, M. Hakim, Y. Y. Broza, S. Billan, R. Abdah-Bortnyak, A. Kuten, U. Tisch, and H. Haick, "Detection of lung, breast, colorectal, and prostate cancers from exhaled breath using a single array of nanosensors," *British journal of cancer*, vol. 103, no. 4, p. 542, 2010.

[17] C. Facts, "Cancer facts and figures (2017)," *Am Cancer Soc*, vol. 64, 2013.

[18] N. Goossens, S. Nakagawa, X. Sun, and Y. Hoshida, "Cancer biomarker discovery and validation," *Translational cancer research*, vol. 4, no. 3, p. 256, 2015.

[19] W. H. Organization *et al.*, *Biomarkers in risk assessment: Validity and validation*, Vol. 222, 2001.

[20] "Committee on the review of omics-based tests for predicting patient outcomes in clinical trials, board on health care services, board on health sciences policy, and institute of medicine, evolution of translational omics: Lessons learned and the path forward," [Online]. Last Date Accessed: 12/1/2018.

[21] H. O'neill, S. Gordon, M. O'neill, R. Gibbons, and J. Szidon, "A computerized classification technique for screening for the presence of breath biomarkers in lung cancer." *Clinical chemistry*, vol. 34, no. 8, pp. 1613–1618, 1988.

[22] M. Phillips, K. Gleeson, J. M. B. Hughes, J. Greenberg, R. N. Cataneo, L. Baker, and W. P. McVay, "Volatile organic compounds in breath as markers of lung cancer: a cross-sectional study," *The Lancet*, vol. 353, no. 9168, pp. 1930–1933, 1999.

[23] X. Chen, F. Xu, Y. Wang, Y. Pan, D. Lu, P. Wang, K. Ying, E. Chen, and W. Zhang, "A study of the volatile organic compounds exhaled by lung cancer cells in vitro for breath diagnosis," *Cancer: Interdisciplinary International Journal of the American Cancer Society*, vol. 110, no. 4, pp. 835–844, 2007.

[24] A. Bajtarevic, C. Ager, M. Pienz, M. Klieber, K. Schwarz, M. Ligor, T. Ligor, W. Filipiak, H. Denz, M. Fiegl *et al.*, "Noninvasive detection of lung cancer by analysis of exhaled breath," *BMC cancer*, vol. 9, no. 1, p. 348, 2009.

[25] H. Handa, A. Usuba, S. Maddula, J. I. Baumbach, M. Mineshita, and T. Miyazawa, "Exhaled breath analysis for lung cancer detection using ion mobility spectrometry," *PloS one*, vol. 9, no. 12, p. e114555, 2014.

[26] P. Fuchs, C. Loeseken, J. K. Schubert, and W. Miekisch, "Breath gas aldehydes as biomarkers of lung cancer," *International Journal of Cancer*, vol. 126, no. 11, pp. 2663–2670, 2010.

[27] M. Phillips, R. N. Cataneo, B. A. Ditkoff, P. Fisher, J. Greenberg, R. Gunawardena, C. S. Kwon, O. Tietje, and C. Wong, "Prediction of breast cancer using volatile biomarkers in the breath," *Breast cancer research and treatment*, vol. 99, no. 1, pp. 19–21, 2006.

[28] J. Li, Y. Peng, Y. Liu, W. Li, Y. Jin, Z. Tang, and Y. Duan, "Investigation of potential breath biomarkers for the early diagnosis of breast cancer using gas chromatography–mass spectrometry," *Clinica chimica acta*, vol. 436, pp. 59–67, 2014.

[29] M. Phillips, R. N. Cataneo, C. Saunders, P. Hope, P. Schmitt, and J. Wai, "Volatile biomarkers in the breath of women with breast cancer," *Journal of breath research*, vol. 4, no. 2, p. 026003, 2010.

[30] H. Amal, D.-Y. Shi, R. Ionescu, W. Zhang, Q.-L. Hua, Y.-Y. Pan, L. Tao, H. Liu, and H. Haick, "Assessment of ovarian cancer conditions from exhaled breath," *International journal of cancer*, vol. 136, no. 6, pp. E614–E622, 2015.

[31] T. Khalid, R. Aggio, P. White, B. D. L. Costello, R. Persad, H. Al-Kateb, P. Jones, C. S. Probert, and N. Ratcliffe, "Urinary volatile organic compounds for the detection of prostate cancer," *PloS one*, vol. 10, no. 11, p. e0143283, 2015.

[32] D. Altomare, M. Di Lena, F. Porcelli, L. Trizio, E. Travaglio, M. Tutino, S. Dragonieri, V. Memeo, and G. De Gennaro, "Exhaled volatile organic compounds identify patients with colorectal cancer," *British journal of surgery*, vol. 100, no. 1, pp. 144–150, 2013.

[33] K. E. Pijls, A. Smolinska, D. M. Jonkers, J. W. Dallinga, A. A. Masclee, G. H. Koek, and F.-J. van Schooten, "A profile of volatile organic compounds in exhaled air as a potential non-invasive biomarker for liver cirrhosis," *Scientific reports*, vol. 6, p. 19903, 2016.

[34] F. Zhang, Y. Zhang, W. Zhao, K. Deng, Z. Wang, C. Yang, L. Ma, M. S. Openkova, Y. Hou, and K. Li, "Metabolomics for biomarker discovery in the diagnosis, prognosis, survival and recurrence of colorectal cancer: a systematic review," *Oncotarget*, vol. 8, no. 21, p. 35460, 2017.

[35] A. Wehinger, A. Schmid, S. Mechtcheriakov, M. Ledochowski, C. Grabmer, G. A. Gastl, and A. Amann, "Lung cancer detection by proton transfer reaction mass-spectrometric analysis of human breath gas," *International Journal of Mass Spectrometry*, vol. 265, no. 1, pp. 49–59, 2007.

[36] P. Španěl, D. Smith, T. A. Holland, W. A. Singary, and J. B. Elder, "Analysis of formaldehyde in the headspace of urine from bladder and prostate cancer patients using selected ion flow tube mass spectrometry," *Rapid communications in mass spectrometry*, vol. 13, no. 14, pp. 1354–1359, 1999.

[37] D. Smith, T. Wang, J. Sulé-Suso, P. Španěl, and A. E. Haj, "Quantification of acetaldehyde released by lung cancer cells in vitro using selected ion flow tube mass spectrometry," *Rapid communications in mass spectrometry*, vol. 17, no. 8, pp. 845–850, 2003.

[38] D. Poli, M. Goldoni, M. Corradi, O. Acampa, P. Carbognani, E. Internullo, A. Casalini, and A. Mutti, "Determination of aldehydes in exhaled breath of patients with lung cancer by means of on-fiber-derivatisation spme–gc/ms," *Journal of Chromatography B*, vol. 878, no. 27, pp. 2643–2651, 2010.

[39] A. R. Lima, M. de Lourdes Bastos, M. Carvalho, and P. G. de Pinho, "Biomarker discovery in human prostate cancer: an update in metabolomics studies," *Translational oncology*, vol. 9, no. 4, pp. 357–370, 2016.

[40] D. Wang, C. Wang, X. Pi, L. Guo, Y. Wang, M. Li, Y. Feng, Z. Lin, W. Hou, and E. Li, "Urinary volatile organic compounds as potential biomarkers for renal cell carcinoma," *Biomedical reports*, vol. 5, no. 1, pp. 68–72, 2016.

[41] D. Poli, P. Carbognani, M. Corradi, M. Goldoni, O. Acampa, B. Balbi, L. Bianchi, M. Rusca, and A. Mutti, "Exhaled volatile organic compounds in patients with non-small cell lung cancer: cross sectional and nested short-term follow-up study," *Respiratory research*, vol. 6, no. 1, p. 71, 2005.

[42] S. Gordon, J. Szidon, B. Krotoszynski, R. Gibbons, and H. O'Neill, "Volatile organic compounds in exhaled air from patients with lung cancer." *Clinical chemistry*, vol. 31, no. 8, pp. 1278–1282, 1985.

[43] M. Bouza, J. Gonzalez-Soto, R. Pereiro, J. de Vicente, and A. Sanz-Medel, "Exhaled breath and oral cavity vocs as potential biomarkers in oral cancer patients," *Journal of breath research*, vol. 11, no. 1, p. 016015, 2017.

[44] J. Devkota, P. R. Ohodnicki, and D. W. Greve, "Saw sensors for chemical vapors and gases," *Sensors*, vol. 17, no. 4, p. 801, 2017.

[45] C. Viespe and C. Grigoriu, "Surface acoustic wave sensors with carbon nanotubes and sio2/si nanoparticles based nanocomposites for voc detection," *Sensors and Actuators B: Chemical*, vol. 147, no. 1, pp. 43–47, 2010.

[46] C. Viespe and D. Miu, "Characteristics of surface acoustic wave sensors with nanoparticles embedded in polymer sensitive layers for voc detection," *Sensors*, vol. 18, no. 7, p. 2401, 2018.

[47] X. Chen, M. Cao, Y. Li, W. Hu, P. Wang, K. Ying, and H. Pan, "A study of an electronic nose for detection of lung cancer based on a virtual saw gas sensors array and imaging recognition method," *Measurement Science and Technology*, vol. 16, no. 8, p. 1535, 2005.

[48] M. Penza, F. Antolini, and M. V. Antisari, "Carbon nanotubes as saw chemical sensors materials," *Sensors and Actuators B: Chemical*, vol. 100, no. 1-2, pp. 47–59, 2004.

[49] A. J. Ricco, R. M. Crooks, and G. C. Osbourn, "Surface acoustic wave chemical sensor arrays: new chemically sensitive interfaces combined with novel cluster analysis to detect volatile organic compounds and mixtures," *Accounts of chemical research*, vol. 31, no. 5, pp. 289–296, 1998.

[50] D. Lange, C. Hagleitner, A. Hierlemann, O. Brand, and H. Baltes, "Complementary metal oxide semiconductor cantilever arrays on a single chip: mass-sensitive detection of volatile organic compounds," *Analytical Chemistry*, vol. 74, no. 13, pp. 3084–3095, 2002.

[51] J.-S. Lee, S.-W. Lee, H.-M. Jeong, S.-W. Lim, E.-Y. Jang, N.-R. Yoon, D.-H. Kwon, and S.-W. Kang, "Volatile organic compounds optical fiber gas sensor based on evanescentl field coupling and solvatochromism," in *SENSORS, 2013 IEEE*. IEEE, 2013, pp. 1–4.

[52] M. C. Janzen, J. B. Ponder, D. P. Bailey, C. K. Ingison, and K. S. Suslick, "Colorimetric sensor arrays for volatile organic compounds," *Analytical chemistry*, vol. 78, no. 11, pp. 3591–3600, 2006.

[53] G. S. Wilson, Y. Zhang, G. Reach, D. Moatti-Sirat, V. Poitout, D. R. Thévenot, F. Lemonnier, and J.-C. Klein, "Progress toward the development of an implantable sensor for glucose." *Clinical Chemistry*, vol. 38, no. 9, pp. 1613–1617, 1992.

[54] J. Janata and A. Bezegh, "Chemical sensors," *Analytical chemistry*, vol. 60, no. 12, pp. 62–74, 1988.

[55] J. Gebicki and A. Kloskowski, "Electrochemical sensor for measurement of volatile organic compounds employing square wave perturbation voltage," *Metrology and Measurement Systems*, vol. 17, no. 4, pp. 637–649, 2010.

[56] A. Daneshkhah, S. Shrestha, A. Siegel, K. Varahramyan, and M. Agarwal, "Cross-selectivity enhancement of poly (vinylidene fluoride-hexafluoropropylene)-based sensor arrays for detecting acetone and ethanol," *Sensors*, vol. 17, no. 3, p. 595, 2017.

[57] A. Daneshkhah, S. Shrestha, M. Agarwal, and K. Varahramyan, "Ppy/pmma/peg-based sensor for low-concentration acetone detection," in *Smart Biomedical and Physiological Sensor Technology XI*, vol. 9107. International Society for Optics and Photonics, 2014, p. 910712.

[58] ——, "Poly (vinylidene fluoride-hexafluoropropylene) composite sensors for volatile organic compounds detection in breath," *Sensors and Actuators B: Chemical*, vol. 221, pp. 635–643, 2015.

[59] B. Szulczyński and J. Gebicki, "Currently commercially available chemical sensors employed for detection of volatile organic compounds in outdoor and indoor air," *Environments*, vol. 4, no. 1, p. 21, 2017.

[60] M. Schuler, N. Helwig, A. Schutze, T. Sauerwald, and G. Ventura, "Detecting trace-level concentrations of volatile organic compounds with metal oxide gas sensors," in *SENSORS, 2013 IEEE*. IEEE, 2013, pp. 1–4.

[61] M. Leidinger, T. Sauerwald, T. Conrad, W. Reimringer, G. Ventura, and A. Schütze, "Selective detection of hazardous indoor vocs using metal oxide gas sensors," *Procedia Engineering*, vol. 87, pp. 1449–1452, 2014.

[62] N. Tayebi and X. Su, "Sensitive and selective gas/voc detection using mos sensor array for wearable and mobile applications," in *Olfaction and Electronic Nose (ISOEN), 2017 ISOCS/IEEE International Symposium on*. IEEE, 2017, pp. 1–3.

[63] S. Some, Y. Xu, Y. Kim, Y. Yoon, H. Qin, A. Kulkarni, T. Kim, and H. Lee, "Highly sensitive and selective gas sensor using hydrophilic and hydrophobic graphenes," *Scientific reports*, vol. 3, p. srep01868, 2013.

[64] S.-Y. Cho, H.-W. Yoo, J. Y. Kim, W.-B. Jung, M. L. Jin, J.-S. Kim, H.-J. Jeon, and H.-T. Jung, "High-resolution p-type metal oxide semiconductor nanowire array as an ultrasensitive sensor for volatile organic compounds," *Nano letters*, vol. 16, no. 7, pp. 4508–4515, 2016.

[65] H. Wohltjen and A. W. Snow, "Colloidal metal- insulator- metal ensemble chemiresistor sensor," *Analytical Chemistry*, vol. 70, no. 14, pp. 2856–2859, 1998.

[66] J. W. Grate, D. A. Nelson, and R. Skaggs, "Sorptive behavior of monolayer-protected gold nanoparticle films: implications for chemical vapor sensing," *Analytical chemistry*, vol. 75, no. 8, pp. 1868–1879, 2003.

[67] E. Dovgolevsky, U. Tisch, and H. Haick, "Chemically sensitive resistors based on monolayer-capped cubic nanoparticles: Towards configurable nanoporous sensors," *Small*, vol. 5, no. 10, pp. 1158–1161, 2009.

[68] K. Beverly, J. Sampaio, and J. Heath, "Effects of size dispersion disorder on the charge transport in self-assembled 2-d ag nanoparticle arrays," *The Journal of Physical Chemistry B*, vol. 106, no. 9, pp. 2131–2135, 2002.

[69] A. W. Snow, M. G. Ancona, and D. Park, "Nanodimensionally driven analyte response reversal in gold nanocluster chemiresistor sensing," *Langmuir*, vol. 28, no. 44, pp. 15 438–15 443, 2012.

[70] Y. Joseph, I. Besnard, M. Rosenberger, B. Guse, H.-G. Nothofer, J. M. Wessels, U. Wild, A. Knop-Gericke, D. Su, R. Schlögl *et al.*, "Self-assembled gold nanoparticle/alkanedithiol films: preparation, electron microscopy, xps-analysis, charge transport, and vapor-sensing properties," *The Journal of Physical Chemistry B*, vol. 107, no. 30, pp. 7406–7413, 2003.

[71] J. S. Cooper, B. Raguse, E. Chow, L. Hubble, K.-H. Muller, and L. Wieczorek, "Gold nanoparticle chemiresistor sensor array that differentiates between hydrocarbon fuels dissolved in artificial seawater," *Analytical chemistry*, vol. 82, no. 9, pp. 3788–3795, 2010.

[72] N. Olichwer, A. Meyer, M. Yesilmen, and T. Vossmeyer, "Gold nanoparticle superlattices: correlating chemiresistive responses with analyte sorption and swelling," *Journal of Materials Chemistry C*, vol. 4, no. 35, pp. 8214–8225, 2016.

[73] Z. Xie, M. V. R. Raju, B. S. Brown, A. C. Stewart, M. H. Nantz, and X.-A. Fu, "Electronic nose for detection of toxic volatile organic compounds in air," in *Solid-State Sensors, Actuators and Microsystems (TRANSDUCERS), 2017 19th International Conference on.* IEEE, 2017, pp. 1425–1428.

[74] G. Peng, U. Tisch, O. Adams, M. Hakim, N. Shehada, Y. Y. Broza, S. Billan, R. Abdah-Bortnyak, A. Kuten, and H. Haick, "Diagnosing lung cancer in exhaled breath using gold nanoparticles," *Nature nanotechnology*, vol. 4, no. 10, p. 669, 2009.

[75] W. H. Steinecker, M. P. Rowe, and E. T. Zellers, "Model of vapor-induced resistivity changes in gold- thiolate monolayer-protected nanoparticle sensor films," *Analytical chemistry*, vol. 79, no. 13, pp. 4977–4986, 2007.

[76] X. Liu, S. Cheng, H. Liu, S. Hu, D. Zhang, and H. Ning, "A survey on gas sensing technology," *Sensors*, vol. 12, no. 7, pp. 9635–9665, 2012.

[77] G. Peng, E. Trock, and H. Haick, "Detecting simulated patterns of lung cancer biomarkers by random network of single-walled carbon nanotubes coated with nonpolymeric organic materials," *Nano letters*, vol. 8, no. 11, pp. 3631–3635, 2008.

[78] S. Chatterjee, M. Castro, and J.-F. Feller, "An e-nose made of carbon nanotube based quantum resistive sensors for the detection of eighteen polar/nonpolar voc biomarkers of lung cancer," *Journal of Materials Chemistry B*, vol. 1, no. 36, pp. 4563–4575, 2013.

[79] Y. Zilberman, U. Tisch, G. Shuster, W. Pisula, X. Feng, K. Müllen, and H. Haick, "Carbon nanotube/hexa-peri-hexabenzocoronene bilayers for discrimination between nonpolar volatile organic compounds of cancer and humid atmospheres," *Advanced Materials*, vol. 22, no. 38, pp. 4317–4320, 2010.

[80] Y. Wang and J. T. Yeow, "A review of carbon nanotubes-based gas sensors," *Journal of Sensors*, vol. 2009, 2009.

[81] G. Lu, L. E. Ocola, and J. Chen, "Reduced graphene oxide for room-temperature gas sensors," *Nanotechnology*, vol. 20, no. 44, p. 445502, 2009.

[82] C. Hagleitner, D. Lange, A. Hierlemann, O. Brand, and H. Baltes, "Cmos single-chip gas detection system comprising capacitive, calorimetric and mass-sensitive microsensors," *IEEE Journal of Solid-State Circuits*, vol. 37, no. 12, pp. 1867–1878, 2002.

[83] Y. Jiang, N. Tang, C. Zhou, Z. Han, H. Qu, and X. Duan, "A chemiresistive sensor array from conductive polymer nanowires fabricated by nanoscale soft lithography," *Nanoscale*, 2018.

[84] F. M. Wisser, J. Grothe, and S. Kaskel, "Nanoporous polymers as highly sensitive functional material in chemiresistive gas sensors," *Sensors and Actuators B: Chemical*, vol. 223, pp. 166–171, 2016.

[85] B. Lakard, S. Carquigny, O. Segut, T. Patois, and S. Lakard, "Gas sensors based on electrodeposited polymers," *Metals*, vol. 5, no. 3, pp. 1371–1386, 2015.

[86] Y. Li, H. Liu, K. Dai, G. Zheng, C. Liu, J. Chen, and C. Shen, "Tuning of vapor sensing behaviors of eco-friendly conductive polymer composites utilizing ramie fiber," *Sensors and Actuators B: Chemical*, vol. 221, pp. 1279–1289, 2015.

[87] Y. Li, P. Pötschke, J. Pionteck, and B. Voit, "Electrical and vapor sensing behaviors of polycarbonate composites containing hybrid carbon fillers," *European Polymer Journal*, vol. 108, pp. 461–471, 2018.

[88] Z. Kennedy, J. Christ, K. Evans, B. Arey, L. Sweet, M. Warner, R. Erikson, and C. Barrett, "3d-printed poly (vinylidene fluoride)/carbon nanotube composites as a tunable, low-cost chemical vapour sensing platform," *Nanoscale*, vol. 9, no. 17, pp. 5458–5466, 2017.

[89] A. N. Mallya and P. C. Ramamurthy, "Selectivity of organic nanocomposite sensor for detection of aldehydes," in *Sensing Technology (ICST), 2013 Seventh International Conference on*, pp. 1-6, 2013.

[90] A. Mallya and P. Ramamurthy, "Organic molecule based sensor for aldehyde detection," in *Sensing Technology: Current Status and Future Trends III*, pp. 299-325, 2015.

[91] S. Antwi-Boampong and J. J. BelBruno, "Detection of formaldehyde vapor using conductive polymer films," *Sensors and Actuators B: Chemical*, vol. 182, pp. 300–306, 2013.

[92] S. Srinives, T. Sarkar, and A. Mulchandani, "Primary amine-functionalized polyaniline nanothin film sensor for detecting formaldehyde," *Sensors and Actuators B: Chemical*, vol. 194, pp. 255–259, 2014.

[93] S. Pirsa and N. Alizadeh, "Design and fabrication of gas sensor based on nanostructure conductive polypyrrole for determination of volatile organic solvents," *Sensors and Actuators B: Chemical*, vol. 147, no. 2, pp. 461–466, 2010.

[94] M. Eberlin *et al.*, "Polyetherimide–silicone: a 10 ám ultrathin composite membrane for faster and more sensitive membrane introduction mass spectrometry analysis," *Analytical Communications*, vol. 36, no. 6, pp. 221–223, 1999.

[95] S. Husain and W. J. Koros, "Mixed matrix hollow fiber membranes made with modified hssz-13 zeolite in polyetherimide polymer matrix for gas separation," *Journal of Membrane Science*, vol. 288, no. 1-2, pp. 195–207, 2007.

[96] D. Wang, W. Teo, and K. Li, "Selective removal of trace h2s from gas streams containing co2 using hollow fibre membrane modules/contractors," *Separation and purification Technology*, vol. 35, no. 2, pp. 125–131, 2004.

[97] A. F. Viero, G. L. SantAnna Jr, and R. Nobrega, "The use of polyetherimide hollow fibres in a submerged membrane bioreactor operating with air backwashing," *Journal of Membrane Science*, vol. 302, no. 1-2, pp. 127–135, 2007.

[98] D. Wang, K. Li, and W. Teo, "Preparation and characterization of polyetherimide asymmetric hollow fiber membranes for gas separation," *Journal of membrane science*, vol. 138, no. 2, pp. 193–201, 1998.

[99] L. Gales, A. Mendes, and C. Costa, "Removal of acetone, ethyl acetate and ethanol vapors from air using a hollow fiber pdms membrane module," *Journal of Membrane Science*, vol. 197, no. 1-2, pp. 211–222, 2002.

[100] W. Zhao and B. Shi, "Removal of volatile organic compounds from water by pervaporation using polyetherimide-polyethersulfone blend hollow fiber membranes," *Separation Science and Technology*, vol. 44, no. 8, pp. 1737–1752, 2009.

[101] S. Deng, A. Tremblay, and T. Matsuura, "Preparation of hollow fibers for the removal of volatile organic compounds from air," *Journal of applied polymer science*, vol. 69, no. 2, pp. 371–379, 1998.

[102] S. Deng, T. Liu, S. Sourirajan, and T. Matsuura, "A study of volatile hydrocarbon emission control by polyetherimide hollow fiber membranes," *Journal of polymer engineering*, vol. 14, no. 4, pp. 219–236, 1995.

[103] T. Schneller, R. Waser, M. Kosec, and D. Payne, *Chemical solution deposition of functional oxide thin films*. Springer, 2013.

[104] J. Creighton and P. Ho, "Introduction to chemical vapor deposition (cvd)," *Chemical vapor deposition*, vol. 2, pp. 1–22, 2001.

[105] H. Li, X. Qian, T. Li, and Y. Ni, "Percolation for coated conductive paper: electrical conductivity as a function of volume fraction of graphite and carbon black," *BioResources*, vol. 10, no. 3, pp. 4877–4885, 2015.

[106] H. Bai and G. Shi, "Gas sensors based on conducting polymers," *Sensors*, vol. 7, no. 3, pp. 267–307, 2007.

[107] L. Han, X. Shi, W. Wu, F. L. Kirk, J. Luo, L. Wang, D. Mott, L. Cousineau, I. Stephanie, I. Lim *et al.*, "Nanoparticle-structured sensing array materials and pattern recognition for voc detection," *Sensors and Actuators B: Chemical*, vol. 106, no. 1, pp. 431–441, 2005.

[108] Q. Zhong, W. H. Steinecker, and E. T. Zellers, "Characterization of a high-performance portable gc with a chemiresistor array detector," *Analyst*, vol. 134, no. 2, pp. 283–293, 2009.

[109] A. Zabet-Khosousi and A.-A. Dhirani, "Charge transport in nanoparticle assemblies," *Chemical reviews*, vol. 108, no. 10, pp. 4072–4124, 2008.

[110] N. Garg, A. Mohanty, N. Lazarus, L. Schultz, T. R. Rozzi, S. Santhanam, L. Weiss, J. L. Snyder, G. K. Fedder, and R. Jin, "Robust gold nanoparticles stabilized by trithiol for application in chemiresistive sensors," *Nanotechnology*, vol. 21, no. 40, p. 405501, 2010.

[111] T. Ogawa, "Vibrational assignments and normal vibrations of trimethylaluminium," *Spectrochimica Acta Part A: Molecular Spectroscopy*, vol. 24, no. 1, pp. 15–20, 1968.

[112] S. Rajasekar and D. Venkatesan, "Synthesis and properties of polyetherimides by nucleophilic displacement reaction," *Polymers & Polymer Composites*, vol. 20, no. 9, pp. 845–852, 2012.

[113] A. Choudhury, "Dielectric and piezoelectric properties of polyetherimide/batio3 nanocomposites," *Materials Chemistry and Physics*, vol. 121, no. 1-2, pp. 280–285, 2010.

[114] M. Rajagopalan, J.-H. Jeon, and I.-K. Oh, "Electric-stimuli-responsive bending actuator based on sulfonated polyetherimide," *Sensors and Actuators B: Chemical*, vol. 151, no. 1, pp. 198–204, 2010.

[115] Y. Bormashenko, R. Pogreb, O. Stanevsky, and E. Bormashenko, "Vibrational spectrum of pvdf and its interpretation," *Polymer testing*, vol. 23, no. 7, pp. 791–796, 2004.

[116] A. M. Díez-Pascual, J. Guan, B. Simard, and M. A. Gómez-Fatou, "Poly (phenylene sulphide) and poly (ether ether ketone) composites reinforced with single-walled carbon nanotube buckypaper: I–structure, thermal stability and crystallization behaviour," *Composites Part A: Applied Science and Manufacturing*, vol. 43, no. 6, pp. 997–1006, 2012.

[117] J. Chen, J. Li, J. Chen, Y. Lin, and X. Wang, "Pervaporation separation of ethyl thioether/heptane mixtures by polyethylene glycol membranes," *Separation and Purification Technology*, vol. 66, no. 3, pp. 606–612, 2009.

[118] J. Kurdi and A. Kumar, "Structuring and characterization of a novel highly microporous pei/bmi semi-interpenetrating polymer network," *Polymer*, vol. 46, no. 18, pp. 6910–6922, 2005.

[119] H. Zhang, S. Wang, S. Zhang, R. Ma, Y. Wang, W. Cao, C. Liu, and C. Shen, "Crystallization behavior of poly (lactic acid) with a self-assembly aryl amide nucleating agent probed by real-time infrared spectroscopy and x-ray diffraction," *Polymer Testing*, vol. 64, pp. 12–19, 2017.

[120] G. Lisa, C. Hamciuc, E. Hamciuc, and N. Tudorachi, "Thermal and thermo-oxidative stability and probable degradation mechanism of some polyetherimides," *Journal of analytical and applied pyrolysis*, vol. 118, pp. 144–154, 2016.

[121] M. Martín, F. Rodríguez-Lence, A. Güemes, A. Fernández-López, L. A. Pérez-Maqueda, and A. Perejón, "On the determination of thermal degradation effects and detection techniques for thermoplastic composites obtained by automatic lamination," *Composites Part A: Applied Science and Manufacturing*, vol. 111, pp. 23–32, 2018.

[122] A. Bajpai, "Fibrinogen adsorption onto macroporous polymeric surfaces: correlation with biocompatibility aspects," *Journal of Materials Science: Materials in Medicine*, vol. 19, no. 1, p. 343, 2008.

[123] M. Rodriguez, J. Lapierre, C. R. Ojha, A. Kaushik, E. Batrakova, F. Kashanchi, S. M. Dever, M. Nair, and N. El-Hage, "Intranasal drug delivery of small interfering rna targeting beclin1 encapsulated with polyethylenimine (pei) in mouse brain to achieve hiv attenuation," *Scientific reports*, vol. 7, no. 1, p. 1862, 2017.

[124] B. Nolin and R. N. Jones, "The infrared absorption spectra of deuterated esters: Ii. ethyl acetate," *Canadian Journal of Chemistry*, vol. 34, no. 10, pp. 1392–1404, 1956.

[125] C.-P. Yang and Y.-Y. Su, "Novel organosoluble and colorless poly (ether imide) s based on 3, 3-bis [4-(3, 4-dicarboxyphenoxy) phenyl] phthalide dianhydride and aromatic bis (ether amine) s bearing pendent trifluoromethyl groups," *Journal of Polymer Science Part A: Polymer Chemistry*, vol. 44, no. 9, pp. 3140–3152, 2006.

[126] H.-W. Wang, K.-C. Chang, J.-M. Yeh, and S.-J. Liou, "Synthesis and dielectric properties of polystyrene-clay nanocomposite materials," *Journal of applied polymer science*, vol. 91, no. 2, pp. 1368–1373, 2004.

[127] S. Banerjee, M. K. Madhra, and V. Kute, "Polyimides 6: synthesis, characterization, and comparison of properties of novel fluorinated poly (ether imides)," *Journal of applied polymer science*, vol. 93, no. 2, pp. 821–832, 2004.

[128] P. Musto, F. Karasz, and W. MacKnight, "Fourier transform infra-red spectroscopy on the thermo-oxidative degradation of polybenzimidazole and of a polybenzimidazole/polyetherimide blend," *Polymer*, vol. 34, no. 14, pp. 2934–2945, 1993.

[129] Q. Zhang, Y. Xu, Y. Yang, L. Li, C. Song, and X. Su, "Conductive mechanism of carbon black/polyimide composite films," *Journal of Polymer Engineering*, vol. 38, no. 2, pp. 147–156, 2018.

[130] K. Hosono, I. Matsubara, N. Murayama, W. Shin, and N. Izu, "The sensitivity of 4-ethylbenzenesulfonic acid-doped plasma polymerized polypyrrole films to volatile organic compounds," *Thin Solid Films*, vol. 484, no. 1-2, pp. 396–399, 2005.

[131] J. Zheng, G. Li, X. Ma, Y. Wang, G. Wu, and Y. Cheng, "Polyaniline–tio2 nanocomposite-based trimethylamine qcm sensor and its thermal behavior studies," *Sensors and Actuators B: Chemical*, vol. 133, no. 2, pp. 374–380, 2008.